Oil Adsorption Performance and Efficiency Study on Novel Silane Functionalized Graphene Polyurethane Sponge

by

Teresa Sung

A thesis

presented to the University of Waterloo

in fulfillment of the

thesis requirement for the degree of

Master of Applied Science

in

Mechanical and Mechatronics Engineering

Waterloo, Ontario, Canada, 2017

Author's Declaration

I hereby declare that I am the sole author of this thesis. This is a true copy of the thesis, including any required final revisions, as accepted by my examiners. I understand that my thesis may be made electronically available to the public.

Abstract

Oil-water separation has been vital in many aspects of our society's operations. This is particularly highlighted during the environmental cleanups of industrial oily wastes and disasters involving petroleum oil spills. These damaging and ever-challenging conditions require novel, adaptive, cost effective materials and technologies that go beyond current practices. Carbon-based materials such as graphene have excellent potential hydrophobic and oleophilic properties. Some of the challenges to date with these adsorbent based materials include structural and stability issues, which hinder their advantages affording it good but limited properties as oil adsorbents. Although there are numerous novel adsorbents with outstanding adsorption capacities and excellent recyclability, there is still a gap between their performances in a laboratory setting and their actual field application. Under field conditions, other parameters such as buoyancy, geometry, strength and durability, transportation, economics, actual amount of oil recovered as well as its quality etc. must be considered altogether. This paper explores some of these topics with a focus on the development of new experimental parameters that allow investigators to study the oil retention efficiency, adsorption capacity efficiency, and adsorption flux efficiency of an adsorbent. There have been many explorations and investigations on the net adsorption capacities of new materials, however, very few focus on the optimization of an adsorbent as a system, maximizing the synergistic effects between its porous structure, morphology and surface chemistry.

In this thesis study, a super-oleophilic and hydrophobic polyurethane sponge (PU) was created by undergoing an acid-pretreatment and subsequently coated with 3-methacryloxypropyl trimethoxysilane (MPTS) functionalized reduced graphene oxide (RGO). Oil adsorption performances were compared between the samples and the controls in order to quantify the effects of acid-pretreatment, RGO and MPTS functionalization. Water and oil contact angles and water uptake were measured to study the hydrophobicity, oleophilicity and selectivity of the samples. Oil adsorption capacities were measured with protocols specifically designed to study oil retention efficiencies. Recyclability and kinetics studies were also performed experimentally. Pump oil was used as the adsorbate for all experiments in this study. The samples were characterized using SEM, Raman, XRD, and FTIR to understand their morphologies and surface chemistries.

Results indicated the net adsorption capacity of the tested adsorbent improved from 18.5 g/g to 28.61 g/g. More importantly, efficiency studies suggest potential further improvement of over 20% in addition to the volumetric oil adsorption, an additional of 10% or so in oil retention, and over 50% in addition to the adsorption mass flux. The recyclability was stable at over 99.4% after 10 adsorption-desorption cycles.

Acknowledgements

Dedication

To all my children.

To my loving husband.

To my family.

For all who bring purpose for tomorrow and instill meaning for yesterday.

Table of Contents

List of Figures

List of Tables

List of Abbreviations and Symbols

Symbol	Name	Units
°	Degree	
δ	Delta	
μL	Microliter	
3D	Three dimensional	
A	Area	(m^2)
ASTM	American society for testing and Materials	
BET	Brunauer-Emmett-Teller	(m^2/g)
C	Celsius	
CA	Contact angle	$(°)$
cm	Centimeter	
cm^3	Cubic centimeter	
CNF	cellulose nanofibrils	
CNT	carbon nanotubes	
cP	centipoise	
DDI	Distilled De-ionized	
DI	De-ionized	
g	gram	
GF	Graphene framework	
GO	Graphene oxide	
hr	Hour	
I	Gravimetric flux improvement factor	

I_D	Raman intensity for D band	
I_G	Raman intensity for G band	
j_m	Gravimetric flux	$(kg/m^2 \cdot s)$
k	Permeability	(m^2)
k_1	Pseudo-first order rate constant	(min^{-1})
k_2	Pseudo-second order rate constant	$(g/g \cdot min)$
Kg	Kilogram	
$Log\ K_{ow}$	Logarithmic octanol/water partition coefficient	
m	Meter	
mm	Millimeter	
mN	Milli-Newton	
mPa	Millipascal	
MPa	Megapascal	
$MPTS$	3-methacryloxypropyl Trimethoxysilane	
μ	Viscosity	(cP)
$MWCNT$	Multiwall carbon nanotubes	
nm	nanometer	
OCA	Oil contact angle	$(°)$
ORR	Oil retention rate	$(\%)$
OWS	Oil-water separator	
p	Pressure	(N/m^2)
Pa	Pascal	
$PBDE$	Polybrominated diphenyl ethers	
PCB	Polychlorinated biphenyls	
$POSS$	Polyhedral oligomeric silsesquioxane	

PU	Polyurethane	
PUF	Polyurethane foam	
PVA	Polyvinyl alcohol	
Q	Adsorption capacity	(g/g)
Q_e	Equilibrium adsorption capacity	(g/g)
$Q_{m/m}$	Gravimetric adsorption capacity	(g/g)
Q_t	Adsorption capacity at time t	(g/g)
$Q_{v/v}$	Volumetric adsorption capacity	(mL/mL)
r	Radius	(m)
RGO	Reduced graphene oxide	
ρ	Density	(g/cm^3)
s	Second(s)	
S_0	Dry weight	(g)
S_{0x}	Dry weight at the beginning of cycle x	(g)
S_D	Weight of oil drainage	(g)
SEM	Scanning electron microscopy	
S_T	Total wet weight	(g)
SWCNT	Single wall carbon nanotubes	
S_{WD}	Weight of drained water	(g)
S_{WT}	Total wet weight (water test)	(g)
T	Temperature	(°C)
V	Volume	(mL)
v/v	Volumetric ratio	
VAE	Volumetric adsorption efficiency	(%)
WCA	Water contact angle	(°)

WRR	Water retention rate	(%)
Wt.%	Weight percent	(%)
ε	Porosity	(%)
θ	Theta, contact angle	(°)
Υ	Surface tension	(N/m)

CHAPTER 1 - INTRODUCTION

1.1 OVERVIEW

The goal of this thesis research is to contribute towards the development of advanced oil-water separation technology aiming at sustainable environmental cleanup applications. Water and oil are two of the mostly used liquids on earth; many operations require these liquids in their purified forms. Although immiscible, the two liquids no longer exist naturally in absence of each other mainly due to anthropogenic wastes and environmental pollutions. Environmental desperation due to oil in water contamination such as gasoline and motor oil via storm drains, oily wastes such as personal care products output from households, and notably accidents such as petroleum oil spills contribute significantly to the need of oil-water separation. There are various devices for the removal of oily contaminants in wastewater, for example, API oil-water separator, gravity plate separator, centrifugal separator, hydrocyclone, which are based on electrochemical emulsification, bioremediation, adsorption, etc.[1-9]. A comprehensive literature review of these mechanisms, advantages and disadvantages of these technologies will be discussed in Chapter 2.

Adsorption is one of the most promising avenues applicable to oil-water separation. It is often used in conjunction with the other methods to accomplish complete removal of oily contaminants and pollutants [5, 8, 9]. Adsorption is the occurrence of the attachment of an adsorbate onto an adsorbent by physical and/or chemical attraction forces between them. Currently, deployed oil sorbents are mostly effective with low oil viscosities, sheen oil films, calm

conditions, least transported distance, and oil that are in continuous phase.[5] Despite there are

numerous organic, inorganic and synthetic sorbents that perform reasonably well, prohibitive

factors such as excessive amounts of secondary hazardous wastes from oil-saturated sorbents,

high transportation costs, harsh conditions such as highly salted and acidic environment demand

for sorbent performances that are well beyond superior. This study evaluates the methodologies

in selecting and modifications of high performing adsorbent materials with a focus particularly

on graphene coated polyurethane foams

1.2   BACKGROUND AND SIGNIFICANCE

Hydrophobicity is the characteristic of a molecule appearing to be repelled from a

network of water molecules. There are various examples of hydrophobicity found in nature.

Some of the most well-known ones include the Lotus effect found on lotus plant leaves. The

rough structure of lotus leaf surface and epicuticle wax create a high static water contact angle

(WCA) and thus a highly hydrophobic, self-cleaning surface. Similarly, this is also found on

water strider legs and bird feathers [10,11].

Oleophilicity is the characteristic of having an affinity toward oil or oil-based materials.

It is oftentimes referred to as a synonym as lipophilicity, the characteristic of having the ability

to dissolve in oils, lipids, fats and non-polar solvents. The term oil usually refers to short chained

fats or unsaturated fatty acids that are liquid at room temperature, whereas lipid is used as a

broader term including fats that are solids at room temperature. Oils and lipids are generally

hydrophobic by nature. The focus of this research is on the adsorption of liquid state oil-based

substances, therefore the term oleophilic or oleophilicity is used throughout the remainder of this paper.

Defined as one of the four macromolecules found in all living things besides water, oils and lipids play significant roles in the biological functions as storage of energy, as signaling messengers, insulation, building blocks for hormones as well as structure components of the cell membrane. Outside of physiological functions, human beings utilize oils and lipids for energy, heat transfer and cooking, cooling and heating, as paint mediums, in consumer products such as personal care products, lubricants, chemical feedstocks such as in pesticides and fertilizers, drug formulations, plastics, rubbers and other synthetic materials; we even commoditized some of these substances, and petroleum oil being one of the pillars of our stock markets globally.

Overall, our world operates on constant cycles from isolation, purification, and refinery of oil; to emulsification, breakdown, absorption or digestion and production of waste products. For as long as we depend on these operations, the need for oil-water separation is inevitable.

Increase in population and demands translate to the increase of a multitude of wastes and their complications in the environment, tipping the balance and becoming increasingly difficult to achieve these processing steps. Accidents such as petroleum oil spills, anthropogenic chemicals such as turpentine, acetone, ethyl acetate, many organic solvents and hydrocarbons have become common oleophilic pollutants. Isolation and purification require more complex processes due to higher amount and novelty of contaminants [12, 15]. Subsequently, the economics, versatility, selectivity, efficiency, durability and recyclability requirements are becoming more challenging.

Oil and gas industry produces an estimated total of 20 billion barrels of wastewater per year [14]. There are over 1.5 billion gallons of used oil along with its toxic contaminants being generated by various industries every year in the United States. Much of the present and past research has been dedicated to the cleanup of these oily wastes. [3, 15-17]

Pollution from Oil-based waste products comes in various forms from different sources. For example, gasoline and motor oil runoffs via storm drains, and petroleum spills have detrimental, long-tailed consequences on economies, environment and the ecosystem [15, 18] Pharmaceutical and personal care products (PCPPs) made up of oil-based compounds are also major contributors to surface and groundwater pollutions. These pollutants make up a great portion of the total water pollution due to continuous discharge by humans and their operations [19].

Beside the detrimental disruptions to the environment and ecosystem, many oleophilic pollutants and toxins are known endocrine disruptors and neuro-intoxicants in humans. These pollutants persist and bioaccumulate due to their high oleophilicity. One of the major sources for such oleophilic toxins is the use of pesticides [15].

A study on oleophilic toxins [20] in eight different brands of Californian milk products, the top dairy producing state of the United States, identified 12 polybrominated diphenyl ethers (PBDEs) and 19 polychlorinated biphenyls (PCBs) congeners from both whole milk and fat free milk. PBDEs and PCBs are both highly oleophilic toxins, and are considered endocrine disruptors as well as neurotoxins. Their highly oleophilic characteristics with log K_{ow} values ranging from 3 to 9 allow them to be highly persistent leading to bioaccumulation in the

environment. It was concluded in the study by Tremolada et. al. that the contaminated vegetation feed contributed the most to the transfer of these contaminants to lactating cow's milk [21].

In Chen et al.'s study [20], the detected levels of PCBs and PBDEs were not significantly different between fat free milk and whole milk. In fact, the lipid adjusted concentrations of these toxins are even higher in fat free milk due to the less lipid content. This suggests that traditional mechanical skimming methods of fat content in milk products are insufficient for the complete removal of certain oleophilic toxins. The observation also suggests that, contrary to what one may expect, the oleophilic toxins do not decrease proportionally when fat content is removed. One possibility is the reduction of interfacial viscosity from the initial heating and agitation step during mechanical skimming allowed the oleophilic substances to move around more freely out of the interfacial film and into water.

This is one example of the reasons for adsorbents to be employed for the complete removal of oily contaminants and pollutions. Adsorbents with special wetting properties readily separate oil or non-polar organic solvents and water without disrupting the immiscibility between them, and therefore using that as an advantage toward removal of one from the other.

1.3   RATIONALE BEHIND STUDY FOCUS

Due to the tremendous volumes of oily wastes generated from these sources together with the social, environmental and economic damages, the amount of secondary hazardous oily wastes generated from these cleanups must be carefully managed. Ideally, recycling of the oil waste minimizes the amount of impact caused by secondary hazardous oily wastes such as accidental spreading and spillage of oily waste during handling and transport, toxic byproducts

from incineration, contamination of groundwater and loss of soil productivity from landfills, etc. The recycling of recovered oil allows for the conversion of liability into potential asset, this creates much economic and environmental advantages.
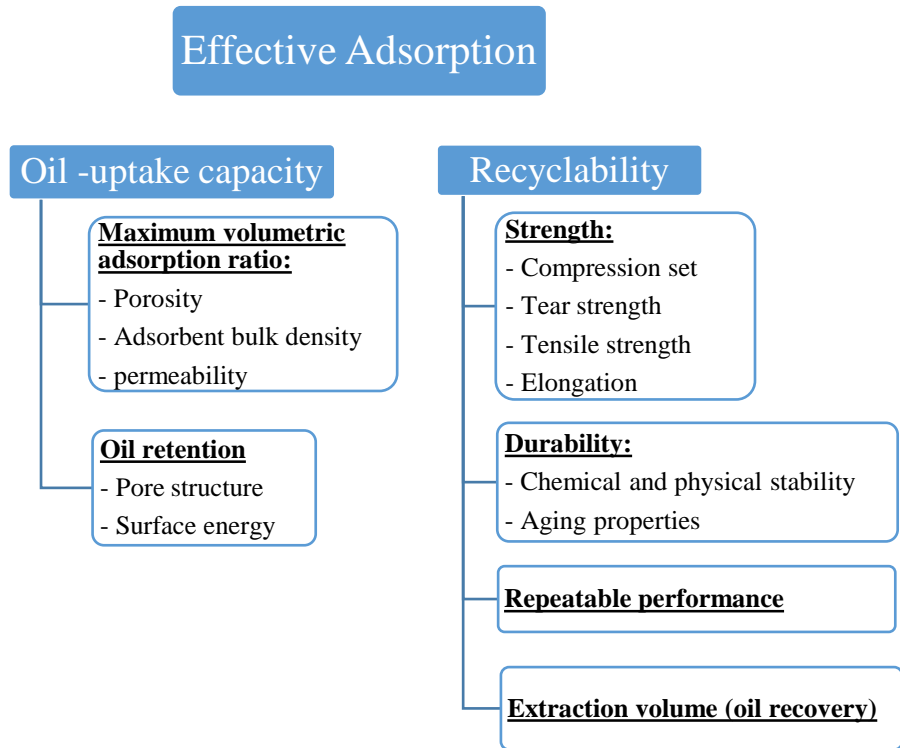
Figure 1.1 Parameters toward effective adsorption applications.

As illustrated in Figure *1.1*, there are two main approaches toward effective adsorption. The oil-uptake of each adsorption cycle and the uptake of all subsequent cycles provide the cumulative oil recovery during the life of an adsorbent. The bottom line of an effective adsorbent is to consider the contribution of the material during its lifetime and weight against all the costs involving the manufacturing, operation and disposal of the material for its services. Therefore,

the value of this research is to contribute towards improving oil retention and recyclability of a promising oil adsorbent.

1.4   OBJECTIVE AND SCOPE

The objectives of this study are

1.   to test the compatibility and stability of 3-methacryloxypropyl trimethoxysilane (MPTS) as a binding agent between reduced graphene oxide (RGO) and polyurethane sponge (PU), its overall effect on wettability, selectivity, oil retention and adsorption recyclability;

2.   to test and compare the effects of HCl etching of PU on the overall wettability, selectivity and oil adsorption capability;

3.   to develop an improved method for MPTS hydrolysis and RGO silanization;

4.   to compare the overall adsorption performance of the samples and to develop experimental parameters for oil adsorption and retention efficiencies.

The scopes of this study include

1.   Review and understanding the overall oil-water separation fundamentals, mechanisms, challenges, trends and development in the area of waste water treatment and oil spill remediation applications;

2.   Review of literature regarding RGO, PU and MPTS, their effects on wetting properties, the methodologies of synthesis and their role in the applications of oil-water separation and oil adsorption;

3.   Characterization of the synthesized adsorbent and controls;

4.   Review and identify relevant industry testing standards and protocols. Design of experiment procedure and parameters for oil adsorption performance data collection.

5.   Perform adsorption kinetics studies;

6.   Data analysis and evaluation of potential improvements to be used in the applications of oil-water separation.

CHAPTER 2 - LITERATURE REVIEW

2.1   OIL PROPERTIES

2.1.1   Overview

Oil-water separation techniques and mechanisms are based on oil properties that define and differentiate it from water. The most important of such properties include density, viscosity, polarity, pressure difference, and molecular size. In technologies based on gravity or centrifugal force, density difference between two liquids dictates the outcome. Pressure difference and molecular size are independent of gravity but they are important to separation by filtration. Viscosity plays an important role in the separation of oil from emulsions [22]. Emulsions are considered heterogeneous and temporary stable dispersions of two or more components that are immiscible, where the components coexist in the mixture in a combination of droplets and continuous phases. At all fronts where oil and water is in contact with each other, an oil-water interfacial film exist and polarity plays an important role in liquids surface tension, determining the immiscibility between them.

2.1.2   Free oil, dispersed oil and emulsion

Oil and grease can exist in different forms in an oil-in-water solution and these forms are differentiated by the oil droplet size. Oil droplet sizes with diameters that are greater than 150 μm are considered as "free oil" and they often coalesce forming larger continuous phases or masses in the water. When oil droplet sizes are within the range of 20 to 150 μm, these are considered to be dispersed oil in water. Typically whenever these droplets fall below 20 μm, the substance is categorized as an emulsified oil [23] as described in Table 2.1.

Table 2.1 Coalesced, dispersed and emulsified oil in water, differentiated by droplet size [23].

Oil droplet size (μm)	Form of oil
> 150	Free oil, coalesced in water
20 - 150	Dispersed oil in water
< 20	Emulsified oil in water

The mechanism of an adsorbent is dependent on both cohesion and adhesion of the adsorbate, where adhesion is a force of attraction between the adsorbent surface and the adsorbate resulting in a layer of adsorbate adhering onto the materials in contact, as well as the forces of cohesion between the adsorbate molecules which allow multiple layers of adsorbate to be adsorbed and thus separation of the two immiscible liquids. Since adhesion and cohesion forces, when combined, require not only the contact of the adsorbate molecules at the surface of the adsorbent but also continuous contact between adsorbate molecules in order for any potential of complete removal from the mixed liquid. The focus of this study is to evaluate an adsorbent adsorption capacity of oil that is in a continued phase, not in the dispersed or emulsified forms of oil in water systems.

Many oil-water-separation of oily water effluents exist in a combination of all three forms. In a real oily water treatment setting, more than one of the separation techniques are necessary to target the various forms and stages of oil-water-separation. Adsorbents are unique with its potential to be tailored to completely remove oily residues. However, it is not economical to be deployed in the primary treatment phase when the bulk of a high volume of oil has yet to be removed, in which case a tremendous volume of oil-saturated adsorbents would be

produced as secondary wastes. Therefore, it is an assumption in this study that low-density and high specific surface area oil adsorbents are to be applied when oil droplets are coalesced into a form of "free oil" that is in a continuous phase. In other circumstances, certain practices require adsorbents that are tailored to target dispersed or emulsified oil in water. In those cases, special oil adsorption testing procedures and parameters would be needed such as submergence and agitation of the adsorbent in the solution. Therefore, adsorption of dispersed or emulsified oil will not be addressed within this study.

2.2   SELECTION OF ADSORBATE OIL

According to the US Environmental Protection Agency's (EPA) Oil and Grease Test Methods 1664A, oil and grease testing standards utilize various solvents to extract and measures the contaminants in groups of compounds rather than specific species. Therefore, the definition of "oil and grease" in all of these cases according to EPA cover a broad spectrum of species including animal fat, vegetable oils, carboxylic acids such as fatty acids, napthenic acids, phenols, petroleum hydrocarbons, and surfactants in addition to other organic compounds. Most of these oils and greases that are discharged into the municipal sewage treatment plants are in forms of dispersed oil or emulsions [23]; they include household and restaurant liquid wastes that are accompanied by high levels of detergents as surfactants Industrial wastes from metals fabrication and manufacturing, detergent manufacturing, car washes and other types of washes and cleaning waste waters are also often highly emulsified due to large amounts of surfactants, dirt, debris and solvents.

Petroleum oil pollution exists in both forms of free oil and emulsions. Tanker washes, petroleum refinery and processed oily waters exist in mostly emulsified forms [23]. On the other

11

hand, crude oil spills are mainly free oils with a smaller percentage of dispersed or emulsified oil compared to the majority of the continuous phase liquid form.

As mentioned earlier, this study focuses on free oil in its continuous phase. Therefore, a logical choice of oil as a targeted adsorbate for this study would be one with properties that are comparable to crude oil. According to ASTM Test Standard F726-12, Standard Test Method for Sorbent Performance of Adsorbents, four representative oil types are categorized by their viscosity and density ranges [24]. As described in Table 2.2, crude oil falls within the medium category with a range of viscosity between 200 to 400 cP and a range of density between 0.86 to 0.97 g/cm^3. For all oil adsorption, kinetics and selectivity studies of this report, pump oil is used as the targeted adsorbate since it falls within the same category, is readily available and has a medium density of 0.869 g$\cdot$cm^{-3} at and a light to medium viscosity of 175 cSt at 60 F. (See Figure A.1 for pump oil properties)

Table *2.2* Testing oil types according to ASTM F726 standard test method for sorbent performance of adsorbents. [24]

Oil Type	Viscosities (cP)	Densities (g/cm^3)	Examples
	(1cP = 10^{-3} Pa$\cdot$s)		
Light	1 - 10	0.82 - 0.87	Diesel fuel, mineral oil
Medium	200 - 400	0.86 - 0.97	Crude oil, canola oil, mineral oil
Heavy	1500 - 2500	0.93 - 1.00	Bunker C or residual fuel, mineral oil
Weathered	8000 -10 000	0.93 - 1.00	Emulsified crude oil, mineral oil

2.3 OIL-WATER SEPARATORS (OWS)

Oil-water separators (OWS) are found in many applications such as oil spill remediation, refineries, waste water treatment, chemical etching, electrospinning, self-assembly processes, etc [25]. Current OWS technologies are mainly based on the mechanisms that revolve around gravity or vortex separation [26,27], chemical treatment [28], coalescence [29], membrane and filtration [30], coagulation [31] and flocculation [32], air flotation [33], biological processes [34], adsorption [35]. They are explained as follows.

2.3.1 Gravity separation

Methods such as an API oil-water separator utilizes the principles of Stoke's law. These types of OWS leverage on the velocity of oil droplets rising to the surface of the solution, which depends on density and size differences between the liquids and the water. Separation by gravity is advantageous for its low cost and simplicity. However, it requires lengthy times, calm conditions, and large footprints[23]. Centrifugal separation methods utilizes centrifugal forces to separate the liquids by density differences, where the lower density liquid would accumulate and be collected at the center of the rotation axis of the device. Centrifugal separation is known for less space required, high speed and high throughput capacity. On the other hand, it requires higher energy consumption than gravitational separation [28].

2.3.2 Chemical treatments

Chemical treatments are often effective in breaking up emulsions. It reduces surface tension at the oil-water interfacial film to enhance water coalescence. However, chemical treatments require specific customization depending on the influent, site and conditions. It can

also result in maintenance issues arising from corrosion and mechanical problems such as clogging [23, 28].

2.3.3   Coalescence OWS

Coalescence OWS are similar to filters where the sludge passes through a coalesce media causing the oil droplets to coalesce. This is effective with higher oil concentrations with certain range of particle sizes depending on the coalescence media. Disadvantages of coalescence methods include poisoning resulted from adhesion of the particles on the media, substantially decreasing its effectiveness.

2.3.4   Membrane and filtration

Membrane filtration is one of few solutions that are best for the separation of highly stable emulsions. Although it generally produces a low liquid throughput compared to other methods, membrane and filtration produces highly uniform and quality output.

2.3.5   Coagulation and flocculation

Coagulation is often followed by flocculation, where coagulation uses chemical or electrochemical coagulants to remove the repulsion force among fine particles, causing them to curdle. Flocculation is a physical process that creates larger masses by joining the coagulated particles into agglomerates or flocs. These flocs are separated out of the water by precipitation. Traditional chemical coagulation is the common type of coagulation deployed in water treatment plants, using coagulants such as inorganic salts of aluminum or iron [29, 36]. Recent years there are increasing interest in electrocoagulation as an alternative to the conventional chemical

coagulation methods, which were used to generate various aluminum or iron coagulants in-situ from the anodic dissolution [37-39]. These methods are effective in removing various oily wastewaters from textiles and industrial discharges, natural organic matter, phenols, and other organic compounds in forms of emulsions [40-43]. However, coagulation and flocculation potentially result in secondary pollution due to the chemical additives used during the processes.

2.3.6 Floatation

Flotation methods leverage on Stoke's law in a similar way as gravity separation methods where the separation is dependent on the density differences between the species to be separated. The mechanism of this method is based on the adhesion of gas bubbles with the dispersed fine particles resulting in agglomerated particles with a reduced net density. With the lowered density, the buoyancy force necessary to bring these particles to the surface is also lowered, causing them to float. Flotation methods are matured technologies that are effective in separating dispersed fine particles. With recent improvements and developments, jet flotation methods are becoming a potential technology in separating dispersed or emulsified particles in water due to its low cost of energy. Disadvantages of flotation methods include high maintenance and issues arising from repairing due to the prolonged periods of time for the equipment to stay submerged in the waste water conditions. Also, it is difficult to handle the frothy layer of particles, debris, oil and other materials that are suspended or floated onto the water surface [6, 31, 33].

2.3.7 Bioremediation

Bioremediation involves the concentration of marine microorganisms that naturally consumes and degrades various types of hydrocarbons as part of their dietary intake for their

sources of carbon and energy to reproduce. Although these types of bioremediation normally allows for a cleanup of petroleum pollution without further introducing secondary pollution or other artificial damages to the environment, this process without intervention is too slow to prevent substantial damages from occurring in the event of major oil spills. Therefore, in order for bioremediation to be effective, fertilizers and dissolved oxygen are deployed in the areas of mitigation in order to boost the concentration of these marine microorganisms. Due to the dynamic conditions and differences in each pollution site, disadvantages of bioremediation include difficulties to produce consistent outcome or to predict them, as well as an incomplete removal of the oil pollutants. Although proven at the laboratory level, field test results were not reliably consistent. Another approach was to identify effective microorganism species and introduce them at the site of pollution. Although these species may be proven effective, the establishment of these species at the pollution site is not reliable [3, 34].

2.3.8 Adsorbents

Adsorbents can be separated into three categories [8, 44]: organic, mineral or inorganic and synthetic. Organic adsorbents are usually referring to waste agricultural products such as peat. Mineral adsorbents include activated carbon, organo-clays, vermiculite, zeolites, etc. Some examples of synthetic adsorbents are polypropylene, polyurethane, nylon, and polyethylene. The forms of adsorbents that are used during oil spill response are bulk, enclosed, continuous and fiber [5]. Bulk adsorbents that are loose are usually used for small oil spill mitigations. Meanwhile, enclosed adsorption make the bulk materials easier to handle by containing the bulk, loose materials into a type of porous material allowing oil to penetrate into the adsorbent. Continuous adsorbents refer to continuous cylindrical sorbents such as booms which are widely used during

oil spills. These are materials with a homogeneous composition with less surface area to volume ratio. Therefore, they are usually higher in structural strength compared to bulk or enclosed materials but the adsorption sites are less accessible to the adsorbates. Therefore, various flat sorbents or other designs such as sheets, rolls, mats and pads, allow for the optimization of accessible surface areas. Loose fiber adsorbents are made to target heavier and weathered oil with a high viscosity. Similar to mops, these are bundles of loose strings or strips attached together called snares. The most common loose fiber adsorbents are made of polypropylene. [2, 45, 46]

Adsorbents are simple to use and they do not require special expertise from operators, but it can be laborious and time consuming. One of the major disadvantages of using adsorbents for the recovery of oil is the amount of secondary waste that it generates. Since adsorbents are specifically tailored as high specific surface area materials, they are difficult to handle due to susceptibility to wind and wave. They are bulky in general and difficult to retrieve. Moreover, adsorbent and oil mixture is more difficult to dispose of than oil itself. Therefore it becomes complicated logistically if the material is needed far from the coastal regions [5].

2.4   ADSORBENTS

2.4.1   Overview

Adsorption is a means to transfer the pollution from one phase to another [47], which requires subsequent methodologies for elimination from the environment.

There are mainly two types of adsorptions between the adsorbate and adsorbent, physisorption and chemisorption. Physisorption describes the attachment of an adsorbate onto

the surface of the adsorbent where weak van der Waals interaction is the main driving force between the two. Chemisorption describes adsorptions when chemical reaction occurs between the adsorbate and adsorbent. Electrostatic adsorption may play a role in either type of adsorption when oppositely charged adsorbent and adsorbate are attracted to each other. The type of adsorption is usually determined by measuring the adsorption energy.

Important factors that affect the cost-effectiveness of an adsorbent in oil-water separation applications include recyclability, wettability, density, specific surface area, geometry, buoyancy, adsorption capacity, saturation, oil retention, strength and durability, cost, availability, ease of storage and transportation [3, 5, 9]. For porous adsorbents with a three dimensional structure, the porosity and pore size distribution also directly affect the sorbent diffusivity. It should be noted that the term "sponge" and "foam" are used interchangeably for the remainder of this paper.

2.4.2 Porosity and pore size distribution

Often times, viscous oils clog the surface pores of an adsorbent, preventing further adsorption by the interior adsorption sites. In these cases, large and accessible pore sizes are essential to the adsorption performances [5, 48]. This phenomenon is explained according to the modified Darcy's law for flow through an unsaturated porous media:

$$j = -D \frac{\delta c}{\delta s} \qquad\qquad 2.1$$

where j is the mass flux through the porous adsorbent; δc is the concentration gradient; δs is the change in distance; and D is the capillary diffusivity defined by the equation below.

$$D = \rho_{liquid} \, K \, \frac{\delta h}{\delta c} \qquad\qquad 2.2$$

where K is the hydraulic conductivity defined by the following equation.

$$K = \frac{\rho g}{\mu} \frac{1}{8} \Sigma_i \ \frac{\pi n_i r_i^2}{A} \cdot r_i^2 \qquad\qquad 2.3$$

In Eqs. (2.1) and (2.2), δh is the hydraulic potential (capillary pressure during adsorption); ρ is the density of the adsorbate liquid; g is the acceleration due to gravity; μ is the viscosity of the adsorbate liquid; n_i is the number of pores having size r_i; A is the total area and $\pi n_i r_i^2$ is the area fraction of pores with radius size r_i.

Here the intrinsic permeability k which represents the latter half of Eq. (2.3) is directly dependent on the pore radius r_i:

$$k \ = \ \frac{1}{8} \Sigma_i \ \frac{\pi n_i r_i^2}{A} \cdot r_i^2 \qquad\qquad 2.4$$

Darcy's law explains that a smaller pore size r_i results in a lower volumetric flux through the porous media. The viscosity μ is indirectly correlated to the volumetric flux. When the viscosity of the adsorbate is high, a relatively larger pore size is needed in order to maintain the flow of adsorbate into the adsorbent until equilibrium is reached.

The clogging of the surface pores by highly viscous oil is attributed to the cohesion forces between the oil molecules in the bulk liquid phase become relatively stronger than the pressure gradient driving force at the oil-solid interface. In this case, since the adsorbent medium is at an unsaturated stage, as distance increases going into the adsorbent and away from the oil-solid interface, the porous medium becomes drier and capillary diffusivity drops significantly. This gradient drop in addition to the radius restriction and viscosity cause a resultant force that is increasingly favorable in the direction of the cohesion forces, and the flow of viscous oil eventually stops.

2.4.3 Wettability

The wettability of a sorbent material is the ability for a liquid to maintain contact with a solid surface; the degree of wettability is a quantifiable indication of hydrophilicity or hydrophobicity if the liquid in question is water. The degree of wettability is often determined by the measurement of liquid contact angle, the angle of which a liquid droplet forms on the solid surface. The wettability of a material is determined by two surface properties, surface energy and surface morphology [9, 49]. How surface energy affects wettability is dependent upon its critical solid surface tension (γ_c) in comparison to the surface tension of the liquid in contact. High critical solid surface tension indicates that the surface has a high surface energy per unit area.

Wetting occurs when the liquid surface tension is lower than the critical solid surface tension (γ_c). In order for an adsorbent material to be called hydrophobic and oleophilic, the adsorbent critical solid surface tension (γ_c) needs to be between the surface tension of water (approximately 60 to 65 mN/m) and the surface tension of oil (depending on different oil composition, typically 20 mN/m). Numerous modification methods have been explored and implemented to tune the surface energy of adsorbents for the desirable wetting properties [50-52].

Young's equation describes the relationship between water contact angle (WCA) and interfacial surface tensions [9, 53, 54]:

$$\gamma_{SV} = \gamma_{SL} + \gamma_{LV} cos\theta \qquad\qquad 2.5$$

Assuming that the surface is smooth and static and that there is no intermolecular interactions, θ is the contact angle and γ_{SV}, γ_{SL}, γ_{LV} are the interfacial surface tensions at the solid-vapor, solid-liquid and liquid-vapor interfaces, respectively. For water, hydrophobicity is indicated by a

contact angle of over 90° where the liquid is beaded on the surface. When the WCA approaches 0°, the liquid spontaneously spreads onto the surface indicating hydrophilicity [55].

In reality, there are various levels of intermolecular interactions at the liquid-solid interface. According to Dupre and Girifalco-Good's theory [9, 53, 56], a correction factor ϕ for this intermolecular interaction is considered:

$$cos\theta = 2\varphi \sqrt{\frac{\gamma_{SV}}{\gamma_{LV}}} - 1 \qquad\qquad 2.6$$

This equation implies the relationship in which a lower solid-vapor interfacial surface tension (or a low surface energy of the solid) results in a high liquid contact angle. Assuming a ϕ value of 1, a γ_{LV} value of 72.8 x 10^{-3} N/m² and the lowest surface energy recorded based on CF_3 alignment at 6 x 10^{-3} N/m² as calculated by Nakajima [53], yields a maximum possible WCA θ value of 115.2° that was obtained by modification of surface energy alone.

Other than surface energy tuning by means of surface chemical composition, the modification of surface morphologies allows the wetting properties to be amplified [9, 49, 53, 57, 58]. The Wenzel model (Figure 2.1.) describes a correction of the contact angle by a factor of roughness on homogeneous rough surfaces.
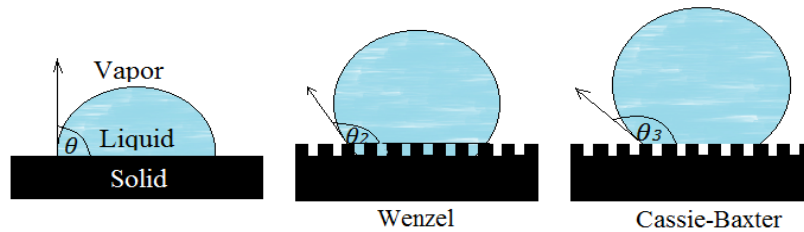
Figure 2.1 Illustrations for a liquid droplet on a smooth, flat surface to the left, Wenzel state in the middle and a Cassie-Baxter to the right.

The roughness of the solid results in an actual surface area that is larger than the perceived or projected surface area:

$$cos\theta^* = Rcos\theta \qquad\qquad 2.7$$

where R is the ratio of the actual surface area to the projected surface area of the solid, θ is the contact angle on a smooth surface and θ^* is the corrected contact angle on the rough surface. According to Eq. (2.7), the corrected contact angle is increased for θ values above 90°, while θ values below 90° results in a decrease in the corrected contact angle. This suggests that surface morphology modifications contribute to wetting as an amplifier [9, 49, 53, 57, 58].

The Cassie-Baxter model describes a heterogeneous surface where a layer of air is trapped in between partial areas of the solid and liquid interfaces. Therefore, a factor "f" is calculated as the fraction of solid surface area in contact with the liquid over the whole solid surface area, including areas where air is trapped in between. The Cassie-Baxter equation is

$$cos\theta^* = r_f f cos\theta_\gamma + f - 1 \qquad\qquad 2.8$$

where r_f is the roughness factor and f is fraction of solid surface area wet by the liquid out of the total solid surface area perceived to be wetted by the liquid.

Combining modifications of surface energy and surface morphology as described in Eqs (2.5 to 2.8), a contact angle of higher than 150°, a superhydrophobic surface can be achieved. There are reports on the fabrication of surfaces with a two-level, nanometer scale to micrometer scale hierarchy that further stabilizes the superhydrophobicity effects from the modifications [59].

2.4.4 Buoyancy, density and surface area

During oil recovery, the conditions are dynamic over time and the oil properties change accordingly. Density and viscosity change as oil evaporates and emulsifies, affecting the buoyancy of the oil and adsorbent mixture. Many of the natural organic materials with good initial buoyancy become affected by these changes during oil recovery and are not able to retain sufficient buoyancy to stay afloat [5]. However, with too high buoyancy, sometimes a layer of light and low density material floating on top of heavier viscous oils may prevent the adsorbent from coming into contact with the oil. Therefore, good adsorbents are required to be able to retain good buoyancy both before and after adsorption.

The number of adsorption sites on the solid surface is limited by its available surface area. Therefore, the adsorption capability of an adsorbent is directly correlated to the amount of accessible surface area [60-62]. Materials that exhibit a high surface area to volume ratio are good candidates since there are relatively more adsorption sites available for the adsorbates.

2.4.5 Geometry, saturation, strength and durability

In order to maximize surface area to volume ratio, 3D porous structured adsorbents gained growing interests in recent years [63-66]. However, 3D porous structured adsorbents with low densities are often too fragile to be handled and deployed in the harsh environments during oil-water separation treatments. Therefore, the use of 3D porous templates to serve only as a support system was reported in earlier studies [8, 67, 69]. Some of these 3D porous template materials are melamine sponge [70], soy protein aerogel [71], kapok wadding [72], polyurethane sponge [68, 73, 74], polypropylene foam [75], and various other natural and synthetic biopolymers [76]. Highly

efficient adsorbent materials that are engineered into these heterogeneous systems are capable of further enhancing wetting properties with nano-micro hierarchy. Scaling 3D porous structures into large size adsorbents such as booms increase the ratio of internal adsorption sites versus external adsorption sites. This potentially obstructs or delays the accessibility of internal surface areas and may consequently affect the overall oil adsorption capacity and saturation. Therefore, a better understanding of the materials' permeability and diffusivity is required for the development of good 3D porous structured adsorbents.

Combining the high surface area to volume ratio, strength and durability of 3D porous templates, these forms of adsorbents are capable of optimizing and harnessing the potential adsorption capacities of the materials.

2.4.6 Oil retention and recyclability

Good oil retention properties are required for good recycling performances. Many materials show the ability to adsorb well, some even adsorb rapidly [8, 9, 35, 44, 48, 66, 77, 79]. However, oil retention is as important which prevents premature drainage of the adsorbate. This is the key for efficient separation of oil from water and is important to avoid recontamination or secondary waste hazard caused by the release and spillage of oil. Adsorbents with low inherent strength are susceptible to deformations easily due to the dynamic conditions of the environment or simply from moving, lifting and handling of the material. The deformations result in pressures upon internal pores, forcing the adsorbed oil to be squeezed out. This phenomenon is often observed with adsorbents that are composed of organic materials [5]. According to Darcy's law as discussed in section 2.4.2, smaller pore sizes reduce the speed of drainage and may improve oil retention.

However, it also affects the speed of adsorbates traveling in the opposite direction during adsorption. Often times, highly viscous oils such as bunker oil occupy the available external surfaces of adsorbents, especially in those cases with small pore sizes, preventing further adsorption into the interior adsorption sites. This greatly reduces the efficiency of the adsorption. The most common adsorbents used for highly viscous heavy oils are polypropylene loose fibers which are better known as snares. According to the studies by Choi, et al. and Zahid, et al. [44, 80], the main mechanism of the oil adsorption of polypropylene snares was based on a combination of capillary bridges across voids between the loose fibers and the crimping effect observed when there is an increase in fiber denier. Without the internal pore structure, polypropylene loose fiber is a poor candidate for light density oils due to its poor oil retention.

On the other hand, recyclability depends on the material's capacity to adsorb and to release the adsorbent when it undergoes extraction. The most common, simple and low cost extraction method is mechanical compression of the adsorbent [81-83]. However, the mechanical extraction is often insufficient to remove all residual oil within the adsorbent. Applications requiring complete extraction of residual oil may be achieved by methods such as immersion in acetone or other organic solvents [81]. Although the complete extraction of residual oil allows the adsorbent to maximize and retain its oil adsorption capacity after repeated use, the use of organic solvents and the resulted oil and organic solvent mixture increase the handling and disposal of secondary hazardous wastes. Therefore, in order to avoid the additional cost of organic solvent uses and the subsequent waste management, a slight drop in oil adsorption capacity due to residual oil retention may be acceptable if the adsorbent material shows stabilization of the oil adsorption capacity in multiple adsorption-desorption cycles. In summary, a balance between the

oil retention capability, flexibility, compressibility, and strength of the structure is needed in order for the adsorbent to retain the oil until it is extracted for recycling purposes.

2.5   OIL ADSORBING SPONGES

As discussed above, truly efficient adsorbents depend on a wide range of factors and many of these factors are interrelated. It is important to understand each of these factors regarding any adsorbent candidate and the degree to which they can be modified without sacrificing other variables. As discussed earlier, accessibility and availability of surface area and pore volume are key factors that enable molecular diffusion and transport in adsorption. However, in most cases the increase of a material's surface area and pore volume often lead to a trade-off with the material's structural strength and mechanical durability. The use of 3D porous templates contribute as structural and mechanical support, aid in maintaining a desired surface area with controllable, tunable pore sizes and porosity, facilitating mass transfer efficiency and diffusion kinetics, as well as providing the compression set properties needed for mechanical desorption of adsorbates.

Types of adsorbents include highly porous and recyclable materials, aerogels, hydrogels, foams, sponges or similar forms of materials, and materials that utilize a 3D porous template as support skeleton. They are reviewed as follows.

2.5.1   Silica and vermiculite based adsorbents

Zhu et al. [81] reported a dip coating method to produce SiO_2 decorated commercial kitchen sponge using octadecyltrichlorosilane as a cross-linking agent. The resulting sponge displayed a WCA of over 150° and an average adsorption capacity of 53 $g \cdot g^{-1}$ for chloroform and 18 $g \cdot g^{-1}$ for

hexadecane. They reported performance degradation down to 94% for chloroform and 72% for hexadecane after 10 adsorption-desorption cycles for each specie. A mechanical squeezing method was combined with immersion into acetone for removal of residual oil. Wang and Geng [83] reported a modified PU sponge by dip coating the sponge into silica nanoparticles with dopamine hydrochloride. Their resulting adsorbent had a WCA of 154˚, with adsorption capacity ranging from 46.8 $g \cdot g^{-1}$ for chloroform to 18.3 $g \cdot g^{-1}$ for paraffin oil. Recyclability was tested for chloroform and linseed oil and adsorption capacity decreased to 74.2 – 82.2% of the initial capacity after 70 adsorption-desorption cycles by mechanically squeezing to extract adsorbed oil from the sponge.

Ge et al. [82] reported a method of fabricating a superhydrophobic, superoleophilic PU sponge. PU sponge was dipped in poly(vinylidene fluoride-hexafluoro-propylene) (PVDF-HFP) solution and then dipped with SiO_2 modified multiwall carbon nanotubes (MWCNT). After curing at 140˚C, the sponge was immersed in perfluoro tetradecanoic acid with ethanol. The resulted sponge had a WCA of 158˚ and adsorption capacities of 52 to 13 $g \cdot g^{-1}$ for chloroform and hexane respectively. Recyclability was tested for 5 adsorption-desorption cycles resulting in a performance degradation to 94% for chloroform, 30% for hexadecane and 8.7% for rap oil. The oil extraction was done by mechanically squeezing only.

Li et al. [84] reported an in situ growth method to synthesize a coating of ZnO microrods with palmitic acid on PU sponge. The adsorbent has a WCA of 168˚ and adsorption capacities of 44 $g \cdot g^{-1}$ for crude oil to 33 $g \cdot g^{-1}$ for pump oil. Recyclability was tested for 95 adsorption-desorption cycles, with the performance for crude oil degrading to 72.7% at the end of the cycles and 92.3% for diesel oil. The desorption data clearly showed that starting at 55th cycle, the

extraction of crude oil from the adsorbent was increasingly inefficient. Desorption was achieved by mechanically squeezing of the sponge, and residual oil continued to build up due to the strong cohesion forces between crude oil molecules.

Zhao et al. [85] reported a sponge-like, vermiculite and CNT hybrid that was grown with CVD method. The adsorbent displayed an adsorption capacity of 26.7 $g \cdot g^{-1}$ for diesel oil. Recycling data was collected by mechanical squeezing for 10 adsorption-desorption cycles. Performance degraded to approximately 92.5% of the initial adsorption capacity. Zhao et al. further improved this vermiculite-CNT hybrid by high shearing and obtained a fluffy sponge with an uptake of 70.6 $g \cdot g^{-1}$ for diesel oil. However no recycling data was reported for the improved material.

2.5.2 Organic synthetic hybrid 3D adsorbents

Jiang and Hsieh [66] reported a method to assemble rice straw cellulose nanofibrils (CNF) into a 3D interconnected ultra-porous aerogel. The CNF aerogels have densities ranging from 1.7 to 8.1 $mg \cdot cm^{-3}$. Young's modulus and yield strain are the highest with the highest density aerogel, having a Young's modulus of 54.5 kPa and a maximum compressive stress of 25.3 kPa at strain, $\varepsilon = 0.8$. These amphiphilic (both hydrophilic and oleophilic) aerogels were modified with triethoxy(octyl) silane, turning the hydrophilic portions of the aerogel into hydrophobic and oleophilic. The resulted samples had adsorption capacities approximately 185 $g \cdot g^{-1}$, 215 $g \cdot g^{-1}$, 240 $g \cdot g^{-1}$ and 356 $g \cdot g^{-1}$ for hexane, hexadecane, pump oil and chloroform, respectively. The sample with the highest density had the lower adsorption capacity among all other samples. Although the least dense samples had a larger adsorption capacity, it was noted that oil retention was poor. The reported adsorption capacities toward non-polar hydrocarbons and oils were

28

superior compared to reports on other cellulose aerogels [86,87]. The study demonstrated

recyclability up to six adsorption-desorption cycles with shrinkages in the aerogels after

recycling. Extraction of the liquids was achieved by distillation and solvent evaporation. The

performance degradation was only reported for octane, cyclohexane and toluene, with 61%, 57%

and 48% of the initial capacities, respectively.

Wang et al. [88] reported a natural luffa sponge modified with polyhedral oligomeric

silsesquioxane (POSS) based compounds. The superhydrophobic adsorbent had a WCA of 155°

and an adsorption capacity of 8 to 12 times its weight. Recyclability was tested for 5 adsorption-

desorption cycles by using the mechanical squeezing method to extract the liquid, degradation of

performance was within approximately 92 to 94% after 5 cycles. The modified luffa sponge

showed excellent oil retention for over a week.

Nagappan et al. [10] reported a superhydrophobic, superoleophilic sponge made with a

combination of lotus leaf powder, poly(methylhydroxysiloxane) (PMHOS), and phenyl

substituted silica ormosil (PSiOr) dip coated onto a melamine sponge. The product displayed a

WCA of 177.87°±1° and initial adsorption capacities for chloroform up to approximately 33

times the adsorbent weight and about 17.5 times for decane. Recycling data was collected for up

to 15 cycles by mechanical squeezing followed by solvent extraction using hexane.

2.5.3 Boron nitride based adsorbents

Zhang et al. [89] reported a freeze drying preparation of boron nitride polyvinyl alcohol

(PVA) aerogel. The aerogel had a WCA of 94.9° to 100.7° and adsorption capacities for hexane

and CCl_4 up to 14 $g \cdot g^{-1}$ and 38 $g \cdot g^{-1}$, respectively. Although it was discussed that the aerogel

would be easily recycled, there was no data collected regarding its recyclability.   Lei et al. [90]

reported the development of a high surface area porous boron nitride nanosheets with BET surface area of 1,427 $m^2 \cdot g^{-1}$ and a WCA of 165˚. Adsorption capacities for used engine oil and ethylene glycol ranged from 29 times to 33 times the adsorbent weight. The saturated nanosheets maintained good buoyancy and remained floating on the water surface. Recyclability data was collected for pump oil adsorption over 5 cycles with performance degradation down to 72% of the initial capacity. Regeneration of the nanosheets was achieved by direct burning in air. The report also discussed alternative methods to recycle the material such as organic solvent extraction using ethanol and petroleum ether, as well as heating at 600 ˚C for 2 hours in air. Song et al. [91] reported an ultralight boron nitride aerogel synthesized by a template-assisted CVD method with an oil adsorption capacity of 160 times the adsorbent weight. The material was regenerated by burning in air.

2.5.4 Organo-silicons

Zhu et al. [92] reported a superhydrophobic sponge by coating a layer of polysiloxane onto a 3D porous PU sponge. PU sponge was immersed and reacted with the hydrolysis of methyltrichlorosilane in hexane solution. Water traces within the hexane solution led to formation of polysiloxane during the hydrolysis reaction. Evaporation of hexane created porous structure on the surfaces. The sponge had a WCA of 157˚ with adsorption capacities ranging from 15 times the adsorbent weight for gasoline and 25 times for crude oil and lubricating oil. Recyclability was tested for 400 adsorption-desorption cycles by mechanical squeezing with clamp plates followed by acetone washing and drying. Water contact angles were measured at the end of each cycle, indicating that WCA remained above 150˚ for the initial 300 cycles. At the

end of 400 cycles, WCA decreased to above 142° mainly due to the cracks on the sponge coating.

Choi et al. [93] reported sugar-templated polydimethylsiloxane (PDMS) sponge that had WCA measurements between 120 to 130°, and adsorption capacities from 4 to 11 times the adsorbent weight for transformer oil and chloroform respectively. The sponge displayed good mechanical stability and recyclability. The sponge had a very low elastic modulus and was able to recover from compression quickly without permanent deformation. Twenty adsorption-desorption cycles were tested by mechanically squeezing and immersion in ethanol. Minimal degradation in performance was observed (within 97% of initial adsorbing capacity). Pham et al.[94] reported a simple solution-immersion process to silanize melamine sponge which modified the material from hydrophilic to superhydrophobic. The silanization was achieved by reacting secondary amine groups on the surface of the melamine sponge with octadecyltrichlorosilane in a toluene solution, forming a self-assembled monolayer on the surfaces of the sponge. Their highest loading sponge had a maximum WCA of 151°±1.1° with adsorption capacities ranging from 82 to 163 times the adsorbent weight for acetone and chloroform respectively. Recyclability was test by mechanically squeezing out the adsorbates. After the initial 100 cycles, oil recovery performances degraded to approximately 93%. Further adsorption-desorption tests were performed for selected organic solvents and oils including toluene, chloroform, diesel oil and motor oil, for up to 1000 cycles. The resulted oil recovery degradation was above 90% for all adsorbates at the end of 1000 cycles. The recyclability is remarkable compared to previous reports.

2.5.5   Carbon and graphene based adsorbents

As mentioned earlier, there are various organic and synthetic materials capable of water purification and carbon-based material is one of the most popular adsorbents. [47,95,96] Some of the reasons for its popularity include high inertness, thermal stability and the ability to perform under broad pH ranges. [47]

Zhao et al. [97] prepared a nitrogen-doped graphene oil adsorbent with a density of 2.1 $mg \cdot cm^3$, which is one of the lightest among 3D graphene structures next to graphene-CNT aerogels. This 3D graphene framework (GF) was prepared by hydrothermally treating graphene oxide aqueous solution with pyrrole followed by freeze drying. The group reported adsorption capacity of 200 $g \cdot g^{-1}$ for toluene, close to 500 $g \cdot g^{-1}$ for chloroform and up to 600 $g \cdot g^{-1}$ for phenoxin. The GF has a high temperature tolerance of up to 600°C in air, and an ability to recover most of its volume after compression at 60% strain. The group predicted the potential recyclability of GF, however no data was collected in this regard.

Sun et al. [98] prepared an elastic graphene-CNT aerogels densities less than 1 $mg \cdot cm^3$. The group performed 1000 cycles of fatigue tests on the aerogels and the samples recovered to its original thickness, macroscopic shape and porous 3D microscopic structure. The samples had a WCA of 132.9° and adsorption capacities of 215 $g \cdot g^{-1}$ for n-hexane, 550 $g \cdot g^{-1}$ for chloroform and 743 $g \cdot g^{-1}$ for phenoxin. The group reported various methods of recycling and regenerating the aerogels including mechanical extrusion, heating, and burning in air and the samples recovered their original shapes and performances. Ten adsorption-desorption cycles of n-hexane were tested by the group and regeneration was done by removing the vapor under an 85°C heat treatment.

Zhang et al. [99] reported the synthesis of a hydrophobic, low density and high porosity spongy material trGO-S-LN prepared from a laundry detergent and graphene oxide solution. The solution was treated with ultrasound, liquid nitrogen freezing, vacuum freeze drying and thermal reduction at 300˚C. The sample had an apparent density of 2 mg·cm^{-3} and adsorption capacities of 260 to 450 g·g^{-1} for ethanol, acetone, methanol, diesel oil, vegetable oil and ethylene glycol. The group performed compression tests and the material was stable up to a maximum strain of 50%. Although the material was stable up to 100 cycles of stress-strain tests, a limited strain of 50% would result in low recovery rate and high performance degradation. Regeneration was limited to vapor removal at 85 ˚C

Li et al. [100] reported a simple dip coating method to prepare 5 wt% graphene-coated polyurethane sponge. The resulted sponge displayed a WCA of 156.1 and adsorption capacities of 50.42 g·g^{-1}, 54.30 g·g^{-1} and 58.95 g·g^{-1} for diesel, soybean and pump oil respectively. Recyclability data was collected over 60 adsorption-desorption cycles by mechanically squeezing out the adsorbates between glass plates. Performance degradation was over 96.5% for all three oils. The group noticed poor oil retention with lower graphene concentration, indicating that pore sizes were adjusted by due to graphene sheets occupying the pore cavities.

2.5.6   Summary on oil adsorbing sponges

Although organic adsorbents materials are the most environmentally benign among available options, synthetic adsorbents are generally the most effective in terms of oil recovery ratio by weight. Inorganic adsorbents are amongst the lowest in terms of oil recovery ratio by weight [5].

As discussed earlier, wettability is dependent on two factors: the surface energy of the material and its roughness. Adsorbent performances can be varied by adjusting the levels of these two factors. Adsorbents may display a high WCA indicating strong hydrophobicity and selectivity, however it does not quantify oil adsorption capacity. According to Wenzel's model and the Cassie-Baxter model, increased surface roughness and hierarchical architecture may amplify the adsorbent wettability and selectivity tendency. Consequently, adsorption speed of the preferred liquid may be increased. The measurement of adsorption capacity is not only based on the speed of adsorption but its capacity to adhere and hold onto the adsorbate. Since the intrinsic surface energy of these materials are not changed with the change in roughness, the increased WCA does not always directly translate to an improvement of the overall adsorption performance. For example, when compared between the studies reported by Zhu et al. [81] Wang et al. [83] and Ge et al. [82], Zhu et al reported a lower WCA at 150˚ compared to Wang et al. at 154˚ and Ge et al.'s 158˚. Yet, Zhu et al.'s reported adsorption capacity of chloroform per weight of the adsorbent is 13% higher than Wang et al.'s and 2% higher than Ge et al.'s. The phenomenon observed in Zhu et al.'s case possibly attribute to better adhesion between the surface material and the liquid, better accessibility to the adsorption sites, higher total pore volume per weight of adsorbent, or a combination of the above.

Therefore WCA alone is not a good indicator of performance degradation during a recyclability study. Also, localized deterioration of the adsorbent may be undetected or misrepresented until adsorption performance of the whole system is counted for. Therefore, an actual adsorption-desorption should be carried out for a true set of recyclability data to be collected.

It is generally observed that adsorbents perform better with high density, high viscosity oils. This may be due to their ability to counter drainage under high cohesive forces, consequently molecules cling onto each other resulting in a better oil retention rate. However in some cases, the performance degradation for dense oils are more severe than lighter oils. Beside better oil retention, strong cohesion forces may work against the recyclability of an adsorbent. Often times this is due to inefficiency in extracting the oil for recovery. This phenomenon may be compensated with optimizing pore sizes, which will further compromise on the ability of the adsorbent to retain lighter oils.

Although there are various potential candidates for oil adsorbents, the methods of material regeneration must be practical on site where oil-spill-cleanups take place. Mechanical extraction of the oil by compression is by far the least costly and simplest method known to date. The recycling data demonstrated by synthetic material such as organo-silicon and polymers are the most promising comparing to other materials. Carbon-based material such as graphene has some of the highest adsorption capacities reported, especially when it expresses low density and high surface area on a 3D framework. Although these 3D carbon frameworks have reasonable mechanical stability, they lack the strength and durability for repetitive use under harsh environments.

There are high potentials in marrying organo-silicon, polymer materials with carbon-based materials. This combination enhances recyclability, mechanical strength and durability, inertness, intrinsic hydrophobic, low-surface-energy and other modifiable properties. In the following chapters, the synthesis of MPTS functionalized reduced graphene oxide coated on polyurethane sponge and its oil adsorption properties are discussed in detail.

2.6   GRAPHENE

2.6.1   Overview

Graphene is an intriguing, single-atomic-layer, two-dimensional nanomaterial. It is comprised of sp^2-hybridized carbon atoms arranged in a hexagonal lattice. Since 2004 when physicists Andre K. Geim and Konstantin S. Novoselov from the University of Manchester (UK) revealed its novelty in a stable form on scotch tape [101], graphene has been highlighted in many active research fields. The material has extremely unique properties. Theoretically, it has a surface area as high as 2630 $m^2 \cdot g$ [102], a charged carrier mobility of approximately 200,000 $cm^2 \cdot V^{-2} \cdot s^{-1}$ [103], thermal conductivity of 5000 $W \cdot m^{-1} \cdot K^{-1}$ [103], and a Young's modulus of 1 TPa [104]. There is a wide range of possibilities to modify and tailor the properties of graphene such as morphology control, chemical doping, and functionalization [105]. Introduction of different oxygen groups onto the planes and edges of the graphene sheets change the polarity of the material, thus allow for hydrophilicity tuning. Although pristine graphene is intrinsically hydrophobic, graphene oxide (GO) is a hydrophilic derivative dispersible in most polar solvent. Figure 2.2 illustrates the typical chemical formula of GO. From the dispersible form, graphene oxide can be further tailored into different morphological variations such as coatings [100], films [106], aerogels [107], hydrogels [108], foams [109], sponges [110], and other 3D frameworks [97] etc. It is important to explore and optimize these morphological variations to allow for the development and incorporation of graphene applications. The van der Waals attractions between graphene sheets cause them to stack upon each other when they are in proximity with each other. This aggregation suppresses its theoretical properties, therefore causes it to behave similar to graphite [97]. Effective

implementation of morphology control is crucial for the end product to benefit from the potentials and properties of graphene.
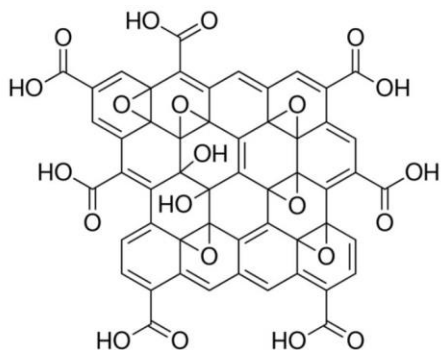
Figure 2.2 Chemical formula of typical graphene oxide.

2.6.2 Graphene synthesis

There are two major approaches to the synthesis of graphene and its derivatives, namely top-down approach and the bottom-up approach [111]. Bottom-up approach describes the assembly and construction of higher ordered structures starting with molecular level precursors, for example, Chemical Vapor Deposition [112]. Top-down approach describes processes that begin with materials such as graphite which naturally contains graphene. Top-down approach processes convert these materials into graphene and its derivatives by means of exfoliations or decomposition via mechanical, chemical, electrochemical, or other methods [112].

Bottom-up approach allow for fabrication of graphene with atomic-level precisions and an infinite variety of carbon sources as its building blocks. While top-down approach result in uncontrollable edge structures and functionalization, resolution limitation and other irregularities that are inherited from its natural sources. Top-down approaches allow bulk production of graphene rapidly and cost effectively relative to the bottom-up approach [111].

For the purpose of this thesis research, the oil adsorbent synthesis does not require a high level of defective-free, large area pristine graphene as such required by applications in electronics, sensors and printable devices. In this thesis research, graphene was synthesized with the top-down approach due to relative scalability and cost effectiveness.

From the late 1800's to 1950's, since Staudenmaier [113], later Hummers and Offeman [114] further developed upon the synthesis of graphite oxide (GO) that was first reported by Brodie [115]. Variations of this process has been widely adopted into the synthesis of GO during the past 20 years. Driven by exponential interest of graphene during the recent years, many researchers have further altered the process into various versions of GO synthesis known as Modified Hummers Methods.

This research focused on the Modified Hummers Method reported by Marcano, et al [116] which was adopted in previous works by Dr. Aiping Yu's research group at the University of Waterloo [117, 118].

2.7   FLEXIBLE POLYURETHANE FOAM (PU)

2.7.1   Overview

Polyurethane foam properties are evaluated according to the oil adsorbent criteria mentioned in the previous sections. PU chemistries are very well studied, the current producers have excellent control over properties such as pore sizes, pore volumes, uniformity of the pores, compression set, etc. PU foams are capable of a wide range of applications including furniture and automobile cushioning, packaging, fire retardants, insulations, and many more. With over 12 million metric tons of global consumption of polyurethane raw materials as of 2007, it is the

largest category of cellular polymeric materials in 2015 [118]. PU formulations and processing are

continuously being improved upon, it is one of the most common and versatile researched

materials in the world. However, there are increasing energy and environmental concerns

regarding its processing, components and precursors [119]. Both industry and academic

communities continued to research on more environmentally friendly substitutions for these

processes, components and precursors [120-122]. For example, vegetable oil has been reported as a

potential ingredient to polyols [118]. In a study conducted by Russell et al. [123] from Yale

University, it is discovered that an Ecuadorian species of fungus was involved in the natural

degradation of polyester PU. Also, there are studies on the use of PU sponge wastes to generate

secondary products. For example, a synthesis method on nitrogen-doped carbon nanostructures

for bio-imaging and catalysis has been created using polyurethane sponge as a carbon source [124].

In spite of these disadvantages and on-going environmental concerns, the need for

immediate improvements for pollution cleanup applications is pressing. Considering the positive

aspects of PU such as commercial availability, low cost, excellent substrate for recyclability,

durability, versatility and possibilities for modifications, PU is a logical oil adsorbent candidate.

In addition, there is a possibility of reusing recycled PU foams from packaging wastes as oil

adsorbents. This is particularly interesting from an environmental sustainability point of view.

In this research, an open-cell polyether based PU with relatively uniform pore sizes was

selected based on the manufacturer's recommendation (See Figure A.2). This PU sponge was

made to target hydrophobic applications which require frequent contact with moisture and water.

All modifications and experiments were performed on the same PU sponge in this research. A

consistent substrate with the same porous structure allowed this research to focus on understanding the effects of the modification components.

2.7.2 PU foam properties

Generally, flexible PU foam product are categorized and distinguished by their properties and the application which they are intended for. These properties include the density, indentation load deflection (ILD), cell count in the number of pores per inch, permeability, tensile strength, elongation, tear strength, compression set, resilience, steam autoclave aging and dry heat aging properties, etc.

There are many varieties of PU foam products available and a wide range of properties. There are numerous possibilities of surface-chemistries and modification for oil adsorption enhancement [74, 82, 125-128]. The initial properties of the PU substrate greatly affect the final outcome of any modified product, therefore it is very important to select a PU with desirable morphology especially the porous structures, and other properties [129]. Ideally, it is beneficial to achieve a synergistic effect between the PU properties and the type of modifications that it will undergo.

In order for a PU sponge to effectively adsorb and retain oil within its pores, the sponge requires an open cell structure with high interconnectivity for accessibility to the pores. Assuming that there is no swelling effect within the PU matrix, the oil flow and the volume retained during adsorption are mainly determined by: 1.) the driving force attracting oil into the porous structure, 2.) the pore volume, and 3.) the interconnectivity among these pores. Pore volume and interconnectivity properties are predetermined properties depending on the selected

PU foam. Using the total relative density of the foam, the maximum volumetric adsorption ratio of the foam can be calculated with the equation [130]:

$$\left(\frac{v_{oil}}{v_{PU}}\right)max = \frac{1-\rho_r}{\rho_r} = \frac{1-\frac{\rho_f}{\rho_s}}{\frac{\rho_f}{\rho_s}} \qquad\qquad 2.9$$

Where v_{oil} is the volume occupied by the adsorbed oil, v_{PU} is the total void volume of the PU sponge, ρ_r is the relative density of the sponge, ρ_f is the apparent density of the foam and ρ_s is the density of the solid PU before expansion into a foam. The known density of solid polyurethane [69] is 1.2 g·cm^{-3}. In the literature, Pinto, et al. [130] equated $(1-\rho_r)$ to the volume of the foam "V_f", however that should not be the case since $\left(\frac{v_{oil}}{v_{PU}}\right)max$ is a dimensionless number.

With a known maximum volumetric adsorption ratio based on the chosen PU foam, the volumetric adsorption efficiency can then be calculated by experimentally determining the actual volumetric adsorption $\left(\frac{v_{oil}}{v_{PU}}\right)$actual as a percentage of the theoretical maximum value $\left(\frac{v_{oil}}{v_{PU}}\right)$max.

2.7.3 Acid treatment of polyurethane sponge

As previously mentioned, morphological modifications of a surface allow tuning of its wettability by amplifying the material's initial wettability tendency. Surface roughness can be increased by various methods including decoration of nanoparticles [70], electropolymerization [131], spray-casting [132], chemical etching [133], etc. Various groups have studied on ways to control and maximize these morphological effects. These studies have demonstrated that besides hierarchical textured surface, the overhang structure or re-entrant surface curvature are major contributors to superb wettability enhancement [134-137]. These special morphological shapes are able to sustain

regions of locally stable Cassie state, satisfying Young's equation along the lengths of these overhangs or curvatures.

In this thesis research, HCl etching of the PU foam was explored prior to other substrate modifications. The acid etching together with the decoration of MPTS-RGO is believed to create a rough surface that has both hierarchical texture and overhang or re-entrant surface curvature features.

Yang et al.[9], Guo et al.[10] and Ren et al.[11] have reported successful etching of the substrate using HCl in order to increase surface roughness for wettability enhancement. The groups have reported a high number of microscale terraces and pores structures on the material's surface as a result of the HCl etching.

2.8   3-METHACRYLOXYPROPYL TRIMETHOXYSILANE (MPTS)
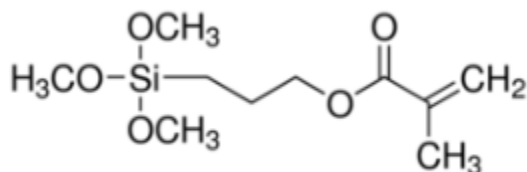
Figure 2.3 Chemical formula of 3-methacryloxypropyl trimethoxysilane (MPTS).

All of the currently known oil adsorbent materials require modifications and enhancements in order to regenerate and recover its liquid adsorbate. Recyclability of natural or mineral adsorbents alone are either impossible or impractical without incorporating a synthetic component into the system [10, 35, 66]. One of the main challenges faced in maintaining performance stability throughout the life of the adsorbents, is the deterioration of the bonding and linkages of

the substrate material with particles which possess the roughness or surface-energy-enhancing

properties [66, 89, 90]. In combining the desirable adsorbent properties of graphene and polyurethane,

a cross-linker is needed to improve bonding and to maintain the performance stability [138, 139].

Organo-silicon is one of the most commonly used, outperforming cross-linkers [93, 94, 109, 125, 139,

131]. Silane coupling agents are unique organo-silicon compounds capable of performance

improvement and inorganic fillers modifications aid [142]. Some of the most used silanes fall into

the categories of vinylsilane, acryloxy silane, epoxysilane, aminosilane, alkylsilane, isocyanato

silane, mercapto silane and others [142]. Table 2.2 lists some of the key materials and resin which

the silane coupling agent is mainly applicable with.

Table 2.3 List of common silane coupling agents and their main applicable resins or other materials [142].

Silane classification	Chemical names	Main applicable resin and/or other materials
Vinylsilane	Vinyltrichlorosilane, Vinyltris (βmethoxyethoxy) silane, Vinyltrimethoxysilane	Unsaturated polyester, crosslinking polyethylene
Acryloxy	ϒ-methacryloxypropyl-trimethoxysilane	UV-cured systems, optical fibber coatings, thermosetting resins, copolymeriations, unsaturated polyester, concrete, elastomers
Epoxysilane	β-(3,4 epoxycyclohexyl)-ethyltrimethoxysilane, ϒ-glycidoxypropyl-trimethoxysilane, ϒ-glycidoxypropyl-methylidiethoxysilane	Epoxy, phenolic and melamine, adhesion of acrylic latex to glass, wood, and various substrates

Aminosilane	N-β (aminoethyl)-r-aminopropyl-trimethoxysilane, N-β (aminoethyl)-r-aminopropyl-methyldimethoxysilane, r-aminopropyl-triethoxysilane, N-phenyl-r-aminopropyl-trimethoxysilane	Epoxy, phenolic, melamine, furan, nylon, polymido, thermosetting resins, epoxies, glass fiber-reinforced thermoplastics
alkylsilane	n-propyltrimethoxysilane	glass, ceramics, concrete, metals
isocyanato silane	2-isocyanatopropyltriethoxysilane	hybrid organic/inorganic urethanes
mercapto silane	3-mercaptopropyltrimethoxysilane, 3-mercaptopropylmethyldimethoxysilane	EPDM rubbers, polysulfide, thiol-ene UV cure systems

MPTS silanes are compatible with water cross-linkable polymers and resins, its chemical formula is illustrated in Figure 2.3.. It is mainly suitable to be used with polyesters and polyurethanes [142]. The methoxy moiety of this silane reacts with various forms of hydroxyl groups, bonds with inorganic particles, pigments or fillers, resulting in an improved adhesion between these molecules with substrates like polyurethane [138]. Therefore, graphene oxide with a rich amount of hydroxyl groups (see Figure 2.2.) functionalized on the edges is theoretically conducive to a better cross-linking efficiency. In addition, alkyl and aryl silanes such as MPTS are specialized in providing hydrophobic properties for applications such as water repellents [138], which is aligned with the purposes of this study.

There have been reports on carbon materials surface modification by chemically grafting of silane coupling agents. Zhao et al. [143] investigated the coupling agent surface treatment of carbon microspheres (CMS) to improve dispersion and reactivity in grafting of polymer monomers for surface imprinting, temperature response and polymer solar cells. The group

reported an optimum ratio of 0.3 g oxidized CMS to 1 ml of MPTS, with a reaction time of 2 hrs at 65℃, and an optimal pH at about 5.60 in 60 mL of ethanol and water (3:1, v/v).

There are four steps to the reaction of silanes: hydrolysis, condensation, hydrogen bonding, and attachment onto the final substrate. During condensation, the hydrolyzed alkoxy groups are condensed to oligomers which have the tendency toward self-condensation, lowering the efficiency of bond formation with the substrate. Dilution with fresh solvents such as ethanol aids to prevent such self-condensation.

Savard, et al. [144] reported that in order for the good adsorption of monolayers of ϒ-methacryloxypropyl-trimethoxysilane (ϒ-MPTS) onto the targeted substrate, amount of time for proper silane hydrolysis prior to coming in contact with the substrate is very important. In addition, it was found that the optimal time of hydrolysis is dependent on the pH of the solution. A prolonged hydrolysis period of the silane results in a condensation time that is too rapid for any possible deposition of silane onto the substrate. It is noted that stable, hydrolyzed silane is needed to react efficiently with the targeted substrate material. The report concluded that within the range of pH 2.4 to 4.0 and a ϒ-MPTS concentration below 0.042 M, a maximum stability is reached for the hydrolyzed ϒ-MPTS in an aqueous solution. On the other hand, an increase in pH favors rapid silane condensation and reduces the rate of hydrolysis, while an increase in the ϒ-MPTS concentration favors polycondensation.

The group reported at a concentration of 0.084 M and a pH of 5.5, a hydrolysis time of 1500 seconds led to a reasonable condensation time allowing for proper deposition of ϒ-MPTS onto the substrate.

CHAPTER 3 - EXPERIMENTAL MATERIALS AND METHODS

3.1   OVERVIEW

This chapter describes and explains the experiment methodologies in detail, including the source of materials, setup, condition, procedure and sampling of the experiment. The objective of the experiment is to investigate the independent variables, and their effects on the oil adsorption performances as well as properties and characteristics of the modified adsorbent. The purpose of these experiments is to better understand the contributions of chemical modifications and morphological architectures of an adsorbent toward its effectiveness and efficiency in oil-water separation applications such as oil spill remediation. There are a total of 6 different types of adsorbent samples prepared in this research plus a control sample made of only the hydrolysis of MPTS onto an HCl treated PU sponge. Figure 3.1 shows a flowchart that illustrates the steps taken to prepare each sample.

Polyether-based PU sponge was modified according to the procedure section of this chapter. Independent variables included

1. PU foams prepared with and without HCl treatment prior to other modifications.
2. PU adsorbents with rGO were added with and without the cross-linking agent 3 - methacryloxypropyl - trimethoxysilane (MPTS).
3. PU adsorbents were made with and without rGO.

There were a total of ten dependent variables in this research, five of which were oil adsorption performance parameters and five of which were material properties and characteristics.

Oil adsorption performance parameters included adsorption rate, time to saturation, oil lost to drainage, oil retention, recycle performance degradation.

The adsorbent properties and characteristics included surface chemistry, apparent density, porosity, surface morphology and wettability.
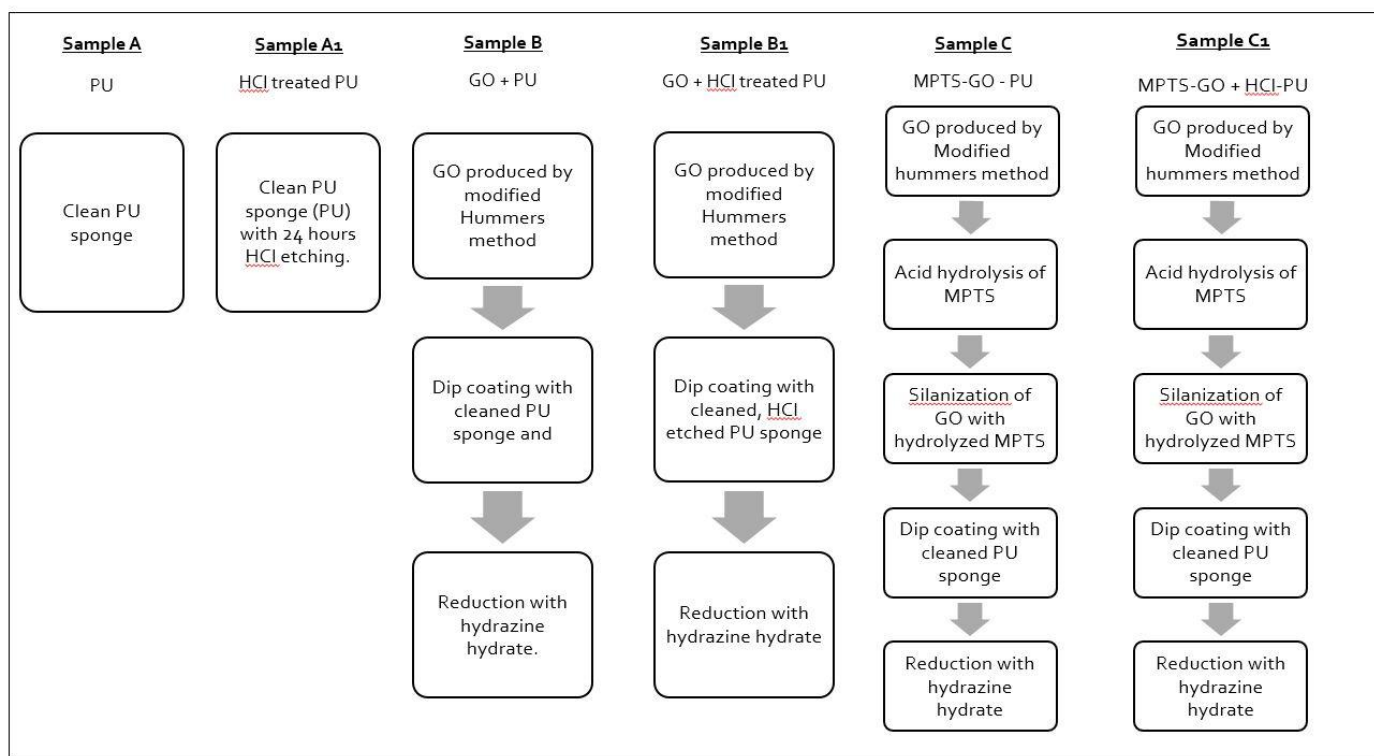
Figure 3.1 Flowchart on the synthesis steps for samples A, A1, B, B1, C and C1.

3.2   MATERIALS

Polyether polyurethane sponge (filter foam, Figure A.2.) was purchased from Foam Factory, Inc. Pump oil was purchased from Citgo Petroleum Corporation (Figure A.1.). Graphite powder (2-15 μm) was purchased from Alfa Aesar. $KMnO_4$ (ACS Reagent, >99%), $NaNO_3$ (ReagentPlus, >99.0%), H_2O_2 (ACS Reagent, 30%), H_2SO_4 (ACS Reagent, 95.0-98.0%), HNO3

(ACS Reagent, 70%), hydrazine hydrate (Reagent grade, 50-60%), MPTS (>98%), HCl (ACS Reagent, 37%), ethanol (ACS Reagent, 200 proof), Sudan blue II (dye content 98%) and ammonia (2.0M in ethanol) were purchased from Sigma-Aldrich and were used as received.

3.3   SYNTHESIS PROCEDURE

3.3.1   Synthesis of GO

GO was obtained via a modified Hummers method chemical oxidation process previously reported by Tjandra et al.[141] In brief, graphite powder (2 g) was stirred into a mixture of H_2SO_4 and HNO_3. The solution temperature was brought near 0°C, $NaNO_3$ and $KMnO_4$ was slowly added. The mixture was kept agitated with a magnetic bar while the temperature increased and maintained at 35°C $\pm 5°$ for 2 hours. The mixture was slowly added in small portions, into a large beaker of deionized water (200 mL). H_2O_2 (30 wt%, 10 mL) was added which changed the mixture into a golden yellow color upon reacting with the $KMnO_4$. The solution was then washed by centrifuge at 4000 rpm three times with HCl (1M) and three times with deionized water. Deionized water (1 L) was added to the filtered material and sonicated until dispersed. At this point the solution becomes brownish in color and formed into a colloid gel. A $BaCl_2$ solution was used for indicating if the SO_4^- disappearance. Filtered GO was dried in an oven at 70°C for 24 hours. GO (150 mg) was dispersed in ethanol (60 mL) and DI water (20 mL) by sonication for 30 minutes.

3.3.2 Acid hydrolysis of MPTS

A mixture of ethanol (60 mL) and DI water (20 mL) was brought to a pH of 5.0 to 5.5 by adding CH_3COOH (36% in DI water). MPTS (2 mL) was added to the ethanol solution and allowed to stir for 25 minutes at room temperature.

3.3.3 Silanization of GO

GO ethanol solution is then added into the MPTS solution and sonicated for 15 minutes. In an oil bath at 80℃, the solution was then refluxed for 2 hours. The obtained MPTS-GO solution was subjected to 30-minutes-wash by centrifuge at 4000 rpm twice with DI water (100 mL) and three times with ethanol (100 mL). The obtained solution was fully dried at 45℃ and redispersed into ethanol (160 mL).

3.3.4 Preparation of PU sponge and etching

The as purchased 0.5-inch thick PU sponges were cut into 6 x 8 cm rectangles, sonicated in ethanol and DI water for cleaning and dried in an oven at 70℃ for several hours. A few dried PU sponges were set aside and labeled as Sample A. The dried PU sponge was then soaked in a HCl solution (5%) for 24 hours and dried in an oven at 70℃ for 4 hours. A few HCl-treated PU sponges were set aside and labeled as Sample A1.

3.3.5 Decorating PU sponge with MPTS-GO and MPTS

The MPTS-GO solution was brought to a pH of 9 by adding ammonia solution. The prepared HCl-treated PU sponge was dipped into the MPTS-GO solution for 1 hour and then sonicated for 30 minutes. Hydrazine hydrate (1 mL, 35%) was added to the sponge in the MPTS-

GO solution and refluxed in an oil bath at 95°C for 1.5 hours. The obtained sponge was washed with DI water, vacuum dried at 30°C for 24 hours and labeled as Sample C1. Separately, Sample C was prepared by the same procedure with a sponge without HCl-treatment. Separately, a control sample MPTS-HCl-PU was prepared by dip coating the hydrolyzed MPTS solution without GO onto a PU sponge treated with HCl.

3.3.6 Preparation of RGO sponges without silane

GO (150 mg) was dispersed into ethanol (160 mL) by sonication for 30 minutes. HCl-treated and non-HCl-treated PU sponges were separately dipped into the GO-ethanol solution for 1 hour, and sonicated for 30 minutes. Hydrazine hydrate (1 mL, 35%) was added into the solution and refluxed in an oil bath at 95°C for 1.5 hours. The resulted sponges were washed with DI water and dried at 30°C for 24 hours, labeled as Sample B for the non-HCl-treated sponges and Sample B1 for the HCl-treated sponges.

3.4 CALCULATION METHODS

3.4.1 Density calculations

Density has units of mass per unit volume. Approximately 2 x 2 x 1 cm thick squares were cut from each foam sample, and their masses were recorded for the density calculations according to standard test method ASTM D 3574-01. This test standard was applicable for flexible polyurethane foams, where a square shaped sample weight was recorded and volume was calculated with measurements of the sample dimensions by a ruler. Density was calculated by dividing the weighted sample mass by the sample volume [145].

3.4.2 Porosity calculations

Porosity was the total void volume divided by the total apparent sample volume. The total void volume was equal to the difference of the total apparent sample volume and the polymer volume. The following equation was used for determining porosity of the foams:

$$\varepsilon = \frac{V_{Bulk} - V_s}{V_{Bulk}} \qquad\qquad 3.1$$

Where V_{Bulk} was the total apparent sample volume, V_s was the volume occupied by the solid material, which is the polyurethane in this case. V_s was calculated using the weight mass recorded for each sample and dividing it by the density of the polymer according to the manufacturer's specifications.

Pore sizes were measured by scanning electron microscopy (SEM) images using a Zeiss Leo 1530 and Ultra Plus FESEM. Where a total of four cross-sections were obtained from sponge samples A, A1, B1 and C1 without regard to orientation. According to the SEM images, the chemical and morphological modifications had negligible effects on the original PU sponge pore sizes. Therefore, pore size distribution was obtained by averaging across all four cross-sections. The diameter of each pore was measured from fitting a circle onto the pores on the images. Note that the pore size measurement technique was an approximation with inaccuracies, the results were not reliable for exact measurements. For exact measurements, porosimetry such as the mercury intrusion porosimetry method is recommended.

3.4.3 Maximum volumetric adsorption ratio

When compared with the experimentally determined volumetric adsorption capacity $Q_{v/v}$, this maximum volumetric adsorption ratio allowed the investigator to obtain the efficiency of the adsorbent. Using the total relative density of the foam, the maximum volumetric adsorption ratio of the foam was calculated with the equation [130]:

$$\left(\frac{v_{oil}}{v_{PU}}\right)_{max} = \frac{1-\rho_r}{\rho_r} = \frac{1-\frac{\rho_f}{\rho_s}}{\frac{\rho_f}{\rho_s}} \qquad 3.2$$

Where v_{oil} was the volume occupied by the adsorbed oil, v_{PU} was the total void volume of the PU sponge, ρ_r was the relative density of the sponge, ρ_f was the apparent density of the foam and ρ_s was the density of the solid PU before expansion into the form of a foam. The known density of solid polyurethane [2] used was 1.2 g·cm⁻³.

The volumetric adsorption efficiency (VAE) of the adsorbent could then be calculated by:

$$VAE = \left[\frac{Q_{v/v}}{\left(\frac{v_{oil}}{v_{PU}}\right)_{max}}\right] \qquad 3.3$$

3.4.4 Theoretical gravimetric flux improvement factor

Theoretically, surface modification of the PU foam has an effect on the pore sizes and its interconnectivity, especially for particle decoration onto the material surface. For example, surface decoration with nanoparticles might increase surface roughness and modify the surface energy. Possible particle overload or agglomeration might narrow the pore channels and diminish effective pore diameters, consequently these could affect the level of interconnectivity. The degree to which these effects take place depend on the dosage of such particle additives. Further complications might result from particles that were not securely bonded to the foam surface. The adsorbate liquid entered the foam through a certain pathway during adsorption,

during desorption the mobility of these weakly-bonded or detached particles might cause the same pathways to be partially or entirely obstructed. A resistance of flow would be created within these channels resulting in poor oil recovery and subsequent adsorption capacities. This phenomenon could create an unpredictable interconnectivity problem and might vary from cycle to cycle.

In order to understand the effectiveness and efficiency of the modifications introduced to the foam, it was helpful to predict the theoretical improvement anticipated from certain modifications in terms of adsorption mass flux. Since it was difficult to determine the attributes of each variable, therefore the follow assumptions were made in order to narrow down the variables:

- There was no swelling with either the substrate material or the modification component(s);

- Good dispersion and stable adhesion of the modification particles on the substrate surface;

- Modification had negligible effect to the pore sizes and interconnectivity;

- Hydraulic potential was driven by matric (capillary) potential only;

- Adsorbed liquid was lost due to drainage is negligible;

- Hydraulic Conductivity remained the same before and after modification;

- The liquid properties (i.e. density and viscosity) and concentration remained the same.

- Liquid contact angle measurements were reliable and accurate.

Then according to the definition of a capillary pressure [136]:

$$\Delta P = \frac{2\gamma cos\theta}{r} \qquad\qquad 3.4$$

Where γ was the oil surface tension, θ was the contact angle between the oil and the PU surface, and r was the radius of the pores.

Upon modifications of the foam surface, the capillary pressure was changed from ΔP to ΔP^* with the assumption that there was no change to the radius of the pores. If the surface tension of oil remained the same, the only change introduced by the modifications would be θ. Hypothetically if a theoretical improvement factor "I" described the change in the capillary drive due to the surface modifications, then:

$$\Delta P^* = \frac{2\gamma\cos\theta^*}{r} = \frac{2\gamma(\cos\theta)I}{r} = I(\Delta P); \qquad\qquad 3.5$$

$$\therefore I = \frac{\cos\theta^*}{\cos\theta}; \qquad\qquad 3.6$$

Where θ and θ^* were the liquid-solid contact angles before and after modification, respectively. As assumed previously, if the liquid properties (density and viscosity), matrix properties (pore radius, pore distribution and interconnectivity) and concentration gradient (concentration of liquid exposed to the foam surface) remained the same, then the following would describe the theoretically improved mass flux of an unsaturated flow according to the modified Darcy's law:

$$j_m^* = I(j_m); \qquad\qquad 3.7$$

Since $\qquad\qquad j_m = -\rho_{liquid}K\frac{\partial h}{\partial c}\frac{\partial c}{\partial s}; \qquad\qquad 3.8$

And $\qquad\qquad \Delta P^* = \partial h^* = I(\partial h); \qquad\qquad 3.9$

Where, j_m^* was the predicted theoretical mass flux of adsorbate entering the modified adsorbent at a given time before equilibrium. j_m was the initial mass flux before modification was made to the adsorbent; and I was the improvement factor.

For example, if the PU foam had an oil contact angle of zero before and after modification, then I would be equal to 1. In that case, according to the Eq. 3.7 the adsorption mass flux would be the same before and after modification of the foam.

The difference between the actual adsorption mass flux and the theoretical value j_m^*

quantified efficiencies due to permeability, pore size distribution, interconnectivities, and other

changes of the porous structure parameters such as pore sizes, pores uniformity, etc..

It must be noted that the limitations and uncertainties of this test include inaccuracies in

OCA measurements and inaccuracies in the actual mass flux measurements. Only apparent liquid

contact angles were measured in this research. According to Eqs. 2.7 and 2.8, the apparent OCA

obtained without considering factors R or f would likely be an overestimate, resulting in an

overestimated theoretical gravimetric flux improvement factor. As described in section 3.5.1

Surface Wettability Measurements, known contact angle measurement methods on porous

surfaces were insufficient to provide accurate, meaningful results. Meanwhile, the improvement

factor I highly depended on the oil contact angle. Therefore, better control and measurement of

contact angles would be required to reflect a true correlation between the theoretical and actual

gravimetric adsorption flux.

A total of nine gravimetric flux measurements were made. Three test samples from each

of A1 and C1 were prepared for the flux measurements. Gravimetric fluxes average across 15-

minutes were recorded in terms of $kg/m^2 \cdot s$, defined as the total wet weight S_{TW} per area of

sponge in contact with the oil per second.

While other parameters such as effective surface area, time to equilibrium, oil retention

rate, and volume adsorption efficiency were not reflected in this correlation, it served as a tool

for the investigator to study the adsorbent flux efficiency and differences in permeability.

Adsorbent flux could be modified by optimizing the dosage of additives such as graphene or

MPTS, minimizing resistances at the pore channels, or customizing pore structures of the foam material, etc.

While the optimum porous structure varied for different adsorbents and liquids, according to the study reported by Pinto et al. [130], pore sizes in the range of 400 to 500 μm was found to produce an optimum oil adsorption efficiency and low oil saturation time for motor oil with a viscosity of 287.23 mPa·s and a density of 0.8787 g·cm^3. It should be noted that a short time to saturation is often required for immediate remediation in order to prevent further environmental damages. Therefore, selection of a small radius must be balanced with the speed of which saturation is required at the site of the oil cleanup, as well as other parameters such as oil retention and ease of extraction for recyclability.

3.5   EXPERIMENT PARAMETERS

3.5.1   Surface wettability measurements

The surface wettability of the samples were determined by measuring the water droplets and oil droplets static contact angles (CA), θ_w and θ_o respectively. However it was concluded in various literatures that static CA on rough and porous surfaces were often meaningless in terms of Young's equation [146] due to the lack of a precise measurement methodology.

The highly porous surfaces of the sponge samples created false apparent CA because of 1) longer liquid to solid contact lines due to the protrusion of struts at the cut edges of the sponge samples; and 2) large pore openings caused water droplet to pin and sit inside of the void, which lowered and rotated the horizontal axis and obscured the view of the true liquid solid contact line.

In this research, water and oil CA were measured to serve as comparisons between the samples. Although the measurements might be inaccurate, the averaged inaccuracies were assumed to be consistent throughout all samples due to the similar roughness and porous nature of the substrates. The CA results were interpreted alongside with the water uptake study, which supported each other in order to quantify the samples' degree of hydrophobicity and oleophilicity.

The static CA of water and oil were measured under room temperature and atmospheric pressure by using an Eppendorf adjustable pipette (0.5 - 10 µL). A total of four dried test samples were prepared, one from each of samples A, A1, C and C1. Where 5 µL water and oil droplets were introduced at 3 different locations on each sample. Three digital images were captured for each liquid droplet introduced. A Nikon D3100 digital camera with a Tamron SP 60mm F/2 Macro lens was used to capture the CA images. The alignment of the field of view was approximated through the digital camera. All seventy-two digital images were analyzed and processed by computer software ImageJ with the Contact Angle plug-in [147]. The recorded CA are averaged for each sample.

3.5.2 Adsorption capacity study

The adsorption test was a modified procedure from ASTM F726 - 9.3 Oil adsorption short test for type I adsorbents [148]. Three approximately 2 x 2 x 1 cm squares were cut from each of samples A, A1, B, B1, C and C1. The dimensions and dry weight "S_0" of each test sample was recorded to 0.01 g accuracy. An amount of 1.5 cm thick pump oil was poured into each of 6 pyrex glass beakers, each beaker was designated for three tests of the same sample type. One

square from each of the 6 samples was carefully lowered with a tweezer into each beaker. The

square samples were allowed to float freely without interruption in the test cells for 15 minutes.

After adsorption, each sample was carefully lifted vertically with a tweezer at its corner,

immediately transferred onto a tared strainer on top of a beaker. The total weight was recorded as

"S_T" and sample was allowed to drain without disturbance for 30 s ± 2 s. It is then lifted carefully

from the strainer in order for recording of the weight of oil drained labeled as "S_D". Photographs

showing the above steps are shown on Figure 3.2.
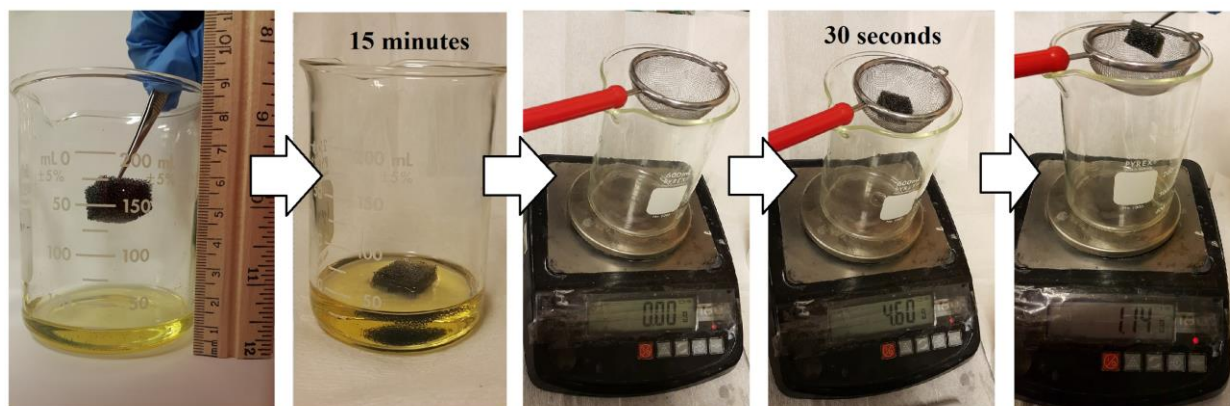
Figure 3.2 Photographs of the adsorption capacity test procedure in the order from left to right.

The same procedure was repeated for the remaining twelve test samples, totaling three

data points for each sample type. The results for each sample type were averaged for

comparison. Calculations of the gravimetric adsorption capacities $Q_{m/m}$ were performed with

the following equation, and the results were reported in terms of grams of oil adsorbed per gram

of adsorbent weight (g·g^{-1}):

$$Q_{m/m} = (S_T - S_D - S_0)/ S_0; \qquad 3.10$$

Where $Q_{m/m}$ was the gravimetric adsorption capacity (g·g⁻¹), S_T was the total wet weight (g) as recorded immediately after it is transferred onto the tared strainer, S_D was the weight (g) of oil drained within 30 s after sample transferred onto the tared strainer and S_0 was the dry weight (g) of the sample. $Q_{m/m}$ was converted to volumetric adsorption capacity $Q_{v/v}$ (mL·mL⁻¹) with the following equation [138]:`

$$Q_{v/v} = Q_{m/m} \cdot \frac{\rho_s}{\rho_o} \qquad\qquad 3.11$$

Where ρ_s was the solid density of the PU before foaming (1.2 g·cm⁻³), and ρ_o was the density of pump oil (0.869 g·cm⁻³ at 60°F, Figure A.1.).

The volumetric adsorption efficiency (VAE) of each sample was calculated from Eq 3.3.

Oil drainage was calculated as a percentage of the initial oil adsorption weight calculated with the following equation:

$$\% \ of \ oil \ drainage \ = \ S_D/(S_T - S_0) \cdot 100\% \qquad\qquad 3.12$$

This parameter was often neglected from other oil adsorption experiments, however it quantified the liquid retention efficiency of the adsorbent upon separation from the bulk liquid. Oil retention rate was calculated by:

$$ORR \ = \ 1 - \% \ of \ oil \ drainage \qquad\qquad 3.13$$

3.5.3 Water uptake study

The water uptake study was designed in order to supplement the WCA characterization of the samples. The purpose of this study was to observe the selectivity and the amount of water uptake by a sample under dynamic conditions. The procedure was designed to be similar to the ASTM F726-9.2 Dynamic Degradation Test for Type I Adsorbents [148]. There were two parts to

this study. The first part of the study involved water uptake in a dynamic condition. The second part involved oil adsorption in the presence of water in order to test the selectivity and performance under such conditions.

Approximately one 2 x 2 x 1 cm square was cut from each of the samples A, A1, C and C1. The dry weight (g) were recorded as "S_0" for each test sample. A centrifuge container (50 mL) was half filled with DI water (25 mL) and a sample was carefully lowered into the container and sealed. The container was then subjected to agitation by a VWR analog vortex mixer at a speed of 500 rpm for 2 minutes. The sample was retrieved carefully with a tweezer and immediately placed onto a tared strainer on top of a beaker. The total weight was recorded as "S_{WT}" and allowed to drain for 30 s. After draining, the sample was removed and the amount of drainage was recorded as "S_{WD}". The gravimetric water uptake was calculated in terms of $g \cdot g^{-1}$ with the following equation:

$$Q_{m/m,w} = (S_{WT} - S_{WD} - S_0)/ S_0; \qquad\qquad 3.14$$

Where S_{WT} was the total wet weight immediately after adsorption, S_{WD} was the weight of the water drained and S_0 was the dry weight of the sample. Drainage and WRR were calculated using the same method in the oil adsorption study.
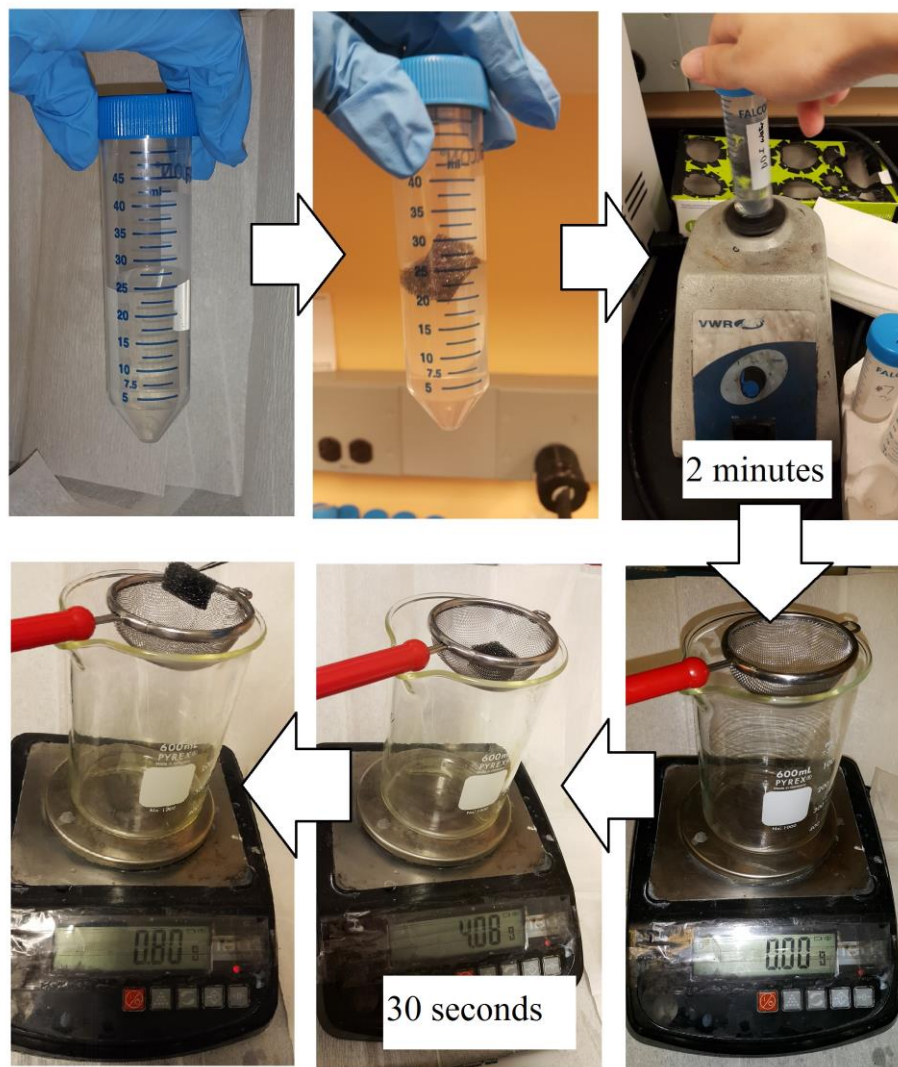
Figure 3.3 Photographic schematic of the water uptake studies procedure.

For the second part of this study, a 500 mL beaker was half filled with DI water. An

amount of 2 mL Pump oil dyed with Sudan blue II was dropped onto the water surface in the

beaker. Sample C1 was retrieved from part one of this study and mechanically squeezed for

water removal. The sample was then placed onto the oil-on-water solution for 15 minutes of

observation. Afterwards, the sample was vertically lifted with tweezers. The sample was then

mechanically squeezed to release the adsorbed liquid into an empty beaker for observation.
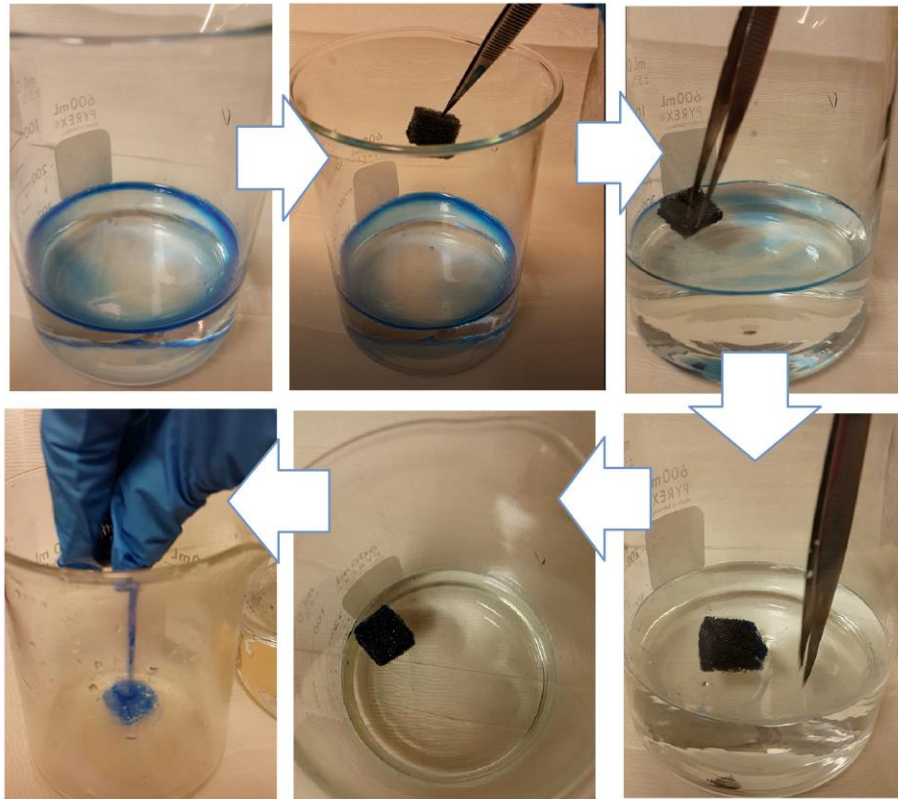
Figure 3.4 Photographs of the water uptake study part two procedure. 2 mL of blue dyed pump oil on top of water was adsorbed by sample C1 for 15 minutes.

3.5.4   Recyclability study

A recyclability study allowed a sample to be tested for its stability under repeated use.

The performance stability, percent of degradation, and the changes of other parameters

throughout the adsorption-desorption cycles were observed.

The adsorption-desorption recycling of sample C1 was tested under this study. An

approximate 2 x 2 x 1 cm square was cut from sample C1 and followed the procedure of the oil

adsorption capacity test except the time of adsorption was shortened to 5 minutes per cycle. After each 5-minutes adsorption period, the initial wet weight was recorded followed by a 30 seconds drainage on the strainer. The amount of drainage was then recorded and the sample was squeezed by hand to remove as much oil as possible into a separate container. The weight of the desorbed sample "S_{0x}" was recorded for each cycle "x" and the procedure is repeated for a total of 10 cycles.

The first cycle's $Q_{m/m}$ was calculated using the same method as in the oil adsorption capacity study (Eq 3.10). For calculating $Q_{m/m}$ for cycles 2 to 10, the dry weight S_0 was substituted with S_{0x} using Eq 3.10. Performance degradation was calculated according to ASTM F726-10.2.2.2 with the following equation:

$$\% \: Performance \: degradation_{nth \: cycle} = \frac{Q_{m/m,n^{th} \: cycle}}{Q_{m/m,initial \: cycle}} \cdot 100\% \qquad\qquad 3.15$$

Potential adsorption capacities $Q_{m/m}$ were calculated by removing S_D from Eq 3.10. Volumetric adsorption capacities $Q_{v/v}$, VAE, drainage and ORR for each cycle were calculated using the same method as in the adsorption capacity study in section 3.5.2.

Separately, a comparison test was performed between the adsorption-desorption cycles of sample C1 and the MPTS-HCl-PU control sample. Three squares approximately 2 cm x 2 cm x 1 cm were cut from the MPTS-HCl-PU control sample. Also, an additional of two squares with approximately the same size were cut from sample C1. All dry samples were immediately weighted. The same recycling procedure was repeated for a total of six cycles. At the end of each cycle, the wet weight after drainage (S_{WT} - S_D) was recorded. Adsorption capacities and performance degradation were calculated using Eqs 3.10 and 3.15.

3.5.5 Adsorption kinetics study

During the process of an adsorption, the concentration of the adsorbate on the surface area of the adsorbent continues to increase until it reaches a dynamic equilibrium with the concentration that exist in the bulk solution. An adsorption kinetics study is a test that investigates the behavior of the sample from the time it is introduced with an adsorbate to the time when it reaches the said dynamic equilibrium. Adsorption kinetics are generally controlled by one or more processes such as bulk diffusion, external mass transfer, chemisorption, and/or intraparticle diffusion [152]. The fitting of the experimental data into various kinetic models help to define the rate expressions characteristics and its possible reaction mechanisms. Also the ability to model and predict the adsorption kinetics of a material helps to optimize designs operating conditions for deployment of the material in applications.

In this research, sample C1 adsorption kinetics for pump oil was investigated with the Lagergren pseudo-first order and pseudo-second order. Respectively, the linear form of the equations corresponding to the two models were as follows:

$$Log(Q - Q_t) = Log\ Q - \frac{K_1 t}{2.303} \qquad\qquad 3.16$$

$$\frac{t}{Q_t} = \frac{1}{K_2 Q_e^2} + \frac{t}{Q} \qquad\qquad 3.17$$

Where Q_e and Q_t were the adsorbate liquid concentrations expressed in mg/L at the time of equilibrium and at time t, respectively and k_1 (min^{-1}) and k_2 (g·g^{-1}·min^{-1}) represented the first-order and second-order rate constants.

One approximate 2 x 2 x 1 cm square was cut from sample C1 and followed the procedure of the adsorption capacity test except that the adsorption was stopped for

measurements at predetermined intervals of 2, 4, 6, 8, 10, 30, 60, 300, 900, 1800, 2700, 3600, 5400, and 7200 seconds. The recorded data was analyzed by fitting into Lagergren pseudo-first-order and second-order kinetic models.

3.6   CHARACTERIZATION

Characterization of the samples and the as-prepared GO were performed using scanning electron microscopy (SEM), powder X-ray diffraction (XRD), Raman spectroscopy and Fourier transform infrared spectroscopy (FTIR). The SEM images were taken with a Zeiss Leo 1530 and Ultra Plus FESEM. A thin layer of gold was sputtered on each sample in order for sufficient conductivity to process imaging. XRD was performed with a Bruker AXS D8 diffractometer using a Cu radiation source with a wavelength of 0.154 nm. Raman spectroscopy was performed with a Bruker SENTERRA with a 532 nm laser source. FTIR was performed with a PerkinElmer 1720 FT-IR spectrometer measured in the range from 4000 cm^{-1} to 400 cm^{-1} with a resolution of 4 cm^{-1}.

CHAPTER 4 - RESULTS AND DISCUSSIONS

4.1 DENSITY, POROSITY AND MAXIMUM VOLUMETRIC ADSORPTION RATIO

Since the samples have similar pore structures, consistency of these parameters are expected. Sample measurements and calculations are listed on Table 4.1. It is noted that except for sample A and C, the majority of samples have similar physical characteristics in terms of density, porosity and maximum volumetric adsorption ratio. Inconsistencies in samples A and C may be caused by their differences in moisture content due to differences in hydrophobicity. Another reason for the inconsistencies may be due to the porous nature of the foams. The weight of the samples vary depending on the locations of vertices at the cut edges, fray edges caused by cutting may exaggerate the true dimensions of the samples.

Table 4.1 List of sample average densities, average porosities and maximum volumetric adsorption ratio.

Sample	Average Apparent Density (g·cm⁻³) $\rho = \dfrac{M}{V_{Bulk}}$	Average Porosity (%) $\varepsilon = \dfrac{V_{Bulk} - V_s}{V_{Bulk}}$	Maximum Volumetric Adsorption Ratio$(\dfrac{v_{oil}}{v_{PU}})max = \dfrac{1-\rho_r}{\rho_r}$
A	0.0322	97.32%	36.25
A1	0.0237	98.03%	49.67
B	0.0239	98.01%	49.29
B1	0.0241	97.99%	49.29
C	0.0207	98.27%	56.91
C1	0.0237	98.03%	49.67

Figure 4.1 shows the pore size distribution histograms averaged from across all samples. It is noted that the distribution is rather narrow between the range of 550 μm to 800 μm. This indicates pore sizes are similar throughout the foam, and therefore there is a lack of a micro-, meso- to macro-pore transition.
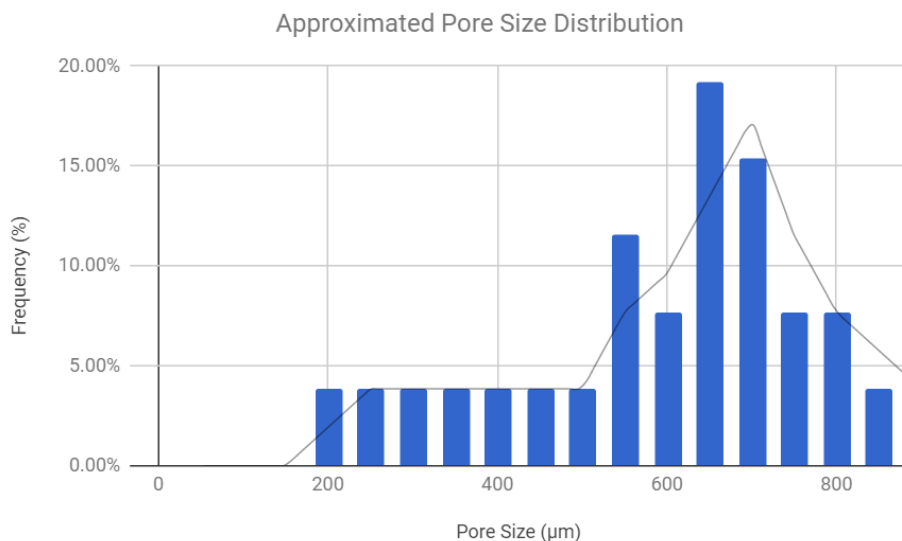
Figure 4.1 Pore size distribution histogram of all PU sponge samples.

4.2   X-RAY DIFFRACTION

XRD was performed to confirm the quality of GO obtained from the synthesis. XRD diffraction of the synthesized GO is shown on Figure 4.2. It has been well documented that GO displays a XRD diffraction peak at approximately 9 to 10° (001 peak), which corresponds to a ~0.89 nm interlayer spacing between the single-layer GO sheets [152]. Also, it has been documented that a diffraction peak at about 26° (002 peak) is observed for graphite [154], indicating its ordered crystallinity. The XRD diffraction on Figure 4.2 displays a peak at 9.43° and the absence of the 26° (002) peak. This is in agreement with literature, suggesting a

successful delamination of the graphite layers and the functionalization of oxygen groups, increasing its interlayer spacing to approximately 0.89 nm.
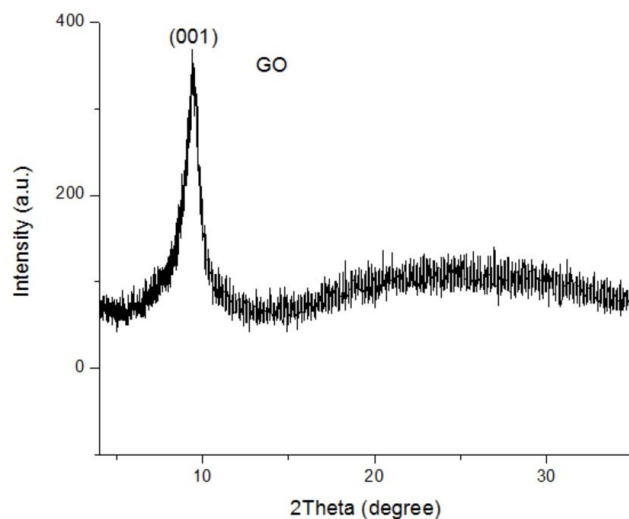
Figure 4.2 XRD pattern obtained for the synthesized GO showing 2θ angles from 4 to 35°. A 001 peak at 9.43° corresponds to an interlayer spacing of 0.89 nm compared to the interlayer spacing of 0.335 nm in graphite [154].

4.3   RAMAN SPECTROSCOPY

Raman spectroscopy enables the differentiation and comparison between various carbon nanostructures. It is well known that all sp^2 carbons forms are featured by a G-band at approximately 1582 cm^{-1}, attributed to the stretching of C-C bond. Disorder-induced D-band at about 1345 cm^{-1} and 1626 cm^{-1} indicate the presence of disorder such as defects and functional groups, such as oxygen groups on graphene oxide (GO). These defects and functional groups disrupt the crystalline sp^2 carbon lattice. The ratio between the D-band and G-band intensities (I_D / I_G) can be used to quantify the level of disorder to the hexagonal carbon lattice. Here the ratio

I_D/I_G is 1.06 for the prepared GO sample. Also common in all sp^2 carbon forms is the G'-band or known as the 2D-band between 2500 to 2800 cm^{-1}, which is a useful indicator for the number of layers present in the sample [149].

The Raman spectra of the synthesized GO from this research is shown in Figure 4.3. The G-band observed at 1576.5 cm^{-1} and a D-band peaked at 1343 cm-1 are in agreement with the Raman profile of a typical GO. The broadened G'-band at 2500 to 3300 cm^{-1} indicates a multi-layered GO sample that is perhaps caused by stacking during the drying process. However, with the XRD characterization corresponding to interlayer spacing of ~0.89 nm, such stacking is weakened by the oxygen functional groups and is expected to be easily re-dispersed into single to few-layered GO sheets.
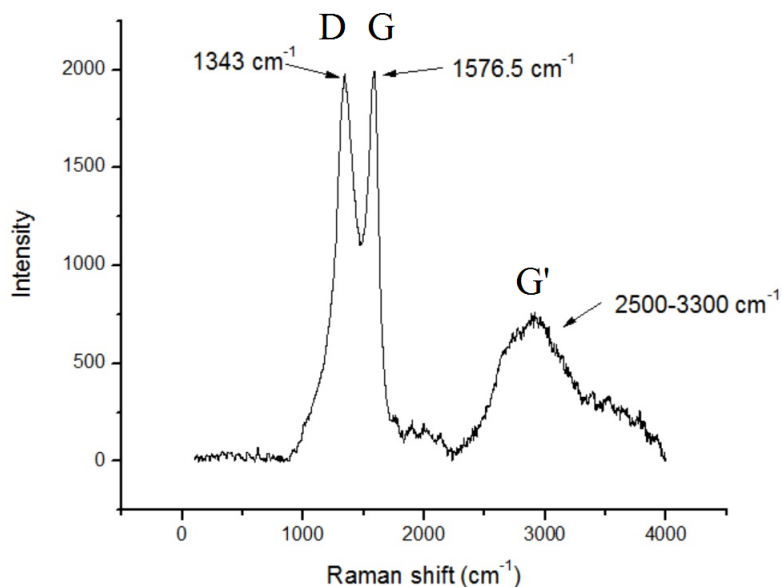
Figure 4.3 Raman spectroscopy of the as-synthesized GO, showing the D-band, G-band and G'-band. The graph shows a ID/IG ratio of 1.06, attributed to a certain level of disorder of the hexagonal carbon lattice.
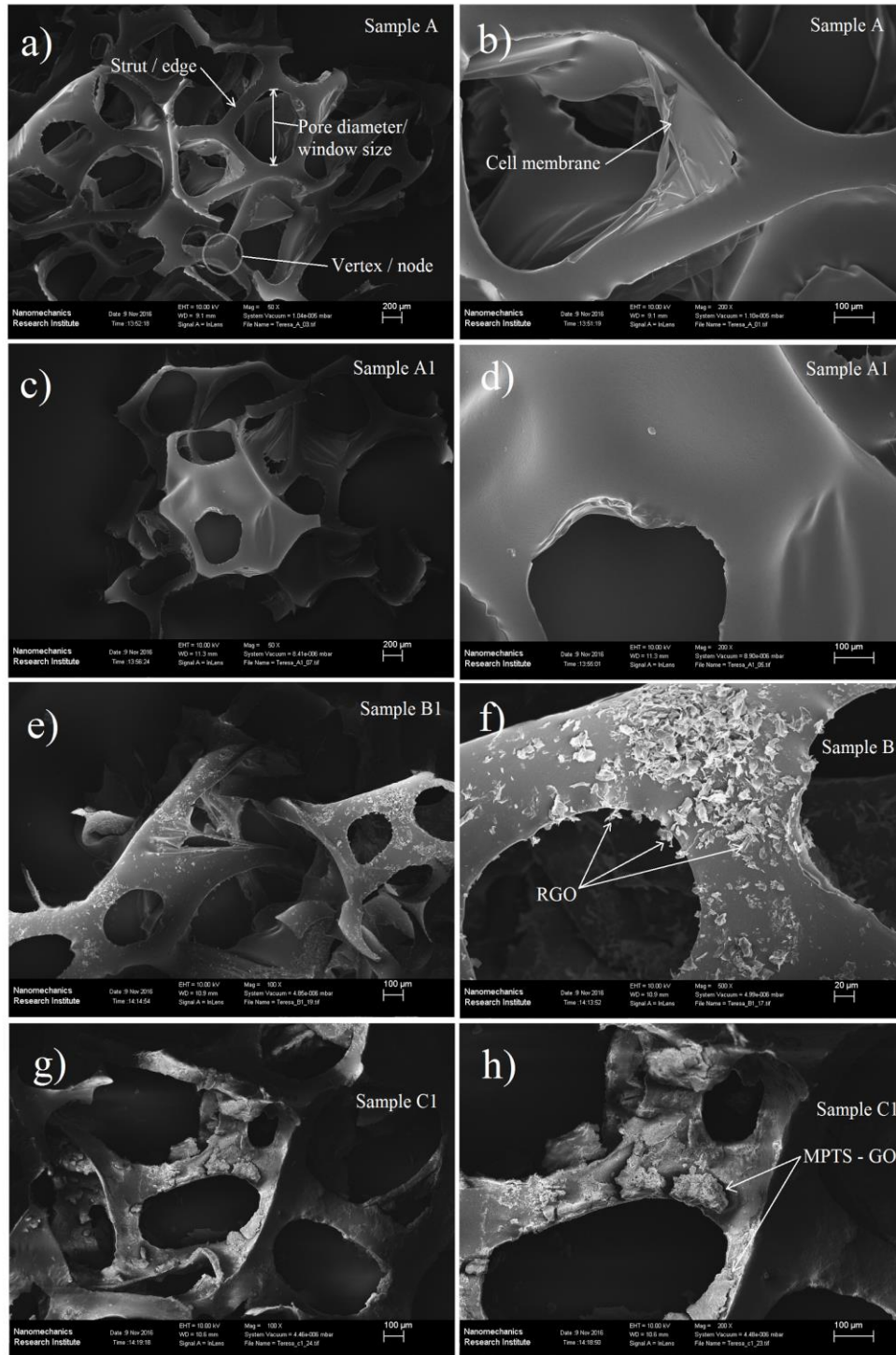
Figure 4.4 SEM images of (a) to (b) Sample A, (c) to (d) Sample A1, (e) to (f) B1, and (g) to (h) Sample C1.

4.4   SCANNING ELECTRON MICROSCOPY

According to Figures 4.4(a) to (h), the SEM images of the samples show a reticulated foam type with completely open cells. Remaining cell membranes are present and visibly attached onto the edges of some of the pore openings. Pore diameter is the same as window openings in this case, and are labeled on Figure 4.4(a). These pore diameters are mostly within the range of 500 to 700 μm and are distributed uniformly across. The narrow pore size distribution together with the completely open cell structure create a skeleton matrix, which is made of struts and open spaces without actual "pores" or "cells" with an enclosed chamber. The porous structure is very well interconnected.

Figure 4.4(a) and (b) shows a subtle difference in surface texture between samples A and A1. The roughened surface in A1 contributed to the increase in water uptake and adsorption capacity. Also, the increase in surface area due to roughness has most likely contributed to better binding between the MPTS-GO and the PU surface.

It is evident from the images that the modifications did not impact the pore diameters between samples. Figure 4.4(e) to (f) shows that the simple dip coating method deposited RGO onto the struts of the sample. Although there are regions where RGO agglomeration is seen and distribution is uneven, the decoration of RGO effectively increased surface area and roughness.

Figures 4.4 (g) and (h) shows MPTS-GO adhesion on the PU sponge skeleton. The clumps observed in Figure 4.4(h) indicate a relatively high loading of MPTS versus RGO. There is potential improvement with better dispersion of the silane solution, possibly by optimizing the ratio of silane to RGO, and lowering self-polymerization.
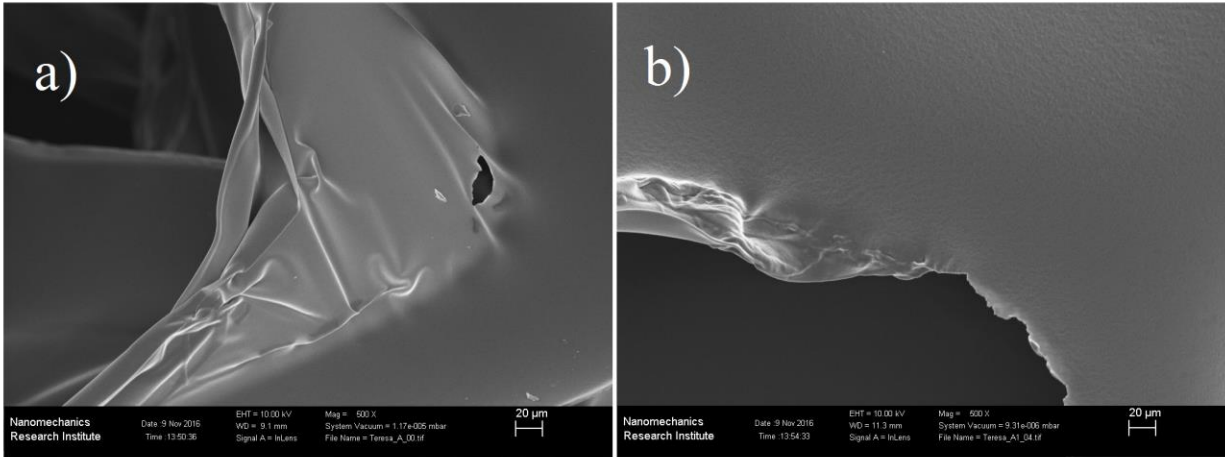
Figure 4.5 SEM images of samples (a) A and (b) A1. The subtle surface roughness is seen in (b) due to HCl etching.
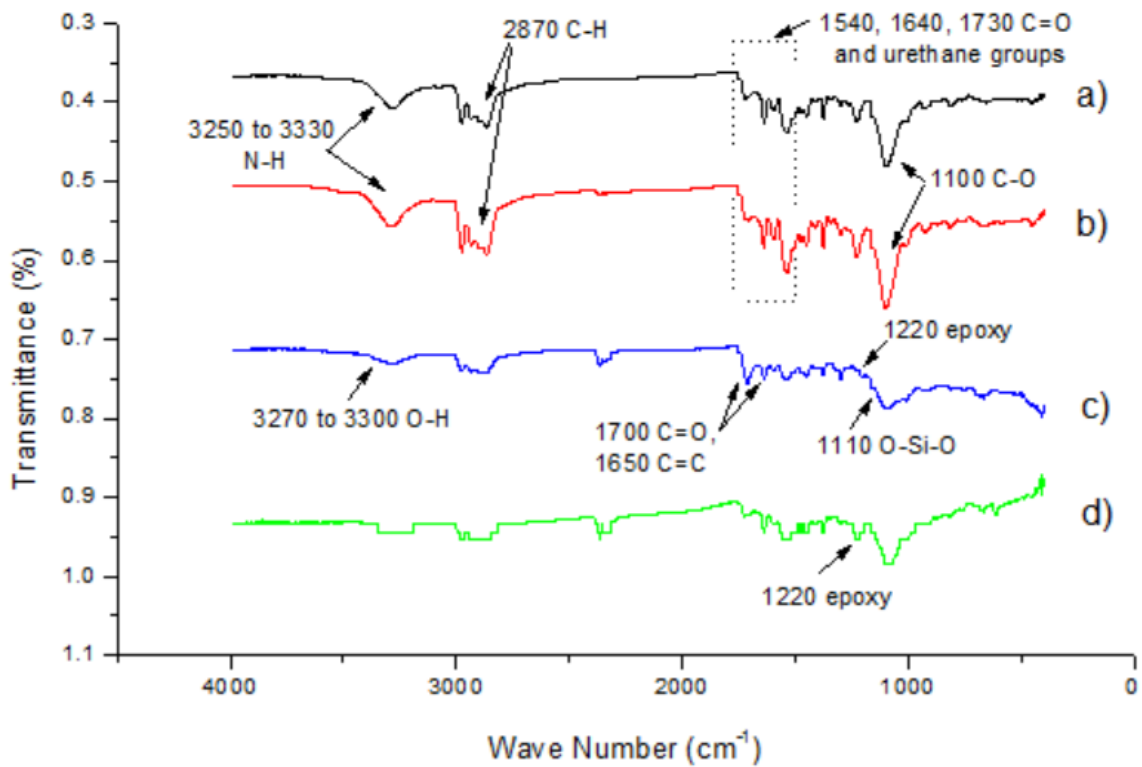
Figure 4.6 FTIR spectrums for (a) sample A, (b) sample A1, (c) sample C1, (d) sample B1.

4.5   FOURIER TRANSFORM INFRARED SPECTROSCOPY

The FTIR spectrum of samples A, A1, B1 and C1 are shown in Figure 4.6(a) to (d). Samples A and A1 show the absorption bands and peaks that are normally observed in polyurethane [73, 118, 141, 158] at 3250 to 3330 cm^{-1} due to N-H stretching and hydroxyl groups, 1100 cm^{-1} due to C-O stretching, 1540 cm^{-1} associated with C-N-H groups, 1640 to 1730 cm^{-1} associated with the urethane groups, and 2870 cm^{-1} from the C-H stretching. There is no observed difference between sample A and A1 spectrums, therefore HCl etching did not affect the sample's molecular structure.

According to literature [138, 139, 144], MPTS has characteristic bands around 3300 to 3500 cm^{-1} assigning to O-H group induced from the hydrolysis process. Other bands and peaks from MPTS include 1700 cm^{-1}, 1650 cm^{-1} and 1110 cm^{-1} approximately, which are due to the stretching of C=O groups, C=C bonds and Si-O-Si groups, respectively. It can be seen that the band at 3270 to 3300 cm^{-1} is weak in sample C1 compared to the others, suggesting that reactions between the silane and the available O-H groups occurred during the coupling between RGO and the PU sponge. The sharpening of the peak around 1720 cm^{-1}, the changes near 1640 cm^{-1} together with the broadening of the band near 1090 cm^{-1} to 1200 cm^{-1} suggest the presence of MPTS in the sample.

Graphene oxide typically display signs of its functional groups in the FTIR spectrum [141, 151]. Namely O-H groups above 3400 cm^{-1}, carboxyl COOH groups forming hydrogen bonds appear between 2500 and 3200 cm^{-1}, carbonyl groups C=O around 1720 cm^{-1}, epoxy C-O-C stretches at 1220 cm^{-1} and alkoxy C-O groups at 1040 cm^{-1}. In the spectrums of samples B1 and

C1, the hydroxyl group band around 3300 cm^{-1} is relatively weak and the carboxyl band is absent. This suggests either effective reduction of the GO or reaction of these groups with the silane during coupling of the GO. While carbonyl and epoxy groups are usually more difficult to remove [151], these bands are relatively weak in samples B1 and C1 compared to the PU samples. This suggests removal of the oxygen functional groups during the hydrazine reduction reaction of the sponges.

4.6   SURFACE WETTABILITY
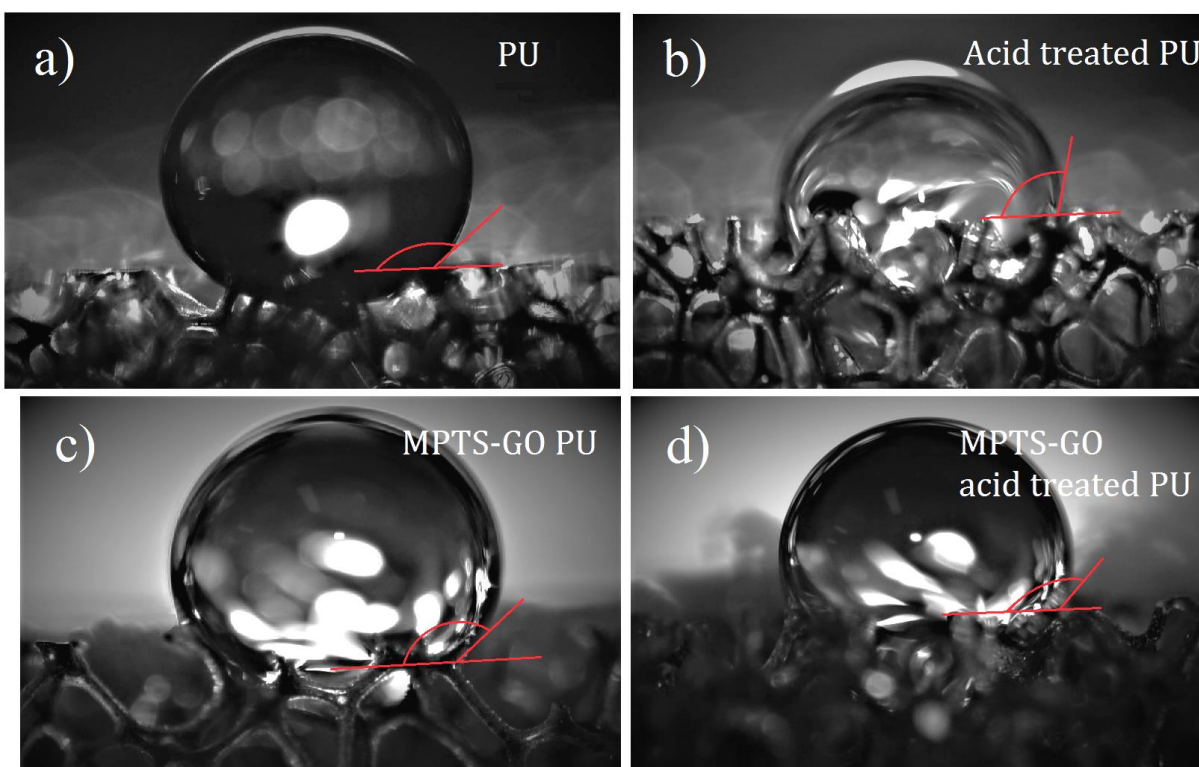
Figure 4.7 Water contact angle images showing 5 μL water droplets on (a) sample A, (b) sample A1, (c) sample C, and (d) sample C1. Contact angles were inaccurate due to the highly porous structure of the substrate.

.
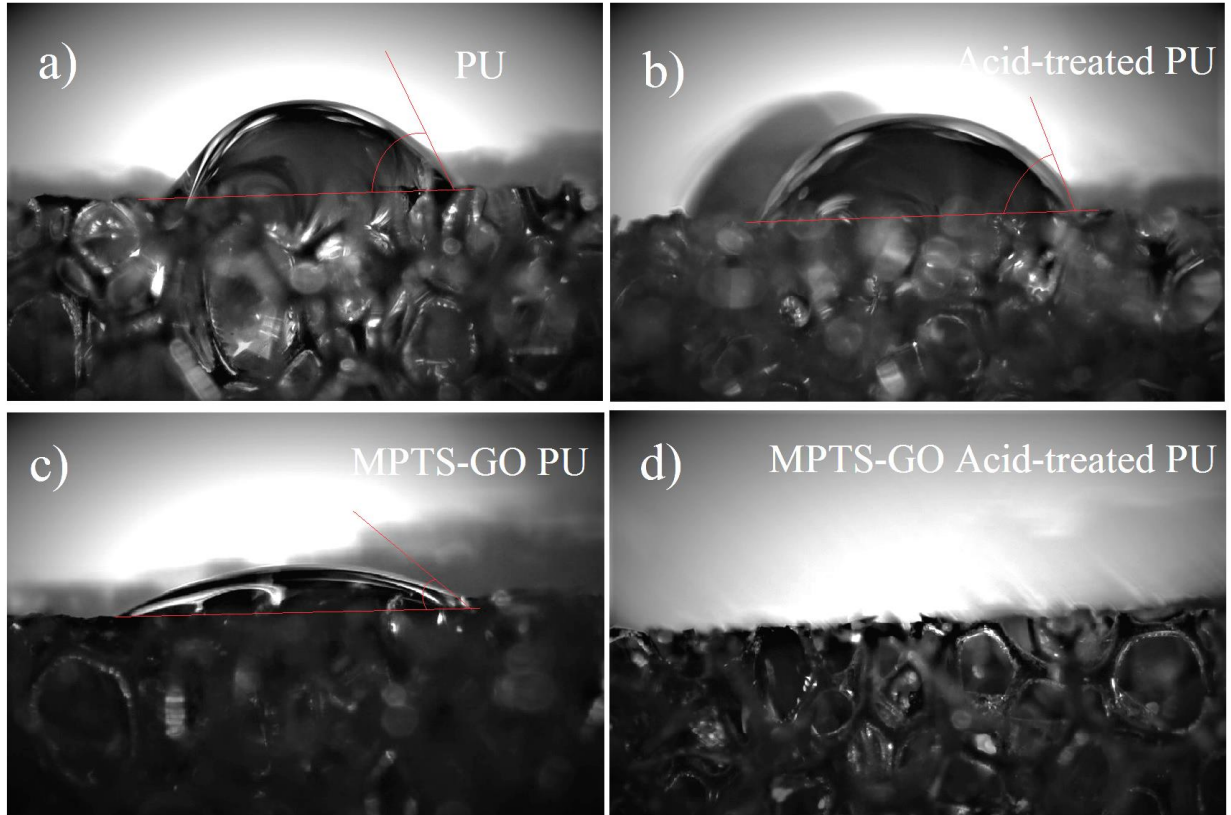
Figure 4.8 Digital images of oil contact angles measured by introducing 5 µL pump oil droplets onto the sponge samples (a) sample A, (b) sample A1, (c) sample C, (d) sample C1.

The measured WCA and OCA are listed in Table 4.2. Although the absolute CA values are inaccurate due to the nature of the porous structures, some information can be interpreted from these results. For example, in combination with the data from the water uptake experiment in section 4.9 it can be confirmed that HCl treatment of the PU sponge increased its hydrophilicity and lowered its WCA. However, if the true WCA of the original PU sponge is higher than 90° which indicates hydrophobicity, an increase of roughness from the HCl treatment would further increase the WCA and hydrophobicity instead. It was observed from the SEM and digital images that the amount of cell membranes decreased substantially after HCl

etching. These cell membranes may have contributed to WCA measurement errors, resulting in

an overestimation of the initial WCA of all samples.

There is no significant change in the overall WCA from modifying sample A into C and

C1. According to this information, the selectivity of oil over water was not improved. However,

the water uptake experiment results confirmed otherwise. (See section 4.9)

On the other hand, HCl treatment clearly enhanced the oleophilicity of sample C1 by

lowering the OCA to 0°. At 0° the oil droplet instantaneously spread across the sample surface.

As previously discussed, surface roughness acts as an amplifier of the material's tendency

toward wettability. The roughness introduced during the HCl etching process enhanced the

oleophilicity for both samples A1 and C1. This is consistent with the previous understanding on

the effects of surface roughness on wettability. Sample C1 displayed a dramatic enhancement of

oleophilicity compared to sample C, other than the amplifying effects from the surface roughness

itself, this may be attributed to the increased surface area which allowed improved binding sites

for the MTPS-GO to adhere onto the PU sponge.

Table 4.2 Static water and pump oil contact angles for samples A, A1, C and C1 at room
temperature and atmospheric pressure.

Sample	WCA (°)	OCA (°)
A - original PU	123.9 ± 10.3	64.2 ± 2.4
A1 - acid-treated PU	110.4 ± 5.9	66.9 ± 2.6
C - MPTS-GO + PU	122.0 ± 2.9	44.2 ± 1.6
C1 - MPTS-GO + Acid-treated PU	123.5 ± 4.4	0

4.7 ADSORPTION CAPACITY

Table 4.3 lists the average $Q_{m/m}$ and $Q_{v/v}$ and their standard deviations for all 6 samples and Figure 4.9 shows the comparison graph between the sample performances. It can be seen that sample C1 outperforms the other samples. It is also observed that HCl etching not only increased the water uptake of sample A1 compared to sample A, the etching also increased the $Q_{m/m}$ by 39.4%. The same improvement applied to sample C1, which has an 8.1% increase in $Q_{m/m}$ compared to sample C. On the contrary, HCl etching appears to negatively affect sample B1 as compared to sample B, which displayed a decrease in the $Q_{m/m}$ by 4.66%. One possibility for this phenomenon may be due to the lack of binding agent between RGO and the PU sponge, an increase of water uptake by the sponge after HCl treatment may wash away more of the deposited RGO during the washing step after synthesis. Performance of samples A1 and B are comparable, indicating that the roughness effect on the PU sponge is comparable with the dip-coated RGO alone.

As seen from Table 4.3, samples A, A1 and C have the lowest oil retention rate (ORR) due to high oil drainage. This also implies that the 3 samples may potentially be improved if these inefficiencies are resolved. C1 is the best-performing sample as well as the most efficient in oil retention. Since the porous structures of all samples are similar, the ORR results allow for a comparison of the oleophilicity between the samples.

The volumetric oil adsorption efficiencies indicate the degree to which samples are filled with adsorbate. According to the result, a substantial percentage of volume of the samples remained empty after adsorption. Sample C1 is relatively more efficient than the others in filling the pores. This is a useful tool to quantify further optimization potentials for the adsorbents.

Table 4.3 Experimentally determined gravimetric and volumetric adsorption capacities, volumetric oil adsorption efficiency (VAE), percent of drainage and oil retention rate (ORR).

Samples	$Q_{m/m}$ (g/g)	$Q_{v/v}$ (cm^3/cm^3)	Volumetric Oil Adsorption Efficiency	Drainage	ORR
A	18.41 ± 0.95	25.43 ± 1.3	$70.15\% \pm 3.6\%$	$24.45\% \pm 1.3\%$	$75.55\% \pm 1.3\%$
A1	25.67 ± 0.44	35.45 ± 0.61	$71.37\% \pm 1.2\%$	$23.17\% \pm 3.5\%$	$76.83\% \pm 3.5\%$
B	25.61 ± 1.7	35.38 ± 2.4	$71.78\% \pm 4.9\%$	$16.82\% \pm 6.1\%$	$83.18\% \pm 6.1\%$
B1	24.42 ± 1.9	33.73 ± 2.6	$68.43\% \pm 5.2\%$	$14.92\% \pm 8.8\%$	$85.08\%\ 8.8\%$
C	26.47 ± 0.31	36.56 ± 0.42	$64.24\% \pm 0.74\%$	$33.52\% \pm 3.4\%$	$66.48\% \pm 3.4\%$
C1	28.61 ± 0.78	39.52 ± 1.1	$79.56\% \pm 2.2\%$	$9.64\% \pm 0.41\%$	$90.36\% \pm 0.41\%$
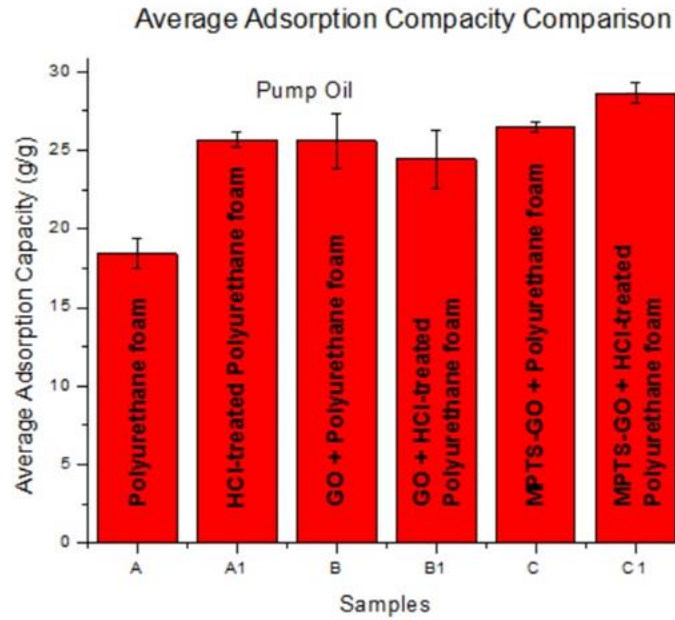
Figure 4.9 Bar chart comparison of average gravimetric adsorption capacities of pump oil for samples A to C1.

4.8 THEORETICAL GRAVIMETRIC FLUX IMPROVEMENT FACTOR

According to Figure 4.10, the 15-minutes average mass flux of samples A1 and C1 were compared with their respective theoretical average mass flux. . The gravimetric flux improvement factors were calculated with Eqs. 3.6 using the measured OCA from section 4.6. The average OCA for sample A1 was 66.9° with a standard deviation of 2.6°. The three improvement factors resulted were 2.31, 2.55 and 2.86, calculated using OCA of 64.3°, 66.9° and 69.5° respectively. Three theoretical flux values were calculated with Eq. 3.7 using these improvement factors, respectively 0.0227, 0.0213 and 0.0205 $kg/m^2 \cdot s$ with an average of 0.0215 $kg/m^2 \cdot s$ (see Figure 4.10).. Three different C1 samples were measured with an average mass flux of 0.00913 $kg/m^2 \cdot s$ and a standard deviation of 6.62 x 10^{-4}. As a control, three different A1 samples were measured and recorded an average mass flux of 0.00837 $kg/m^2 \cdot s$ with a standard deviation of 4.35 x 10^{-4}. The actual average mass flux measured for sample C1 was approximately 42% of the theoretical value, indicating a significant potential for improvements if the permeability properties of the material are optimized.

As mentioned earlier, a theoretical value based on the improvement fact is highly dependent on the accuracy of the OCA. Therefore, apparent contact angles used in this case do not take into account the surface roughness or air trapped between the solid and liquid. A reliable CA measurement method capable accurate measurements on rough surfaces is needed in order to calculate a true theoretical flux value.
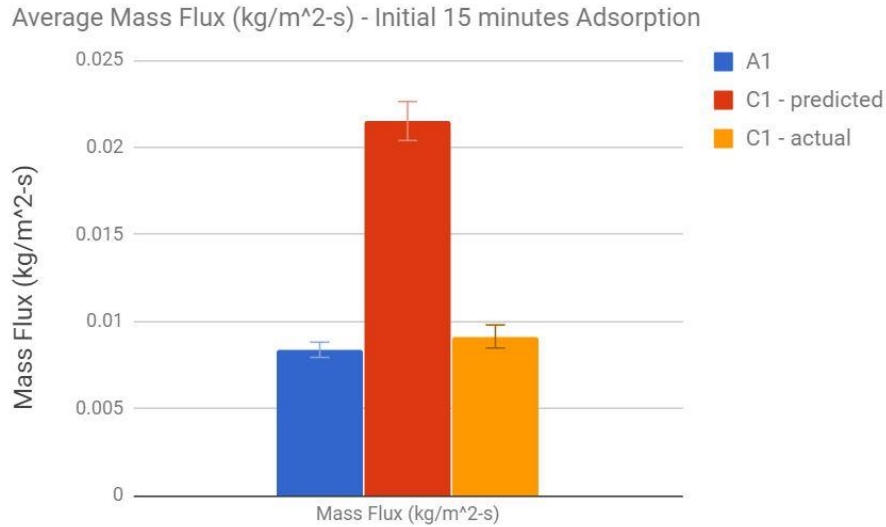
Figure 4.10 Comparison between the 15-minutes average mass flux of samples A1, the predicted and actual average mass flux of sample C1 using the theoretical gravimetric flux improvement factor (average I = 2.57).

4.9   WATER UPTAKE STUDY

As the results indicate in Table 4.4, samples A1 followed by A had the highest water uptake compared to C and C1. Besides high water adsorption capabilities, it is noted that the drainage of water is almost negligible for samples A and A1. Meanwhile the low water uptake of C and C1 are mainly due to high drainage of the liquid. Since all four samples have similar porous structure as observed in the SEM characterizations (section 4.4), WRR results allow for the comparison of hydrophilicity and hydrophobicity differences between the samples.

As shown in Figure 3.4, the second part of the water uptake study demonstrates the oleophilic properties of sample C1 and its selectivity of oil over water.

The water surface appeared to be clear at around 7 minutes after placing adsorbent onto the solution. A thin ring of blue oil adhered to the side of the glass beaker and was separated from the water surface due to liquid level slightly lowered after the adsorption. A small amount

80

of oil was leaked and returned into the water when it was handled. No major drainage occurred, this was likely due to the adsorption did not reach its capacity. The sample had very good buoyancy, which allowed the sample to remain floating throughout the test. The entire sample was above the water line initially and about two thirds of its body lowered below the water line after 15 minutes.

Only one test per sample was performed in the first part of this study, and only one sample C1 was tested in the second part on selectivity. The results obtained in this study served as an indicator complementary to the liquid contact angles study. However, due to the limited sample size, it may not be reliable or representative of the overall adsorbent properties. It is recommended that for future research, this experiment should be repeated with a higher sample number for better confirmation of the results.

Table 4.4 Water adsorption capacity $(g \cdot g^{-1})$, drainage and water retention rate (WRR) results from the water uptake study.

Sample	$Q_{m/m}$, w (g/g)	Drainage	WRR
A	19.00	<1%	99.00%
A1	30.80	<1%	99.00%
C	4.33	27.78%	72.22%
C1	2.50	28.57%	71.43%

4.10   RECYCLABILITY STUDY

The recyclability study results are shown in Figure 4.11 and the recyclability calculations are listed in Table 4.5. According to the recyclability test results, there is potential improvements

of 20% or more on the overall adsorption capacity of the adsorbent. Performance degradation is minimal, which demonstrates stable recyclability. Adsorption capacity after 10 cycles stays above 99% of the initial adsorption capacity.

It should be noted that performance degradations above 100% were fluctuations caused by human and measurement errors. These errors most likely resulted from inaccuracies during mechanical squeezing of the sponges, and inability to capture all of the drained oil. An interesting observation was noted from the oil drainage measurements, which increased throughout the cycles. Although drainage increased, there was no noticeable change to the overall adsorption capacity. Most interestingly, potential adsorption capacity $Q_{m/m, potential}$ was the only factor that changed to compensate for this increase of inefficiency throughout the cycles.

The increase in $Q_{m/m, potential}$ suggested that the adsorbent had improved after repeated adsorption-desorption. This was consistent with Darcy's law on capillary diffusivity, which stated that as moisture content increased in a porous media, capillary diffusivity increased as well. Also, it was possible that sample C1 was initially impeded by an excess amount of MPTS according to Figure 4.4. The SEM images revealed agglomerates of the silane agent, these agglomerates covered most of the RGO which made them inaccessible. Excess amount of MPTS could result from various factors, such as an imperfect MPTS, GO and ethanol solution ratio, self-polymerization of MPTS, improper timing or temperature of the silane coupling process, or insufficient washing. The liquid flow from repeated adsorption-desorption possibly helped to remove excess MPTS, exposing the RGO sheets underneath. However, the existing porous structure might not be ideal for oil retention due to the excessive drainage.

82

Additionally, recyclability was compared between sample C1 and the MPTS-HCl-PU control. Figure 4.12 compared their average adsorption capacities for six adsorption-desorption cycles. Results from the first to sixth cycle of the previous sample C1 recyclability test were combined and averaged with the results of this test. MPTS-HCl-PU had an average adsorption capacity of 27.98 $g \cdot g^{-1}$ with a standard deviation of 1.75 and performance degradation of 97.04% after the sixth cycle. C1 had an average adsorption capacity of 29.75 $g \cdot g^{-1}$ with a standard deviation of 3.51 and performance degradation of 99.33% after the sixth cycle. The MPTS-HCl-PU demonstrated an 8% adsorption improvement compared to the original HCl treated PU sponge (see Table 4.3). The functionalization of rGO on MPTS-HCl-PU increased the adsorption capacity by an additional 6%.

Table 4.5 Recyclability performance data. Potential and actual gravimetric adsorption capacities, actual volumetric adsorption capacities, volumetric oil adsorption efficiencies, oil drainage, oil retention rate, and performance degradations resulted from 10 adsorption-desorption cycles.

Cycle	$Q_{m/m}$, potential (g/g)	$Q_{m/m}$, actual (g/g)	$Q_{v/v}$, actual (cm^3/cm^3)	Volumetric Oil Adsorption Efficiency	Drainage	ORR	Performance Degradation (%)
1	31.33	28.50	39.36728712	77.69%	9.04%	90.96%	-
2	32.67	29.00	40.05794128	79.05%	11.22%	88.78%	101.75%
3	31.33	28.33	39.13706907	77.23%	9.57%	90.43%	99.42%
4	35.33	29.00	40.05794128	79.05%	17.92%	82.08%	101.75%
5	34.00	28.83	39.82772323	78.60%	15.20%	84.80%	101.17%
6	34.33	28.17	38.90685101	76.78%	17.96%	82.04%	98.83%
7	35.00	29.50	40.74859544	80.41%	15.71%	84.29%	103.51%
8	34.17	29.00	40.05794128	79.05%	15.12%	84.88%	101.75%
9	35.50	27.83	38.44641491	75.87%	21.60%	78.40%	97.66%
10	35.00	28.33	39.13706907	77.23%	19.05%	80.95%	99.42%
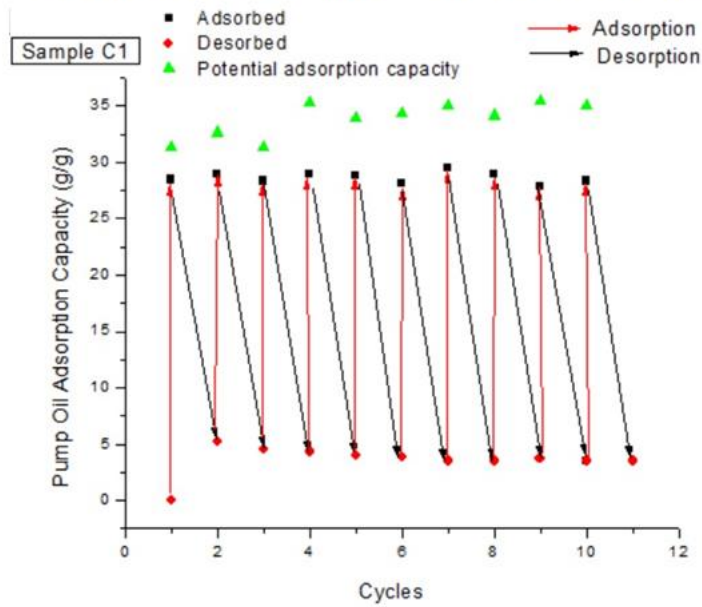
Figure 4.11 Potential and actual adsorption capacities of pump oil measured over 10 adsorption-desorption cycles for sample C1.
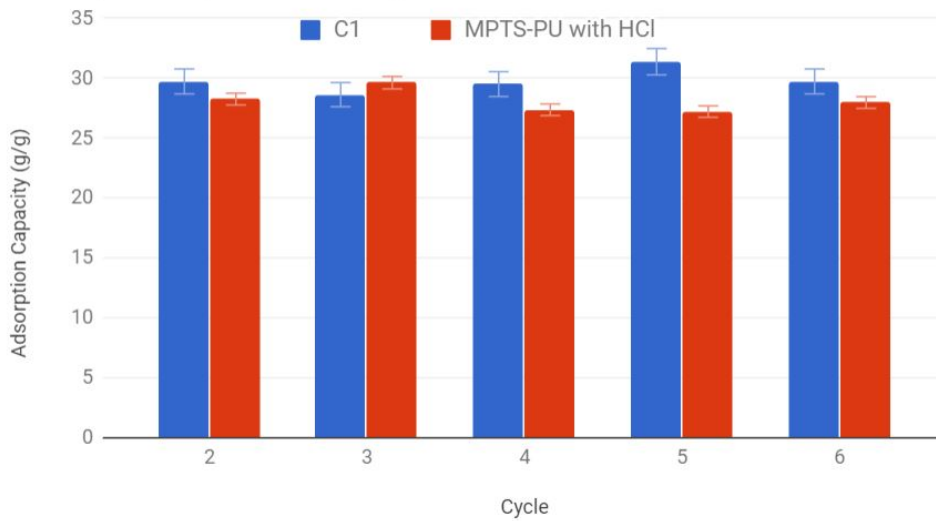
Figure 4.12 Adsorption capacity comparison for six adsorption-desorption cycles between samples C1 and MPTS-HCl-PU.

4.11   ADSORPTION KINETICS STUDY

The kinetics data is shown in Figure 4.13. The graph illustrated the relationship between the oil adsorption capacities versus time. During the kinetics study, it was observed that the adsorbent rapidly increased in its adsorption capacity within the first 5 seconds.
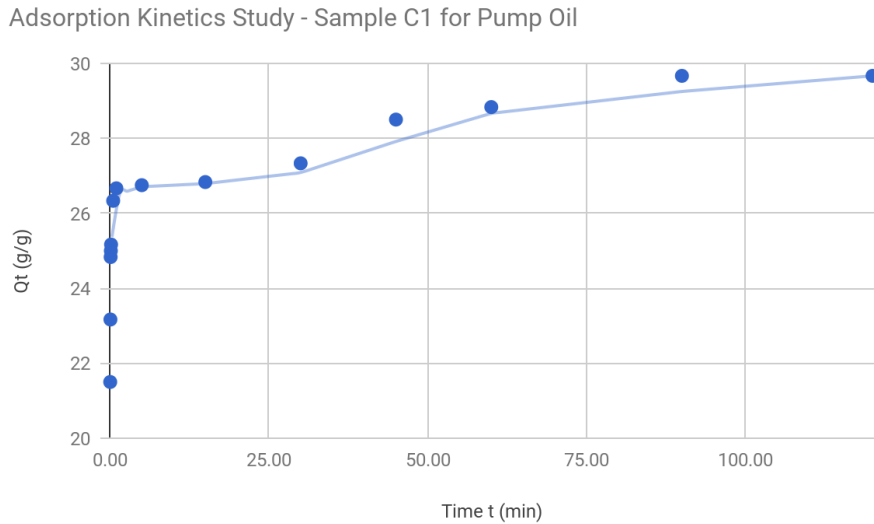
Figure 4.13 Adsorption kinetics of sample C1, the relationship between adsorption capacity and time from t = 0 to 120 minutes.

The adsorption capacity tapered until it came to an equilibrium at t = 90 minutes. The rate constants solved from Eq 3.16 and 3.17 are listed in Table 4.6. The Lagergren pseudo-second order models yielded a better fitting with the equilibrium data from the experiment (See Figures 4.14 and 4.15). Therefore suggesting that the rate limiting step may be associated with chemisorption which involve valence forces between the adsorbent and adsorbate in terms of sharing or exchange of electrons [149].

Table 4.6 Fitted Lagergren pseudo first and second order rate constant and R2 for sample C1 pump oil adsorption.

Pseudo-first order kinetic		Pseudo-second order kinetic	
k_1 (min^{-1})	R^2	k_2 (g·g^{-1}·min^{-1})	R^2
0.062	96.90%	0.065	99.70%
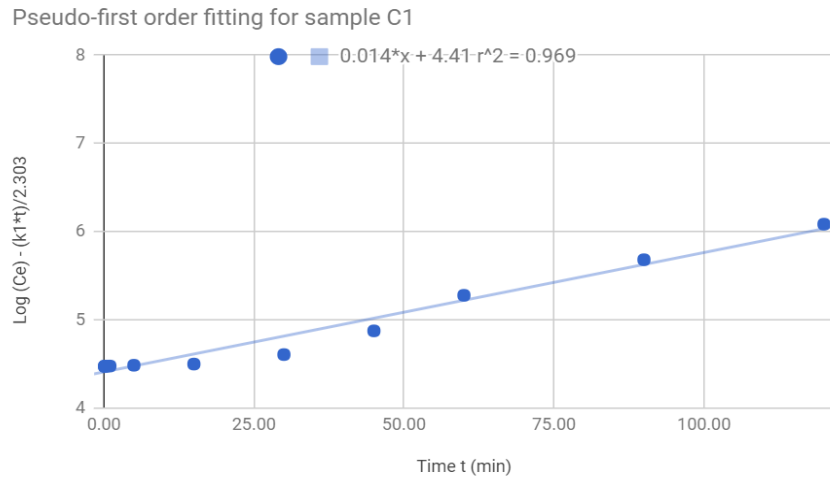
Figure 4.14 Lagergren pseudo-first order model fitting with kinetic data from sample C1.
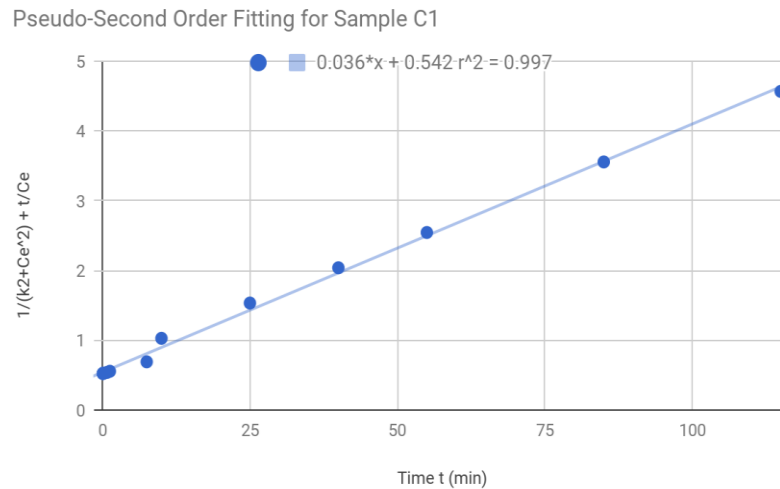
Figure 4.15 Lagergren pseudo-second order model fitting with kinetics data from sample C1.

CHAPTER 5 - SUMMARY AND CONCLUSION

5.1   SUMMARY

A novel oleophilic polyurethane (PU) sponge adsorbent, functionalized with reduced graphene oxide (RGO) and crosslinked with 3-methacryloxypropyl trimethoxysilane (MPTS), was successfully synthesized. Raman and XRD characterizations provided evidence that graphite was completely converted to GO. SEM confirmed the modification of morphology with surface roughness increase. FTIR confirmed successful silanization and reduction of the graphene oxide (GO) on the final PU sponge.

As explained previously in section 3.5.1, liquid contact angle measurements on porous surfaces were challenging. Although inaccurate, apparent contact angles were obtained in this thesis research mainly for comparison purposes. There was no obvious change of the WCA between the samples, which was likely an interference with measurements due to the disappearance of PU cell membranes after modifications. However there was substantial improvements in the OCA from 64.2° in sample A to 0° in C1, which displayed a superoleophilic spreading. Despite inaccuracies, together with the water uptake studies, it was evident that: 1) HCl caused the neat PU sponge to become more hydrophilic, 2) HCl improved hydrophobicity of MPTS-GO modified PU and contributed to its superoleophilic properties.

The novel adsorbent had an average recorded gravimetric adsorption capacity of 28.61 g/g as compared to 18.41 g/g from the original PU sponge without modification. The increase in oil uptake was an improvement of over 50%. HCl etching, rGO and MPTS all demonstrated contribution to the significant adsorption capacity improvement. Recyclability studies results

demonstrated the stability of repetitive adsorption-desorption cycling of the novel adsorbent. Performance maintained at about 99.42% from the initial adsorption capacity.

Adsorption kinetics modeling yielded a best fit with the Lagergren pseudo-second order model with a k_2 value of 0.065 with a coefficient of determination R^2 at 99.7%.

5.2   CONCLUSION

In general, experiments results on high surface area and low density adsorbent materials are highly sensitive to fluctuations of the sample's physical measurements, such as its apparent density. In these cases, larger sample dimensions and larger sample size from each sample type are necessary in order to offset some of these uncertainties and inaccuracies.

Several experimental parameters were implemented to analyze the adsorbent efficiency. These included 1) volumetric oil adsorption efficiency, which was a measurement of the amount of voids occupied by oil after adsorption as a percentage of a theoretical maximum amount of voids available in the adsorbent. 2) oil Retention Rate, which was a measurement of the amount of oil actually retained in the sponge as a percentage of the total amount of oil adsorbed before leakage or drainage occurred and 3) comparison of the gravimetric flux with a theoretically predicted value. The predicted value was calculated based on the changes in OCA. Uncertainties in the contact angle measurements resulted in unreliable theoretical gravimetric improvement factor values, consequently an overestimate of the theoretical flux was documented in this thesis research. A more reliable method for contact angle measurement would be required in order to achieve a meaningful flux comparison.

It was observed that the liquid contact angles changed gradually over time. For future research on related subject, it is recommended that dynamic water and oil contact angles to be obtained with the change of time. In addition, surface energies comparison between the samples and the liquid surface tensions would allow a better understanding of the surface energy and wettability changes introduced by the sample modifications.

During contact angle measurements, a large percentage of the liquid droplets sagged into the surface pores within the first three to five minutes. It is recommended that future research to be performed on the effects of contact angle measurement using droplets larger than 3 mm in diameter.

Results from the efficiency parameters demonstrated substantial potential for further improvement in the samples. The results indicated reduction of drainage or leakage of the adsorbed oil may greatly improve the final adsorption capacities.

During actual field application of oil-water separation, adsorbents are often bulky and difficult to handle especially after it is oil saturated. The amount of these secondary wastes generated cannot be overlooked. Leakages risk the spread of contaminants and loss of efficiency, consequently negating the initial benefits that it should bring. Therefore, the experimental parameters reported in this thesis should be carefully considered during the process of adsorbent modification and selection.

Adsorption isotherm studies were not performed as part of this thesis, however it is suggested that isotherm studies to be carried out in conjunction with investigations of various geometries. It was visually observed that the angle of which the adsorbent was placed onto the

liquid surface had a significant effect on the adsorption behavior. Therefore, it is of interest to investigate various shapes which introduce the adsorbent onto the liquid surface at various angles. Varying geometries may control the angle at which the direction of the liquid enters the adsorbent surface. Since diffusivity changes with the change in moisture content, using geometries to allow for multiple entry angles may create a differential of diffusivities within the adsorbent at a given point in time. Comparisons between varying dosages of the adsorbent by keeping the same geometries to scale versus varying dosages by changing the geometries may provide further insights into controlling such adsorption behaviors.

CHAPTER 6 - FURTHER STUDIES

Optimal design and engineering of an adsorbent material is highly dependent on the adsorbate properties. The structural designs of an adsorbent are often as important as the modification of material by itself. The product's success and realistic performance depends on the synergistic effect among all facets in the material's engineering.

As discussed earlier in section 2.4.2 on porosity and pore size distributions, strong cohesive forces in viscous liquids resist adsorption at the bulk liquid phase. This results in clogging near the surface of an adsorbent, causing poor adsorption at the interior surface areas of the adsorbent mass. Due to this phenomenon, the thickness of an adsorbent should be designed accordingly to minimize the distance required for an adsorbate to travel through the porous media.

While these cohesive forces work against the capillary pressure during adsorption, the same forces are desirable and needed for oil retention. When a saturated adsorbent is removed from the liquid surface and transferred to a location for oil recovery, a majority of the adsorbed liquid is held in place due to cohesive forces and the result is oil retention.

Oil retention and the prevention of drainage is significant and yet it is not well studied. According to the experimental data from this thesis research, drainage can account for up to 30% of the initially adsorbed liquid. Whereas it is common for adsorption researches to focus on the net adsorption capacities without reporting the amount of drainage.

Often times, the only mitigation to decrease oil lost due to drainage, is by decreasing pore sizes of the adsorbent substrate material. This selection of pore sizes is passive and is a result of

trial and error from experiments and tests. Furthermore, this decrease of pore sizes most likely decreases the ratio of total pore volume to adsorbent volume due to the extra number of pore walls partitioning these pores. This not only compromises the maximum adsorption capacity by reducing the total volume available for adsorbate occupancy, reducing pore sizes result in a high number of pore cells in a given volume, therefore interconnectivity must be increased in order to maintain a high level of accessibility throughout the adsorbent. In order to address this oil retention inefficiency, further study is needed to focus on the hydrodynamic forces that govern drainage.

The drainage of liquid from porous media is well studied in the area of ground water hydraulics [153] where water occupies and recedes from pores in response to hydraulic pressure differences. Drainage occurs when the water pressure in the pores become less than the air pressure outside of the pores.
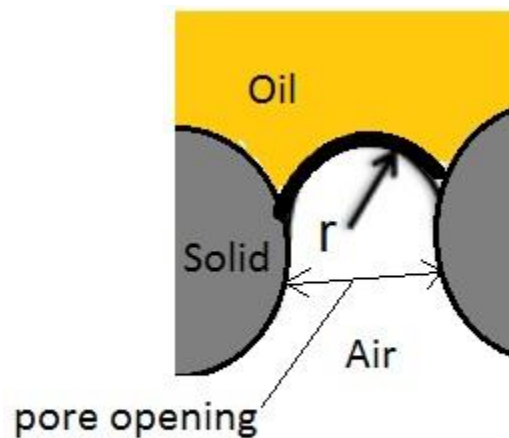

Figure 6.1 Illustration of an oil-saturated pore opening with an oil-solid-air interface, with radius r representing the sustainable pore opening size in order to maintain the balance of the pressure driving force.

As illustrated in Figure 6.1, Interfacial tension prevents displacement of the oil from the pore. In the case of water drainage [153], the force balances are described by the following equation:

$$2\pi r \gamma = \pi r^2 \Delta p \qquad\qquad 6.1$$

Solving for r yields: $\qquad\qquad r = \dfrac{2\gamma}{\Delta p} \qquad\qquad 6.2$

Where r is the radius of the pore opening, γ is the surface tension of the liquid, and Δp is the capillary which is the pressure difference across the interface. When Δp increases, r must decrease in order to balance the capillary force, otherwise drainage occurs because the surface tension with the existing radius can no longer support the force imbalance.

Similarly, in the case of an adsorbent pore saturated with oil, capillary force in this case is countered by gravity. When adsorption reaches equilibrium while the adsorbent sits on top of the bulk liquid, all forces are in balance. However when the adsorbent is lifted up and away from the liquid, the imbalance of forces result in a net positive pressure that is only sustainable up to a certain radius r. As in the water drainage example, the smaller the radius, the better it can maintain the force balance necessary to prevent drainage.

However, this radius r describes the *pore opening* radius and must not be confused with the radius of the pore chamber. Coincidentally, whenever a smaller pore size adsorbent material is selected, the pore opening is often smaller and therefore seemingly fulfills the requirement to decrease drainage. While a decrease in the pore diameter allow better oil retention due to a tighter network of cohesion forces among the oil molecules, it hinders the potential of the material by decreasing its total pore volume to adsorbent volume ratio, preventing it from

maximizing its oil adsorption capacities. Therefore, a better alternative is to study the effects of an optimal pore diameter to pore opening ratio.

Although a high pore chamber diameter to opening diameter ratio may suggest oil retention improvement without compromising the potential oil adsorption capacity of a material, a smaller opening will be relatively more restrictive for the adsorption flux flowing into the pore. This will undesirably increase the time to saturation as well as restricting the adsorption of viscous liquids due to possible plugging. As discussed earlier in Chapter 3, high interconnectivity, in which each pore is connected with all surrounding pores [130], is necessary for reaching maximum oil adsorption capacity. In this case, an ideal porous structure is one with high pore chamber diameter to opening diameter ratio, very high interconnectivity with a large number of pore openings, and high porosity. As reported by Bernardini et al. [154], a synthesis of lignin based flexible PU foam using water as a blowing agent, was optimize with substitution of up to 12% of common petroleum derived polyol. Their resulted open-cell PU foam shows good porosity, high interconnectivity as well as a good pore chamber diameter to opening diameter ratio as shown in their SEM images.
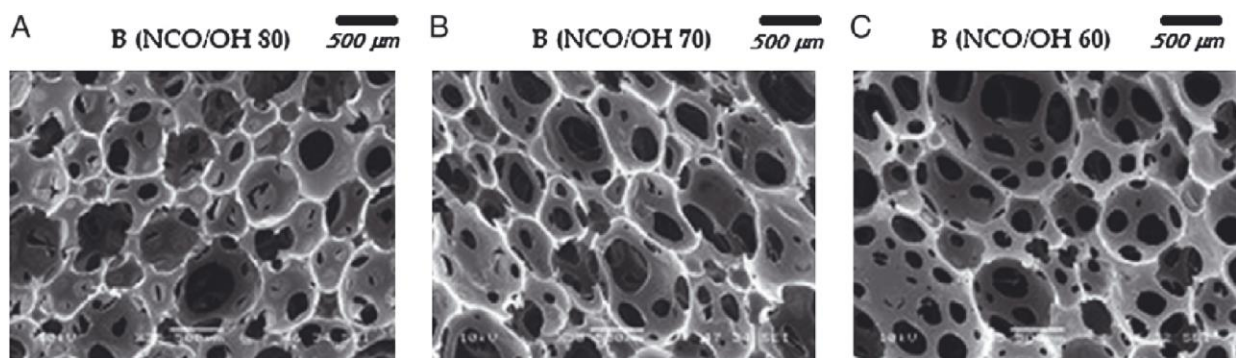
Figure 6.2 Reprinted from Polymer International, Vol 64, Jacopo Bernardini, Irene Anguillesi, Maria-Beatrice Coltelli, Patrizia Cinelli, Andrea Lazzeri, "Optimizing the lignin based synthesis of flexible polyurethane foams employing reactive liquefying agents", Page 1243, Copyright (2015), with permission from John Wiley and Sons.

This is an excellent example of the possibility to architect and fine tune according to the required

porous structure. Aviv et al. [155] demonstrated another example of a PU foam with a high pore

chamber diameter to opening diameter ratio.
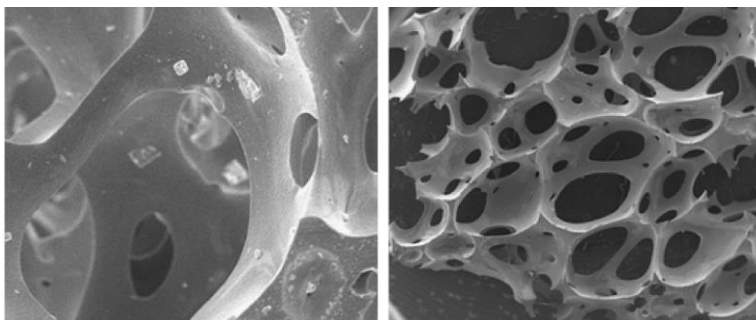
Figure 6.3 Reprinted from Journal of Controlled Release, Vol 172 issue 3, Oren Aviv, Natalia
Laout, Stanislav Ratner, Oshrat Harik, Konda Reddy Kunduru, Abraham J. Domb, "Controlled
iodine release from polyurethane sponges for water decontamination", Page 637, Copyright
(2013), with permission from Elsevier.

The SEM images of their sample showcased a desirable structure for liquid retention. The group

demonstrated the effectiveness of their adsorbent with an application that required slow release

of the adsorbate in an aqueous environment. In contrast, an example of a PU foam with low

interconnectivity and a pore diameter to pore opening ratio of 1 or less is shown in Figure 6.4.
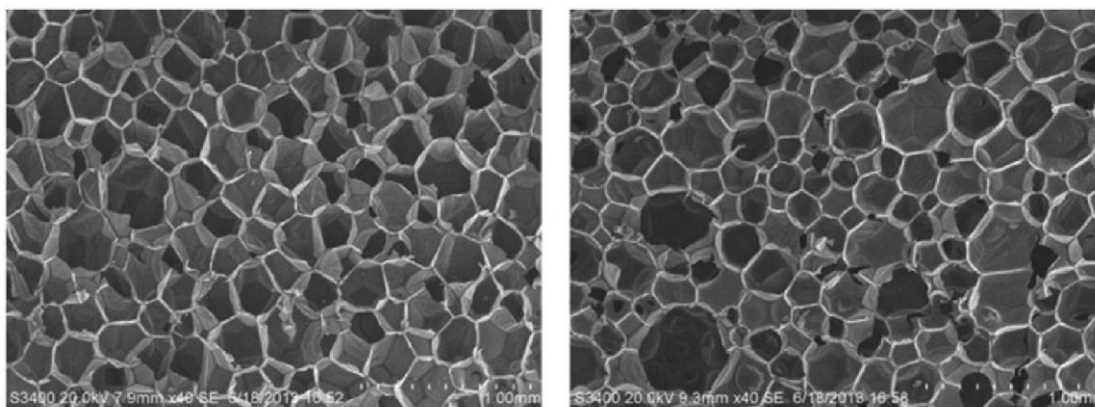
*Figure 6.4 (Reprinted from New Journal of Chemistry, Vol 38 issue 8, Xiaolin Li, Zheng Fang,
Xin Li, Shigui Tang, Kai Zhang, Kai Guo, "Synthesis and application of a novel bio-based polyol
for preparation of polyurethane foams", Page 3877, Copyright (2014), with permission from
Royal Society of Chemistry.*

95

Theoretically a high interconnectivity shortens the time to saturation due to a high network of accessible entry points, however this type of structure remains inefficient for highly viscous and heavy oils.

The study of fluid dynamic as a function of pore opening sizes rather than simply pore diameters have been documented in literatures. Mills[156] suggested in a wet Kelvin foam model using Computational Fluid Dynamics (CFD) that the air flow-permeability is a function of the area of the largest hole in a pore.

With a vast range of oily pollution properties, it is difficult to remain effective for a single type of adsorbent to target a wide spectrum of adsorbates. On the other hand, a more targeted adsorbent with optimized oil recovery and recyclability is capable to be highly effective and efficient. This will greatly benefit downstream applications in oil-water separation. Therefore, future investigations on the architecture of an ultrafast-adsorbing, leakage-proof, and highly recyclable adsorbent shall be considered.

LETTERS OF COPYRIGHT PERMISSION

License Number	4136631132711
License date	Jun 26, 2017
Licensed Content Publisher	John Wiley and Sons
Licensed Content Publication	Polymer International
Licensed Content Title	Optimizing the lignin based synthesis of flexible polyurethane foams employing reactive liquefying agents
Licensed Content Author	Jacopo Bernardini,Irene Anguillesi,Maria-Beatrice Coltelli,Patrizia Cinelli,Andrea Lazzeri
Licensed Content Date	Mar 27, 2015
Licensed Content Pages	10
Type of use	Dissertation/Thesis
Requestor type	University/Academic
Format	Electronic
Portion	Figure/table
Number of figures/tables	1
Original Wiley figure/table number(s)	Figure 14. SEM micrographs (35×) for comparing the formulations produced at the same isocyanate index
Will you be translating?	No
Title of your thesis / dissertation	Effects of 3-methacryloxypropyl-trimethoxysilane Functionalized Graphene on the Oil Adsorption Performance of Polyurethane Sponge
Expected completion date	Oct 2017
Expected size (number of pages)	100
Requestor Location	Mrs. Teresa Sung
	Attn: Mrs. Teresa Sung
Publisher Tax ID	EU826007151
Billing Type	Invoice
Billing Address	Mrs. Teresa Sung

This Agreement between Mrs. Teresa Sung ("You") and Royal Society of Chemistry ("Royal Society of Chemistry") consists of your license details and the terms and conditions provided by Royal Society of Chemistry and Copyright Clearance Center.

License Number	4136630073735
License date	Jun 26, 2017
Licensed Content Publisher	Royal Society of Chemistry
Licensed Content Publication	New Journal of Chemistry
Licensed Content Title	Synthesis and application of a novel bio-based polyol for preparation of polyurethane foams
Licensed Content Author	Xiaolin Li,Zheng Fang,Xin Li,Shigui Tang,Kai Zhang,Kai Guo
Licensed Content Date	Jun 3, 2014
Licensed Content Volume	38
Licensed Content Issue	8
Type of Use	Thesis/Dissertation
Requestor type	academic/educational
Portion	figures/tables/images
Number of figures/tables/images	1
Format	electronic
Distribution quantity	5
Will you be translating?	no
Order reference number	
Title of the thesis/dissertation	Effects of 3-methacryloxypropyl-trimethoxysilane Functionalized Graphene on the Oil Adsorption Performance of Polyurethane Sponge
Expected completion date	Oct 2017
Estimated size	100
Requestor Location	Mrs. Teresa Sung
	Attn: Mrs. Teresa Sung
Billing Type	Invoice
Billing Address	Mrs. Teresa Sung

REFERENCES

1. Ivshina IB, Kuyukina MS, Krivoruchko AV, et al. Oil spill problems and sustainable response strategies through new technologies. *Environmental science. Processes & impacts*. 2015;17(7):121-1219. http://www.ncbi.nlm.nih.gov/pubmed/26089295. doi: 10.1039/c5em00070j.

2. Prendergast DP, Gschwend PM. Assessing the performance and cost of oil spill remediation technologies. *Journal of Cleaner Production*. 2014;78:233-242. doi: 10.1016/j.jclepro.2014.04.054.

3. Ivshina IB, Kuyukina MS, Krivoruchko AV, et al. Oil spill problems and sustainable response strategies through new technologies. *Environ Sci : Processes Impacts*. 2015;17(7):1201-1219.

4. Ivshina IB, Kuyukina MS, Krivoruchko AV, et al. Oil spill problems and sustainable response strategies through new technologies. *Environmental science. Processes & impacts*. 2015;17(7):1201-1219. http://www.ncbi.nlm.nih.gov/pubmed/26089295. doi: 10.1039/C5EM00070J.

5. ITOPF. Use of oil sorbent materials in oil spill response. *THE INTERNATIONAL TANKER OWNERS POLLUTION FEDERATION LIMITED*. 2014.

6. Saththasivam J, Loganathan K, Sarp S. An overview of oil-water separation using gas flotation systems. *Chemosphere*. 2016;144:671-680.

http://www.ncbi.nlm.nih.gov/pubmed/26408973. doi:

10.1016/j.chemosphere.2015.08.087.

7. Dean RB. Hazardous and toxic wastes: Technology, management and health effects. *Waste*

Management & Research. 1985;3(3):283-284.

http://www.sciencedirect.com.proxy.lib.uwaterloo.ca/science/article/pii/0734242X85901

20X. doi: //dx.doi.org.proxy.lib.uwaterloo.ca/10.1016/0734-242X(85)90120-X ".

8. Adebajo MO, Frost RL, Kloprogge JT, Carmody O, Kokot S. Porous materials for oil spill

cleanup: A review of synthesis and absorbing properties. *Journal of Porous Materials*.

2003;10(3):159-170.

9. Ge J, Zhao H, Zhu H, Huang J, Shi L, Yu S. Advanced sorbents for Oil-Spill cleanup: Recent

advances and future perspectives. *Advanced Materials*. 2016;28(47):10459-10490.

http://onlinelibrary.wiley.com/doi/10.1002/adma.201601812/abstract. doi:

10.1002/adma.201601812.

10. Nagappan S, Park JJ, Park SS, Lee W, Ha C. Bio-inspired, multi-purpose and instant

superhydrophobic–superoleophilic lotus leaf powder hybrid micro–nanocomposites for

selective oil spill capture. *Journal of Materials Chemistry A*. 2013;1(23):6761. doi:

10.1039/c3ta00001j.

11. Barthlott W, Neinhuis C. Purity of the sacred lotus, or escape from contamination in

biological surfaces. *Planta*. 1997;202(1):1-8.

12. Wallace T, Gibbons D, O'Dwyer M, Curran TP. International evolution of fat, oil and grease

(FOG) waste management – A review. *J Environ Manage*. 2017;187:424-435.

13. Richardson SD, Kimura SY. Emerging environmental contaminants: Challenges facing our next generation and potential engineering solutions. *Environmental Technology & Innovation*. 2017;8:40-56.

14. John Pichtel. Oil and gas production wastewater: Soil contamination and pollution prevention. *Applied and Environmental Soil Science*. 2016;2016:1-24. http://dx.doi.org/10.1155/2016/2707989. doi: 10.1155/2016/2707989.

15. Schäfer RB, Bundschuh M, Rouch DA, et al. Effects of pesticide toxicity, salinity and other environmental variables on selected ecosystem functions in streams and the relevance for ecosystem services. *Science of the Total Environment*. 2012;415:69-78. http://www.sciencedirect.com/science/article/pii/S0048969711005912. doi: 10.1016/j.scitotenv.2011.05.063.

16. yu li, han mei, he fang. Review of treating oily waste water. .

17. László Kiss Z, Talpas L, Seres Z, Beszédes S, Hodúr C, László Z. Treatment of model oily waste water by microfiltration. *Per Pol Chem Eng*. ;57(1):21.

18. JSTOR is a not-for-profit service that helps scholars, researchers, students discover, et al. Long, slow recovery predicted for alaska author(s): Leslie roberts source: Science, new series, vol. 244, no. 4900 (apr. 7, 1989), pp. 22-24 published by: American association for the advancement of science stable URL: Http://Www.jstor.org/stable/1703422 accessed: 22-03-2017 23:50 UTC. . ;244.

19. Kaplan S. Review: Pharmacological pollution in water. *Critical Reviews in Environmental Science and Technology*. 2013;43(10):1074-1116. http://search.proquest.com/docview/1318604987. doi: 10.1080/10934529.2011.627036.

20. Xiaopeng Chen, Yanping Lin, Katherine Dang, Birgit Puschner. Quantification of polychlorinated biphenyls and polybrominated diphenyl ethers in commercial cows' milk from california by gas chromatography-triple quadruple mass spectrometry. *PLoS One*. 2017;12(1):e0170129. http://search.proquest.com/docview/1858297462. doi: 10.1371/journal.pone.0170129.

21. Tremolada P, Guazzoni N, Parolini M, Rossaro B, Bignazzi MM, Binelli A. Predicting PCB concentrations in cow milk: Validation of a fugacity model in high-mountain pasture conditions. *Sci Total Environ*. 2014;487:471-480.

22. Nordvik AB, Simmons JL, Bitting KR, Lewis A, Strøm-Kristiansen T. Oil and water separation in marine oil spill clean-up operations. *Spill Science and Technology Bulletin*. 1996;3(3):107-122. http://www.sciencedirect.com/science/article/pii/S1353256196000217. doi: 10.1016/S1353-2561(96)00021-7.

23. Cheryan M. Rajagopalan. eryan M, Rajagopalan N. Membrane processing of oily streams. wastewater treatment and waste reduction. *Journal of Membrane Science*. 1998;151(1):13-28. http://www.sciencedirect.com/science/article/pii/S0376738898001902. doi: 10.1016/S0376-7388(98)00190-2.

24. American Society for Testing and Materials. *ASTM standards on hazardous substances and oil spill response.* United States: ; 1994. http://catalog.hathitrust.org/Record/008341810.

25. Zhao T, Zhang D, Yu C, Jiang L. Facile fabrication of a polyethylene mesh for oil/water separation in a complex environment. *ACS Appl Mater Interfaces*. 2016;8(36):24186-24191.

26. LIU H, XU J, ZHANG J, SUN H, ZHANG J, WU Y. Oil/water separation in a liquid-liquid cylindrical cyclone. *Journal of Hydrodynamics, Ser. B*. 2012;24(1):116-123. http://www.sciencedirect.com.proxy.lib.uwaterloo.ca/science/article/pii/S1001605811602 254. doi: //dx.doi.org.proxy.lib.uwaterloo.ca/10.1016/S1001-6058(11)60225-4.

27. Zeevalkink JA, Brunsmann JJ. Oil removal from water in parallel plate gravity-type separators. *Water Res*. 1983;17(4):365-373.

28. Hande Gursoy-Haksevenler B, Idil Arslan-Alaton. Treatment of olive mill wastewater by chemical processes: Effect of acid cracking pretreatment. *Water Science and Technology*. 2014;69(7):1453-1461.

29 Chawaloesphonsiya N, Painmanakul P. Study of cutting-oil emulsion separation by coalescer process in terms of medium characteristics and bed packing. *Sep Sci Technol*. 2014;49(18):2960-2967.

30. Zhang W, Zhu Y, Liu X, et al. Salt-Induced fabrication of superhydrophilic and underwater superoleophobic PAA-g-PVDF membranes for effective separation of Oil-in-Water emulsions. *Angewandte Chemie International Edition*. 2014;53(3):856-860.

http://onlinelibrary.wiley.com/doi/10.1002/anie.201308183/abstract. doi:
10.1002/anie.201308183.

31. Zouboulis AI, Avranas A. Treatment of oil-in-water emulsions by coagulation and dissolved-air flotation. *Colloids and Surfaces A: Physicochemical and Engineering Aspects*. 2000;172(1):153-161. http://www.sciencedirect.com.proxy.lib.uwaterloo.ca/science/article/pii/S0927775700005616. doi: //dx.doi.org.proxy.lib.uwaterloo.ca/10.1016/S0927-7757(00)00561-6.

32. Lu Q, Yan B, Xie L, Huang J, Liu Y, Zeng H. A two-step flocculation process on oil sands tailings treatment using oppositely charged polymer flocculants. *Science of The Total Environment*. 2016;565:369-375. http://www.sciencedirect.com.proxy.lib.uwaterloo.ca/science/article/pii/S0048969716308944. doi: //dx.doi.org.proxy.lib.uwaterloo.ca/10.1016/j.scitotenv.2016.04.192.

33. Al-Shamrani AA, James A, Xiao H. Destabilisation of oilwater emulsions and separation by dissolved air flotation. *Water Res*. 2002;36(6):1503-1512.

34. Wang X, Wang X, Liu M, Zhou L, Gu Z, Zhao J. Bioremediation of marine oil pollution by brevundimonas diminuta: Effect of salinity and nutrients. *Desalination and Water Treatment*. 2016;57(42):19768-19775.

35. Angelova D, Uzunov I, Uzunova S, Gigova A, Minchev L. Kinetics of oil and oil products adsorption by carbonized rice husks. *Chem Eng J*. 2011;172(1):306-311.

36. Zhao YX, Gao BY, Shon HK, Cao BC, Kim J-. Coagulation characteristics of titanium (ti)

salt coagulant compared with aluminum (al) and iron (fe) salts. *Journal of Hazardous Materials*. 2011;185(2):1536-1542. http://www.sciencedirect.com/science/article/pii/S0304389410013725. doi: 10.1016/j.jhazmat.2010.10.084.

37. Holt PK, Barton GW, Mitchell CA. The future for electrocoagulation as a localised water treatment technology. *Chemosphere*. 2005;59(3):355-367. http://www.sciencedirect.com/science/article/pii/S0045653504009774. doi: 10.1016/j.chemosphere.2004.10.023.

38. Mollah MYA, Schennach R, Parga JR, Cocke DL. Electrocoagulation (EC) — science and applications. *Journal of Hazardous Materials*. 2001;84(1):29-41. http://www.sciencedirect.com/science/article/pii/S0304389401001765. doi: 10.1016/S0304-3894(01)00176-5.

39. Bazrafshan E, Kord Mostafapour F, Farzadkia M, Ownagh KA, Mahvi AH. Slaughterhouse wastewater treatment by combined chemical coagulation and electrocoagulation process. *PloS one*. 2012;7(6):e40108. http://www.ncbi.nlm.nih.gov/pubmed/22768233. doi: 10.1371/journal.pone.0040108.

40. Cañizares P, Martínez F, Jiménez C, Sáez C, Rodrigo MA. Coagulation and electrocoagulation of oil-in-water emulsions. *Journal of Hazardous Materials*. 2008;151(1):44-51. http://www.sciencedirect.com/science/article/pii/S0304389407007650. doi: 10.1016/j.jhazmat.2007.05.043.

41. Fajardo A, Seca H, Martins R, et al. Phenolic wastewaters depuration by electrochemical oxidation process using ti/IrO2 anodes. *Environ Sci Pollut Res*. 2017;24(8):7521-7533. doi: 10.1007/s11356-017-8431-9.

42. Zongo I, Maiga AH, Wéthé J, et al. Electrocoagulation for the treatment of textile wastewaters with al or fe electrodes: Compared variations of COD levels, turbidity and absorbance. *Journal of Hazardous Materials*. 2009;169(1):70-76. http://www.sciencedirect.com/science/article/pii/S0304389409004634. doi: 10.1016/j.jhazmat.2009.03.072.

43. Sahu O, Mazumdar B, Chaudhari P. Treatment of wastewater by electrocoagulation: A review. *Environ Sci Pollut Res*. 2014;21(4):2397-2413. http://www.ncbi.nlm.nih.gov/pubmed/24243160. doi: 10.1007/s11356-013-2208-6.

44. Choi HM, Cloud RM. Natural sorbents in oil spill cleanup. *Environmental Science & Technology*. 1992;26(4):772-776. http://search.proquest.com/docview/230112596. doi: 10.1021/es00028a016.

45. AlMajed AA, Adebayo AR, Hossain ME. A sustainable approach to controlling oil spills. *Journal of environmental management*. 2012;113:213-227. http://www.ncbi.nlm.nih.gov/pubmed/23037316. doi: 10.1016/j.jenvman.2012.07.034.

46. Ventikos NP, Vergetis E, Psaraftis HN, Triantafyllou G. A high-level synthesis of oil spill response equipment and countermeasures. *J Hazard Mater*. 2004;107(1–2):51-58.

47. QU J search progress of novel adsorption processes in water purification: A review. *Journal*

of Environmental Sciences. 2008;20(1):1-13.

http://www.sciencedirect.com.proxy.lib.uwaterloo.ca/science/article/pii/S1001074208600

017. doi: //dx.doi.org.proxy.lib.uwaterloo.ca/10.1016/S1001-0742(08)60001-7.

48. Abdelwahab O, Nasr SM, Thabet WM. Palm fibers and modified palm fibers adsorbents for

different oils. *Alexandria Engineering Journal*. 2017.

49. Zhang L, Zhong Y, Cha D, Wang P. A self-cleaning underwater superoleophobic mesh for

oil-water separation. *Scientific reports*. 2013;3:2326.

http://www.ncbi.nlm.nih.gov/pubmed/23900109. doi: 10.1038/srep02326.

50. Gong H, Chen Z, Fan Y, Zhang M, Wu W, Wang W. Surface modification of activated

carbon for siloxane adsorption. *Renewable Energy*. 2015;83:144-150.

51. Chibowski E, Delgado AV, Rudzka K, Szcześ A, Hołysz L. Surface modification of glass

plates and silica particles by phospholipid adsorption. *Journal of Colloid and Interface

Science*. 2011;353(1):281-289.

http://www.sciencedirect.com.proxy.lib.uwaterloo.ca/science/article/pii/S0021979710010

799. doi: //dx.doi.org.proxy.lib.uwaterloo.ca/10.1016/j.jcis.2010.09.028.

52. Yu Z, Zhang C, Zheng Z, et al. Enhancing phosphate adsorption capacity of SDS-based

magnetite by surface modification of citric acid. *Appl Surf Sci*. 2017;403:413-425.

53. Akira Nakajima. Design of hydrophobic surfaces for liquid droplet control. *NPG Asia

Materials*. 2011;3:49. http://search.proquest.com/docview/1024546597. doi:

10.1038/asiamat.2011.55.

54. Young T. An essay on the cohesion of fluids. *Journal of Natural Philosophy, Chemistry, and the Arts*. 1806;14:158. http://search.proquest.com/docview/1310932429.

55. Kanicky JR, Lopez-Montilla J-, Pandey S, Shah D. Surface chemistry in the petroleum industry. In: *Handbook of applied surface and colloid chemistry*. New York: Wiley; 2001:251–267.

56. Good RJ, Girifalco LA, Kraus G. A theory for estimation of interfacial energies. II. application to surface thermodynamics of teflon and graphite. *J Phys Chem*. 1958;62(11):1418-1421.

57. Xue Z, Wang S, Lin L, et al. A novel superhydrophilic and underwater superoleophobic Hydrogel-Coated mesh for oil/water separation. *Adv Mater*. 2011;23(37):4270-4273.

58. Hui Li, Mengnan Qu, Zhe Sun, Jinmei He, Anning Zhou. Facile fabrication of a hierarchical superhydrophobic coating with aluminate coupling agent modified kaolin. *Journal of Nanomaterials*. 2013;2013:1-5. http://dx.doi.org/10.1155/2013/497216. doi: 10.1155/2013/497216.

59. Su Y, Ji B, Zhang K, Gao H, Huang Y, Hwang K. Nano to micro structural hierarchy is crucial for stable superhydrophobic and water-repellent surfaces. *Langmuir*. 2010;26(7):4984-4989.

60. Züttel A, Sudan P, Mauron P, Wenger P. Model for the hydrogen adsorption on carbon nanostructures. *Applied Physics A*. 2004;78(7):941-946.

61. Ströbel R, Jörissen L, Schliermann T, et al. Hydrogen adsorption on carbon materials.

Journal of Power Sources. 1999;84(2):221-224.

http://www.sciencedirect.com.proxy.lib.uwaterloo.ca/science/article/pii/S0378775399003

201. doi: //dx.doi.org.proxy.lib.uwaterloo.ca/10.1016/S0378-7753(99)00320-1.

62. Ansón A, Jagiello J, Parra JB, et al. Porosity, surface area, surface energy, and hydrogen adsorption in nanostructured carbons. *J Phys Chem B*. 2004;108(40):15820-15826.

63. Chin SF, Binti Romainor AN, Pang SC. Fabrication of hydrophobic and magnetic cellulose aerogel with high oil absorption capacity. *Mater Lett*. 2014;115:241-243.

64. Li Y, Zhu X, Ge B, Men X, Li P, Zhang Z. Versatile fabrication of magnetic carbon fiber aerogel applied for bidirectional oil-water separation. *Applied Physics A*. 2015;120(3):949-957.

65. Jiao C, Xiong J, Tao J, et al. Sodium alginate/graphene oxide aerogel with enhanced strengthtoughness and its heavy metal adsorption study. *Int J Biol Macromol*. 2016;83(Complete):133-141.

66. Jiang F, Hsieh Y. Amphiphilic superabsorbent cellulose nanofibril aerogels. *Journal of Materials Chemistry A*. 2014;2(18):6337. doi: 10.1039/c4ta00743c.

67. Smirnova I, Gurikov P. Aerogels in chemical engineering: Strategies toward tailor-made aerogels .

68. Wang Z, Ma H, Chu B, Hsiao BS. Super-hydrophobic polyurethane sponges for oil absorption. *Sep Sci Technol*. 2017;52(2):221-227.

69. Barry E, Mane AU, Libera JA, Elam JW, Darling SB. Advanced oil sorbents using sequential

infiltration synthesis. *J. Mater. Chem. A*. 2017;5(6):2929-2935. doi: 10.1039/C6TA09014A.

70. Cho E, Chang-Jian C, Hsiao Y, Lee K, Huang J. Interfacial engineering of melamine sponges using hydrophobic TiO2 nanoparticles for effective oil/water separation. *Journal of the Taiwan Institute of Chemical Engineers*. 2016;67:476-483. http://www.sciencedirect.com.proxy.lib.uwaterloo.ca/science/article/pii/S1876107016302 772. doi: //dx.doi.org.proxy.lib.uwaterloo.ca/10.1016/j.jtice.2016.08.002.

71. Zhuang Y, Yu F, Ma J, Chen J. Graphene as a template and structural scaffold for the synthesis of a 3D porous bio-adsorbent to remove antibiotics from water. *RSC Adv*. 2015;5(35):27964-27969. doi: 10.1039/C4RA12413H.

72. Shouying Huang, Jiafu Shi. Monolithic macroporous carbon materials as high-performance and ultralow-cost sorbents for efficiently solving organic pollution. . 2014. doi: 10.1021/ie5003558.

73. Guo J, Wang J, Zhang S, et al. One-step modification of PU sponges for selective absorption of oil-water mixtures. *New J. Chem*. 2016;41(1):9-96. doi: 10.1039/c6nj03239g.

74. Li H, Liu L, Yang F. Hydrophobic modification of polyurethane foam for oil spill cleanup. *Marine Pollution Bulletin*. 2012;64(8):1648-1653. http://www.ncbi.nlm.nih.gov/pubmed/22749062. doi: 10.1016/j.marpolbul.2012.05.039.

75. Miyamoto R, Yasuhara S, Shikuma H, Ohshima M. Preparation of micro/nanocellular polypropylene foam with crystal nucleating agents. *Polymer Engineering & Science*.

2014;54(9):2075-2085. http://onlinelibrary.wiley.com/doi/10.1002/pen.23758/abstract. doi: 10.1002/pen.23758.

76. Udeni Gunathilake TM Sampath, Yern Chee Ching, Cheng Hock Chuah, Johari J Sabariah, Pai-Chen Lin. Fabrication of porous materials from natural/synthetic biopolymers and their composites. *Materials*. 2016;9(12):991. http://search.proquest.com/docview/1858315569. doi: 10.3390/ma9120991.

77. Maes J, De Meulenaer B, Van Heerswynghels P, et al. Removal of dioxins and PCB from fish oil by activated carbon and its influence on the nutritional quality of the oil. *J Amer Oil Chem Soc*. 2005;82(8):593-597. http://search.proquest.com/docview/274956259. doi: 10.1007/s11746-005-1114-1.

78. Khin MM, Nair AS, Babu VJ, Murugan R, Ramakrishna S. A review on nanomaterials for environmental remediation. *Energy & Environmental Science*. 2012;5(8):875-819. doi: 10.1039/c2ee21818f.

79. Mondal S. Preparation, properties and applications of nanocellulosic materials. *Carbohydr Polym*. 2017;163:301-316.

80. Zahid MA, Halligan JE, Johnson RF. Oil slick removal using matrices of polypropylene filaments. *Ind Eng Chem Proc Des Dev*. 1972;11(4):550-555.

81. Zhu X, Zhang Z, Ge B, Men X, Zhou X, Xue Q. A versatile approach to produce superhydrophobic materials used for oil–water separation. *Journal of Colloid and Interface Science*. 2014;432:105-108.

http://www.sciencedirect.com.proxy.lib.uwaterloo.ca/science/article/pii/S0021979714004

858. doi: //dx.doi.org.proxy.lib.uwaterloo.ca/10.1016/j.jcis.2014.06.056.

82. Ge B, Zhang Z, Zhu X, Men X, Zhou X. A superhydrophobic/superoleophilic sponge for the

selective absorption oil pollutants from water. *Colloids and Surfaces A: Physicochemical*

and Engineering Aspects. 2014;457:397-401.

http://www.sciencedirect.com.proxy.lib.uwaterloo.ca/science/article/pii/S0927775714005

585. doi: //dx.doi.org.proxy.lib.uwaterloo.ca/10.1016/j.colsurfa.2014.06.020.

83. Wang J, Geng G. Highly recyclable superhydrophobic sponge suitable for the selective

sorption of high viscosity oil from water. *Marine Pollution Bulletin*. 2015;97(1):118-124.

http://www.sciencedirect.com.proxy.lib.uwaterloo.ca/science/article/pii/S0025326X1500

3938. doi: //dx.doi.org.proxy.lib.uwaterloo.ca/10.1016/j.marpolbul.2015.06.026.

84. Li B, Liu X, Zhang X, Zou J, Chai W, Lou Y. Rapid adsorption for oil using

superhydrophobic and superoleophilic polyurethane sponge. *Journal of Chemical*

Technology & Biotechnology. 2015;90(11):2106-2112. doi: 10.1002/jctb.4646.

85. Zhao M, Huang J, Zhang Q, Luo W, Wei F. Improvement of oil adsorption performance by a

sponge-like natural vermiculite-carbon nanotube hybrid. *Applied Clay Science*.

2011;53(1):1-7.

http://www.sciencedirect.com.proxy.lib.uwaterloo.ca/science/article/pii/S0169131711001

359. doi: //dx.doi.org.proxy.lib.uwaterloo.ca/10.1016/j.clay.2011.04.003.

86. Korhonen JT, Kettunen M, Ras RHA, Ikkala O. Hydrophobic nanocellulose aerogels as

floating, sustainable, reusable, and recyclable oil absorbents. *ACS applied materials &*

interfaces. 2011;3(6):1813. http://www.ncbi.nlm.nih.gov/pubmed/21627309.

87. Xiao-Feng Sun, RunCang Sun, Jing-Xia Sun. Acetylation of rice straw with or without catalysts and its characterization as a natural sorbent in oil spill cleanup. *Journal of agricultural and food chemistry*. 2002;50(22):6428-6433. http://www.ncbi.nlm.nih.gov/pubmed/12381129. doi: 10.1021/jf020392o.

88. Wang Z, Ma H, Chu B, Hsiao BS. Super-hydrophobic modification of porous natural polymer "luffa sponge" for oil absorption. *Polymer*.

89. Zhang R, Wan W, Qiu L, Wang Y, Zhou Y. Preparation of hydrophobic polyvinyl alcohol aerogel via the surface modification of boron nitride for environmental remediation. *Appl Surf Sci*. 2017;419:342-347.

90. Weiwei Lei, David Portehault, Dan Liu, Si Qin, Ying Chen. Porous boron nitride nanosheets for effective water cleaning. *Nature Communications*. 2013;4:1777. http://www.ncbi.nlm.nih.gov/pubmed/23653189. doi: 10.1038/ncomms2818.

91. Song Y, Li B, Yang S, Ding G, Zhang C, Xie X. Ultralight boron nitride aerogels via template-assisted chemical vapor deposition. *Sci Rep*. 2015;5:10337.

92. Zhu Q, Chu Y, Wang Z, et al. Robust superhydrophobic polyurethane sponge as a highly reusable oil-absorption material. *Journal of Materials Chemistry A*. 2013;1(17):5386. doi: 10.1039/c3ta00125c.

93. Choi S, Kwon T, Im H, et al. A polydimethylsiloxane (PDMS) sponge for the selective absorption of oil from water. *ACS applied materials & interfaces*. 2011;3(12):4552.

http://www.ncbi.nlm.nih.gov/pubmed/22077378.

94. Viet Hung Pham, James H Dickerson. Superhydrophobic silanized melamine sponges as high efficiency oil absorbent materials. *ACS applied materials & interfaces*. 2014;6(16):14181-14188. http://www.ncbi.nlm.nih.gov/pubmed/25039789. doi: 10.1021/am503503m.

95. Kayvani Fard A, Mckay G, Manawi Y, Malaibari Z, Hussien MA. Outstanding adsorption performance of high aspect ratio and super-hydrophobic carbon nanotubes for oil removal. *Chemosphere*. 2016;164:142-155.

96. Kemp KC, Seema H, Saleh M, et al. Environmental applications using graphene composites: Water remediation and gas adsorption. *Nanoscale*. 2013;5(8):3149-3171. http://www.ncbi.nlm.nih.gov/pubmed/23487161. doi: 10.1039/c3nr33708a.

97. Zhao Y, Hu C, Hu Y, Cheng H, Shi G, Qu L. A versatile, ultralight, nitrogen-doped graphene framework. *Angewandte Chemie (International ed. in English)*. 2012;51(45):11371-11375. http://www.ncbi.nlm.nih.gov/pubmed/23060007. doi: 10.1002/anie.201206554.

98. Sun H, Xu Z, Gao C. Multifunctional, Ultra-Flyweight, synergistically assembled carbon aerogels. *Advanced Materials*. 2013;25(18):2554-2560. http://onlinelibrary.wiley.com/doi/10.1002/adma.201204576/abstract. doi: 10.1002/adma.201204576.

99. Rujing Zhang Yachang Cao Peixu Li Xiaobei Zang Pengzhan Sun Kunlin wang Minlin Zhong Jinquan Wei Dehai Wu Feiyu Kang Hongwei Zhu. Three-dimensional porous

graphene sponges assembled with the combination of surfactant and freeze-drying. Nano

Research. 2014;7(10):1477-1487.

http://lib.cqvip.com/qk/71233X/201410/666115666.html. doi: 10.1007/s12274-014-

0508-x.

100. Li B, Liu X, Zhang X, Chai W, Ma Y, Tao J. Facile preparation of graphene-coated

polyurethane sponge with superhydrophobic/superoleophilic properties. *J Polym Res*.

2015;22(10):1-6.

101. Novoselov KS, Geim AK, Morozov SV, et al. Electric field effect in atomically thin carbon

films. *Science*. 2004;306(5696):666-669.

http://www.sciencemag.org/cgi/content/abstract/306/5696/666. doi:

10.1126/science.1102896.

102. Stoller MD, Park S, Zhu Y, An J, Ruoff RS. Graphene-based ultracapacitors. *Nano Lett*.

2008;8(10):3498-3502.

103. Balandin AA, Ghosh S, Bao W, et al. Superior thermal conductivity of single-layer

graphene. *Nano Lett*. 2008;8(3):902-907.

104. Lee C, Wei X, Kysar JW, Hone J. Measurement of the elastic properties and intrinsic

strength of monolayer graphene. *Science*. 2008;321(5887):385-388.

http://www.sciencemag.org/cgi/content/abstract/321/5887/385. doi:

10.1126/science.1157996.

105. Shahrima Maharubin, Xin Zhang, Fuliang Zhu, Hong-Chao Zhang, Gengxin Zhang, Yue

Zhang. Synthesis and applications of semiconducting graphene. *Journal of Nanomaterials*. 2016;2016. http://search.proquest.com/docview/1846088664. doi: 10.1155/2016/6375962.

106. Park S, An J, Piner RD, et al. Aqueous suspension and characterization of chemically modified graphene sheets. *Chemistry of Materials*. 2008;20(21):6592-6594. doi: 10.1021/cm801932u.

107. Wang J, Shi Z, Fan J, Ge Y, Yin J, Hu G. Self-assembly of graphene into three-dimensional structures promoted by natural phenolic acids. *Journal of Materials Chemistry*. 2012;22(42):22459-22466. doi: 10.1039/c2jm35024f.

108. Nguyen BH, Nguyen VH. Promising applications of graphene and graphene-based nanostructures. *Adv Nat Sci: Nanosci Nanotechnol*. 2016;7(2):023002.

109. Yun-Seok Jun, Serubbabel Sy, Wook Ahn, et al. Highly conductive interconnected graphene foam based polymer composite. . 2015. doi: 10.1016/j.carbon.2015.08.079.

110. Zhao J, Ren W, Cheng H. Graphene sponge for efficient and repeatable adsorption and desorption of water contaminations. *Journal of Materials Chemistry*. 2012;22(38):20197. doi: 10.1039/c2jm34128j.

111. Department of Chemistry, Department of Computer Science, Department of Mechanical Engineering, et al. Top-down versus bottom-up fabrication of graphene-based electronics. . 2013. doi: 10.1021/cm402179h.

112. Choi W, Lahiri I, Seelaboyina R, Kang YS. Synthesis of graphene and its applications: A

review. *Critical Reviews in Solid State and Materials Sciences*. 2010;35(1):52-71.

113. Staudenmaier L. Untersuchungen ber den graphit. *Berichte der deutschen chemischen Gesellschaft*. 1899;32(3):2824-2834.

114. WILLIAMS HUMMERSJR, RICHARDE OFFEMAN. Preparation of graphitic oxide. .

115. B. C. Brodie. On the atomic weight of graphite. *Philosophical Transactions of the Royal Society of London*. 1859;149:249-259. http://www.jstor.org/stable/108699. doi: 10.1098/rstl.1859.0013.

116. Daniela C Marcano, Dmitry V Kosynkin, Jacob M Berlin, et al. Improved synthesis of graphene oxide. *ACS nano*. 2010;4(8):4806-4814. http://www.ncbi.nlm.nih.gov/pubmed/20731455. doi: 10.1021/nn1006368.

117. Higgins D, Hoque MA, Seo MH, et al. Development and simulation of sulfur-doped graphene supported platinum with exemplary stability and activity towards oxygen reduction. *Advanced Functional Materials*. 2014;24(27):4325-4336. http://onlinelibrary.wiley.com/doi/10.1002/adfm.201400161/abstract. doi: 10.1002/adfm.201400161.

118. Akindoyo JO, Beg MDH, Ghazali S, Islam MR, Jeyaratnam N, Yuvaraj AR. Polyurethane types, synthesis and applications - a review. *RSC Adv*. 2016;6(115):114453-114482. doi: 10.1039/c6ra14525f.

119. Lithner D, Larsson Å, Dave G. Environmental and health hazard ranking and assessment of plastic polymers based on chemical composition. *Science of the Total Environment*.

2011;409(18):3309-3324.

http://www.sciencedirect.com/science/article/pii/S0048969711004268. doi:

10.1016/j.scitotenv.2011.04.038.

120. Tryznowski M, Świderska A, Żołek-Tryznowska Z, Gołofit T, Parzuchowski PG. Facile

route to multigram synthesis of environmentally friendly non-isocyanate polyurethanes.

Polymer. 2015;80:228-236. doi: 10.1016/j.polymer.2015.10.055.

121. Lu Y, Larock RC. Synthesis and properties of grafted latices from a soybean oil-based

waterborne polyurethane and acrylics. *Journal of Applied Polymer Science*.

2011;119(6):3305-3314. http://onlinelibrary.wiley.com/doi/10.1002/app.29029/abstract.

doi: 10.1002/app.29029.

122. Rafiemanzelat F, Zonuz A, Abdollahi E. Fast and eco-friendly synthesis of new

hydrolysable and biodegradable copolyurethanes derived from L-leucine cyclodipeptide

and different molecular weights of PEG in TBAB under microwave irradiation.

Macromol Res. 2012;20(9):902-911. doi: 10.1007/s13233-012-0137-8.

123. Jonathan R. Russell, Jeffrey Huang, Pria Anand, et al. Biodegradation of polyester

polyurethane by endophytic fungi. *Applied and Environmental Microbiology*.

2011;77(17):6076. http://aem.asm.org/content/77/17/6076.abstract. doi:

10.1128/AEM.00521-11.

124. Yong Yang, Jingchao Zhang, Jing Zhuang, Xun Wang. Synthesis of nitrogen-doped carbon

nanostructures from polyurethane sponge for bioimaging and catalysis. *Nanoscale*.

2015;7(29):12284-12290. http://www.ncbi.nlm.nih.gov/pubmed/26148902. doi:

10.1039/c5nr03481g.

125. Li B, Liu X, Zhang X, Zou J, Chai W, Xu J. Oil-absorbent polyurethane sponge coated with KH-570-modified graphene. *Journal of Applied Polymer Science*. 2015;132(16):n/a. http://onlinelibrary.wiley.com/doi/10.1002/app.41821/abstract. doi: 10.1002/app.41821.

126. Madkour TM, Abdelazeem EA, Tayel A, Mustafa G, Siam R. In situ polymerization of polyurethane-silver nanocomposite foams with intact thermal stability, improved mechanical performance, and induced antimicrobial properties. *Journal of Applied Polymer Science*. 2016;133(11):n/a. http://onlinelibrary.wiley.com/doi/10.1002/app.43125/abstract. doi: 10.1002/app.43125.

127. Appel A, Thomann R, Mülhaupt R. Hydroxyalkylation and polyether polyol grafting of graphene tailored for graphene/polyurethane nanocomposites. *Macromolecular Rapid Communications*. 2013;34(15):1249-1255. http://onlinelibrary.wiley.com/doi/10.1002/marc.201300363/abstract. doi: 10.1002/marc.201300363.

128. Krupadam RJ, Khan MS, Das S. Adsorption of fluoride from water by surface-functionalized polyurethane foam. *Water science and technology : a journal of the International Association on Water Pollution Research*. 2010;62(4):759. http://www.ncbi.nlm.nih.gov/pubmed/20729576. doi: 10.2166/wst.2010.190.

129. Rengasamy RS, Das D, Praba Karan C. Study of oil sorption behavior of filled and structured fiber assemblies made from polypropylene, kapok and milkweed fibers. *Journal of Hazardous Materials*. 2011;186(1):526-532.

http://www.sciencedirect.com.proxy.lib.uwaterloo.ca/science/article/pii/S0304389410014 55X. doi: //dx.doi.org.proxy.lib.uwaterloo.ca/10.1016/j.jhazmat.2010.11.031.

130. Pinto J, Athanassiou A, Fragouli D. Effect of the porous structure of polymer foams on the remediation of oil spills. *J Phys D: Appl Phys*. 2016;49(14):145601.

131. Darmanin T, Guittard F. Super oil-repellent surfaces from conductive polymers. *Journal of Materials Chemistry*. 2009;19(38):7130. doi: 10.1039/b904766b.

132. Steele A, Bayer I, Loth E. Inherently superoleophobic nanocomposite coatings by spray atomization. *Nano Lett*. 2009;9(1):501-505.

133. Meng H, Wang S, Xi J, Tang Z, Jiang L. Facile means of preparing superamphiphobic surfaces on common engineering metals. *J Phys Chem C*. 2008;112(30):11454-11458.

134. Ren G, Zhang Z, Zhu X, et al. A facile method for imparting superoleophobicity to polymer substrates. *Appl Phys A*. 2014;114(4):1129-1133. doi: 10.1007/s00339-013-7660-0.

135. Tuteja A, Choi W, Ma M, et al. Designing superoleophobic surfaces. *Science*. 2007;318(5856):1618-1622. http://www.sciencemag.org/cgi/content/abstract/318/5856/1618. doi: 10.1126/science.1148326.

136. Extrand CW. Model for contact angles and hysteresis on rough and ultraphobic surfaces. *Langmuir*. 2002;18(21):7991-7999. doi: 10.1021/la025769z.

137. Cao L, Price TP, Weiss M, Gao D. Super water- and oil-repellent surfaces on intrinsically hydrophilic and oleophilic porous silicon films. *Langmuir : the ACS journal of surfaces*

and colloids. 2008;24(5):1640-1643. http://www.ncbi.nlm.nih.gov/pubmed/18198916. doi: 10.1021/la703401f.

138. Witucki GL. A silane primer: Chemistry and applications of alkoxy silanes. *The Journal of Coatings Technology*. 1993;65(822):57.

139. Han MS, Kim YH, Han SJ, Choi SJ, Kim SB, Kim WN. Effects of a silane coupling agent on the exfoliation of organoclay layers in polyurethane/organoclay nanocomposite foams? *Journal of Applied Polymer Science*. 2008;110(1):376-386. http://onlinelibrary.wiley.com/doi/10.1002/app.28521/abstract. doi: 10.1002/app.28521.

140. Ke Q, Jin Y, Jiang P, Yu J. Oil/water separation performances of superhydrophobic and superoleophilic sponges. *Langmuir : the ACS journal of surfaces and colloids*. 2014;30(44):13137. http://www.ncbi.nlm.nih.gov/pubmed/25340643.

141. Tjandra R, Lui G, Veilleux A, Broughton J, Chiu G, Yu A. Introduction of an enhanced binding of reduced graphene oxide to polyurethane sponge for oil absorption. *Ind Eng Chem Res*. 2015;54(14):3657-3663.

142. Mitsubishi International PolymerTrade Corporation. Silane coupling agents. http://www.micchem.com/silane_coupling_agents.html Web site. http://www.micchem.com/silane_coupling_agents.html. Accessed June 22, 2017.

143. X X Zhao, H J Zhao, S Li, Y Z Yang, Z Yang, X G Liu. Functionalization of carbon microspheres using 3-methacryloxypropyl trimethoxysilane and its theoretical elucidation. *Asian Journal of Chemistry*. 2013;25(17):9622.

http://search.proquest.com/docview/1513751194. doi: 10.14233/ajchem.2013.15103.

144. Savard S, Blanchard L-, L onard J, Prud'homme RE. Hydrolysis and condensation of silanes in aqueous solutions. *Polymer Composites*. 1984;5(4):242-249. doi: 10.1002/pc.750050403.

145. Standard test methods for flexible cellular materials - slab, bonded, and molded urethane foams. *ASTM*. 2008;08(02). http://www.astm.org/Standards/D3574. doi: 10.1520/D3574-08.

146. Kwok DY, Lam CNC, Li A, et al. Measuring and interpreting contact angles: A complex issue. *Colloids Surf Physicochem Eng Aspects*. 1998;142(2–3):219-235.

147. Brugnara M. Contact angle. https://imagej.nih.gov/ij/plugins/contact-angle.html Web site. https://imagej.nih.gov/ij/plugins/contact-angle.html. Updated 2006. Accessed July 8, 2017.

148. American Society for Testing and Materials. Standard test method for sorbent performance of adsorbents. . 2012. https://global.ihs.com/doc_detail.cfm?gid=LLJEVEAAAAAAAAAA&input_doc_number=ASTM F726.

149. Mildred S Dresselhaus, Ado Jorio, Mario Hofmann, Gene Dresselhaus, Riichiro Saito. Perspectives on carbon nanotubes and graphene raman spectroscopy. *Nano letters*. 2010;10(3):751-758. http://www.ncbi.nlm.nih.gov/pubmed/20085345. doi: 10.1021/nl904286r.

150. Yang S, Song C, Qiu T, Guo L, Li X. Synthesis of polystyrene/polysilsesquioxane core/shell composite particles via emulsion polymerization in the existence of poly(γ-methacryloxypropyl trimethoxysilane) sol. *Langmuir : the ACS journal of surfaces and colloids*. 2013;29(1):92. http://www.ncbi.nlm.nih.gov/pubmed/23231420.

151. Strankowski M, Włodarczyk D, Piszczyk Ł, Strankowska J. Polyurethane nanocomposites containing reduced graphene oxide, FTIR, raman, and XRD studies. *Journal of Spectroscopy*. 2016;2016:1-6. https://doaj.org/article/1e5846d5b6894023a91a55562a68a0c9. doi: 10.1155/2016/7520741.

152. Lagergren S. About the theory of so-called adsorption of soluble substances. *Kungliga Svenska Vetenskapsakademiens Handlingar,*. 1898;24(4):1-39.

153. Karkare MV, Fort T. Water movement in "unsaturated" porous media due to pore size and surface tension induced capillary pressure gradients. *Langmuir*. 1993;9(9):2398-2403. doi: 10.1021/la00033a023.

154. Bernardini J, Anguillesi I, Coltelli M, Cinelli P, Lazzeri A. Optimizing the lignin based synthesis of flexible polyurethane foams employing reactive liquefying agents. *Polymer International*. 2015;64(9):1235-1244. http://onlinelibrary.wiley.com/doi/10.1002/pi.4905/abstract. doi: 10.1002/pi.4905.

155. Aviv O, Laout N, Ratner S, Harik O, Kunduru K, Domb A. Controlled iodine release from polyurethane sponges for water decontamination. *Journal of Controlled Release*. 2013;172(3):634-640. http://www.ncbi.nlm.nih.gov/pubmed/24096017. doi:

10.1016/j.jconrel.2013.09.018.

156. Mills NJ. The wet kelvin model for air flow through open-cell polyurethane foams. *J Mater Sci*. 2005;40(22):5845-5851. doi: 10.1007/s10853-005-5018-5.

157. Citgo, Petroleum Corporation. Citgo hytherm oil 46 specifications. http://www.docs.citgo.com/msds_pi/C10083.pdfC Web site. http://www.docs.citgo.com/msds_pi/C10083.pdfC. Updated 2015. Accessed July 10th, 2017.

158. Trovati G, Sanches EA, Neto SC, Mascarenhas YP, Chierice GO. Characterization of polyurethane resins by FTIR, TGA, and XRD. *Journal of Applied Polymer Science*. 2010;115(1):263-268. doi: 10.1002/app.31096.

APPENDICES

PRODUCT INFORMATION

CITGO HYTHERM® OIL 46

Date 07/15

DESCRIPTION: CITGO Hytherm Oil 46 is a premium quality heat transfer oil formulated with high viscosity index paraffinic base stocks and a special high temperature detergent/dispersant additive package.

QUALITIES: CITGO Hytherm Oil 46 provides high specific heat and good thermal conductivity at all temperatures for highly efficient heat transfer. CITGO Hytherm Oil 46 contains rust and oxidation inhibitors and a special additive package to help maintain system cleanliness and operational performance, reducing downtime and maintenance costs.

APPLICATIONS: CITGO Hytherm Oil 46 meets the exacting requirements of both open and closed heat transfer systems, at temperatures up to 600°F.

CITGO HYTHERM® OIL 46 PHYSICAL DATA

Temp., °F	Specific Gravity	Specific Heat BTU/lb/°F	Thermal Conductivity BTU/hr/ft²/°F	Viscosity cSt
60	0.871	0.442	0.0790	175
100	0.857	0.463	0.0770	51
200	0.824	0.517	0.0738	8.0
300	0.792	0.570	0.0715	2.9
400	0.761	0.624	0.0697	1.6
500	0.731	0.678	0.0675	1.0
600	0.697	0.732	0.0647	0.8

TYPICAL PROPERTIES:

CITGO HYTHERM® OIL 46

ISO VIS Grade (SAE Grade)	46
Material Code	637130001
Gravity, ASTM D 4052, °API	31.5
Density, lb/gal at 60°F	7.25
Flash Point, ASTM D 92, °F	453
Viscosity, ASTM D 445, cSt, at 40°C	48.5
cSt, at 100°F	7.0
Viscosity Index, ASTM D 2270	100
Pour Point, ASTM D 97, °F	16
Color, ASTM D 1500	2.0
Acid No., ASTM D 974	<0.01
Volume Factor, % per °F	0.033
Distillation, °F, ASTM D 2887, IBP, °F	650
5%	734
10%	771
50%	858
95%	944

CITGO and Hytherm are registered trademarks of CITGO Petroleum Corporation. All other registered trademarks or trademarks are the property of their respective owners.

CITGO Petroleum Corporation • 800/248-4684 • Houston, Texas • Made in USA
C10083

Figure A.1 Manufacturer specifications on the pump oil [158].

Speaker / Filter Foam - 30 PPI - Physical Data Sheet

Product General and Technical Information

Date: 12/10/2014   Name: Speaker / Filter Foam

General Information
Filter foam is a good-quality foam with a medium/firm feel. Filter foam has a high dust collection rate, while still providing high air flow. Common applications include speaker covers, filters, and cleaning sponges. Typical life is 5 to 10 years.

Property	Test Method	Values
Density (LB/Cubic Ft.)	ASTM D 3574-91	1.8
25% ILD (LB)	ASTM D 3574-91	30
Cell Count (Pores Per Inch)	ASTM D 3574-91	30
Air Flow (CFM)	ASTM D 3574-91	18.0
Tensile (PSI) Min.	ASTM D 3574-91	20
Elongation (%) Min.	ASTM D 3574-91	180
Tear (PPI) Min.	ASTM D 3574-91	5.0
Compression Set (@ 50% Deflection) % Max.	ASTM D 3574-91	15
25% CLD Autoclave Loss (% Max.)	ASTM D 3574-91	25
Compression Set (@ 50% Deflection Autoclave Loss)% Max.	ASTM D 3574-91	10

Figure A.2 Polyurethane sponge specifications by the manufacturer Foam Factory, Inc.